

Contract N0bsr 95349  
Project Serial SFF101-03-17  
Task 8139  
TRACOR Project 002 025 04  
Document Number 67-017-U

SUMMARY REPORT

EXPLORATORY DEVELOPMENT DOME STUDIES

Volume I

by

W. C. Moyer

Submitted to

Commander, Naval Ship Systems Command  
Department of the Navy  
Washington, D. C. 20360  
Attention: Code 00V1E

9 October 1967

THIS DOCUMENT MAY BE REPRODUCED WITHOUT  
RESTRICTIONS OF DISSEMINATION

D D C  
JAN 11 1968

**TRACOR**

AD 663556



6506 TRACOR LANE AUSTIN TEXAS 78721

Contract NObsr 95349  
Project Serial SFF101-03-17  
Task 8139  
TRACOR Project 002 025 94  
Document Number 67-917-U

SUMMARY REPORT

EXPLORATORY DEVELOPMENT DOME STUDIES

Volume I

by

W. C. Moyer

Submitted to

Commander, Naval Ship Systems Command  
Department of the Navy  
Washington, D. C. 20360  
Attention: Code 00V1E

9 October 1967

Approved:

E. A. Tucker  
Director of Hydrospace Programs

Submitted:

W. C. Moyer  
Program Manager



6500 TRACOR LANE AUSTIN TEXAS 78721

## ACKNOWLEDGEMENTS

Principal investigator for the general studies conducted under Task IA was R. F. Pohler. Dr. R. E. Douglass was primarily responsible for the elliptical dome studies, Task IB. He was assisted by J. W. Duran and B. E. Jay. These individuals together with K. B. Hamilton contributed to the supporting studies conducted in addition to Tasks IA and IB.

The experimental phase of the program was conducted at the TRACOR facility in Rockville, Maryland. Chief investigators were R. R. Whymark and K. E. Feith.

## ABSTRACT

This report presents the results obtained during the first year of a program for the analysis of the effects of sonar dome-transducer interactions on transmit performance. The analytical work has been directed toward (a) modeling a cylindrical transducer surrounded by an elliptical dome, (b) the application of an integral formulation of the radiation problem to sonar domes and transducers, and (c) limited analysis of a spherical transducer and concentric dome and a cylindrical dome with supporting structure. The analytical phases of the program have been supported by an experimental study whose main purpose has been the development of a small, high frequency transducer and appropriate instrumentation for measuring beam patterns and transducer displacements.

Numerical results for the elliptical dome model demonstrate the dependence of side lobe structure and level on beam steering angle. While beam patterns lack symmetry about the beam axis if the beam axis is not normally incident on the dome surface, no beam steering errors are incurred. The computed source level is strongly dependent on beam steering angle.

The development of several modifications to the usual application of the integral formulation of radiation problems has led to the successful modeling of large transducers. Numerical results applicable to several current sonar equipments have been obtained. The integral formulation now offers considerable promise of application to fairly general dome-transducer configurations.

The computed effects of a concentric dome on the beam patterns of a spherical array are similar qualitatively to those for a concentric cylindrical system: namely, a general increase in side lobe level with no significant change in the major lobe. The changes in transducer element interaction coefficients due



6500 TRACOR LANE AUSTIN, TEXAS 78721

to the dome also were computed. It was found that the dome did not alter the oscillatory nature of the coefficients (as a function of element separation); however, the amplitudes of both the reactive and resistive components varied appreciably, depending on dome-transducer spacing. A very limited analysis of a dome with simple supporting structure has demonstrated that the presence of the structure alters both beam pattern and source level compared to a homogeneous shell-type dome.



6500 TRACOR LANE. AUSTIN, TEXAS 78721

## TABLE OF CONTENTS

| <u>Section</u>  | <u>Page</u> |
|---|-------------|
| ACKNOWLEDGEMENTS                                      | ii          |
| ABSTRACT  | iii         |
| LIST OF ILLUSTRATIONS                                 | vii         |
| 1. INTRODUCTION                                       | 1           |
| 2. BACKGROUND   | 5           |
| 3. SUMMARY  | 7           |
| 3.1 Task IA - General Analytical Methods              | 7           |
| 3.2 Task IB - Elliptic Dome                           | 8           |
| 3.3 Related Studies                                   | 8           |
| 3.3.1 Studies of Dome Geometry                        | 9           |
| 3.3.2 Dome Structure                                  | 10          |
| 3.3.3 Comparison of Two- and Three-Dimensional Models | 10          |
| 3.4 Task II - Experimental Program                    | 11          |
| 4. GENERAL METHODS                                    | 13          |
| 4.1 Introduction                                      | 13          |
| 4.2 Outline of Present Technique                      | 16          |
| 4.3 Numerical Results                                 | 18          |
| 4.4 Summary   | 26          |
| 5. ELLIPTIC DOME                                      | 29          |
| 5.1 Introduction                                      | 29          |
| 5.2 Numerical Results                                 | 31          |
| 5.3 Discussion of Results                             | 42          |



TABLE OF CONTENTS (Cont'd.)

| <u>Section</u> |   | <u>Page</u> |
|----------------|---|-------------|
| 5.4            | Summary                                     | 43          |
| 6.             | OTHER DOME-TRANSDUCER MODELS                | 45          |
| 6.1            | Three-Dimensional Concentric Dome Model     | 45          |
| 6.2            | Spherical Dome Model                        | 50          |
| 6.3            | Thick Dome Model                            | 61          |
| 6.4            | Structured Model                            | 63          |
| 6.5            | Nonconcentric Circular Dome Model           | 69          |
| 6.6.           | Infinite Planar Dome-Transducer Model       | 72          |
| 7.             | EXPERIMENTAL PROGRAM                        | 77          |
| 7.1            | Introduction                                | 77          |
| 7.2            | Measurement Techniques                      | 77          |
| 7.3            | Beam Pattern Measurements                   | 83          |
| 7.4            | Measurement Apparatus                       | 85          |
| 7.5            | Model Source Design                         | 87          |
| 7.6            | Summary                                     | 98          |
| 8.             | CONCLUSIONS                                 | 99          |
| 9.             | PROPOSED PROGRAM FOR SECOND YEAR OF STUDIES | 103         |
|                | REFERENCES                                  | 105         |



## LIST OF ILLUSTRATIONS

| <u>Figure</u>   |   | <u>Page</u> |
|-----------------|---|-------------|
| 1               | Farfield Beam Pattern for a Circular Transducer                                   | 19          |
| 2               | Farfield Beam Pattern for a Circular Transducer                                   | 21          |
| 3               | Farfield Beam Pattern for a Circular Transducer                                   | 23          |
| 4               | Broadside Beam Pattern for an Elliptical Baffle                                   | 24          |
| 5               | Endfire Beam Pattern for an Elliptical Radiator                                   | 25          |
| 6               | Farfield Beam Pattern for a Spherical Transducer                                  | 27          |
| 7               | Geometry of Elliptic Dome and Circular Transducer                                 | 30          |
| 8<br>thru<br>16 | Beam Pattern for Elliptic Dome-Circular Transducer                                | 32-40       |
| 17              | Source Level Versus Steering Angle  | 41          |
| 18              | Geometry of Cylindrical Dome - Transducer Model                                   | 46          |
| 19              | Horizontal Beam Pattern for Cylindrical Array and Concentric Dome                 | 48          |
| 20              | Vertical Beam Pattern for Cylindrical Array and Concentric Dome                   | 49          |
| 21              | Geometry of Spherical Dome - Transducer Model                                     | 52          |
| 22              | Horizontal Beam Pattern for Spherical and Cylindrical Arrays with Domes           | 53          |
| 23              | Vertical Beam Pattern for Spherical and Cylindrical Arrays with Domes             | 54          |
| 24              | Vertical Beam Patterns for Spherical and Cylindrical Arrays without Domes         | 55          |
| 25              | Real Part of Normalized Mutual Acoustic Impedance for Elements on Bare Transducer | 57          |



## LIST OF ILLUSTRATIONS (Cont'd.)

| <u>Figure</u>    |   | <u>Page</u> |
|------------------|---|-------------|
| 26               | Imaginary Part of Normalized Mutual Acoustic Impedance for Elements on Bare Transducer                                | 58          |
| 27               | Real Part of Normalized Mutual Acoustic Impedance for Elements under Dome for Various Dome-Transducer Spacings        | 59          |
| 28               | Imaginary Part of Normalized Mutual Acoustic Impedance for Elements for Various Dome-Transducer Spacings              | 60          |
| 29               | Normalized Self Impedance Versus Dome-Transducer Spacing  | 62          |
| 30<br>thru<br>32 | Beam Patterns for Cylindrical Transducer, Thick Dome and Thin Dome Models   | 64-66       |
| 33               | Beam Pattern for Cylindrical Transducer and Concentric Dome, with Structure   | 68          |
| 34               | Nonconcentric Dome-Transducer Geometry  | 70          |
| 35               | Beam Pattern for Nonconcentric Dome-Circular Transducer Model and Elliptic Dome Model                                 | 71          |
| 36               | Geometry of Infinite Planar Dome-Transducer Model   | 74          |
| 37               | Radiated Intensity of Planar Dome-Transducer Model Versus $kd \cos \theta$  | 75          |
| 38               | Experimental Apparatus for Measuring the Displacement Profile of a Model Sound Source                                 | 78          |
| 39a              | Typical FM Discriminator Curve  | 80          |
| b                | Typical Displacement Sensor Calibration Curve   | 80          |
| 40               | Simplified Experimental Arrangement for the Measurement of Small Displacement Amplitudes Using a Laser Interferometer | 82          |



## LIST OF ILLUSTRATIONS (Cont'd.)

| <u>Figure</u> |   | <u>Page</u> |
|---------------|---|-------------|
| 41            | Geometric Arrangement of Probe Hydrophone and Model Sound Source for Measurement of Azimuthal Beam Patterns | 84          |
| 42            | Electronic Apparatus for Measuring Beam Patterns of the Model Sound Source                                  | 86          |
| 43            | Displacement Mapping Scheme for a Double Segmentally Active Piezoelectric Ring Source                       | 89          |
| 44            | Relative Displacements of 6.3" Dia. Segmentally Polarized Cylinder  | 90          |
| 45            | Horizontal Beam Pattern for Segmentally Excited PZT Cylinder  | 91          |
| 46            | Horizontal Beam Pattern at 5 ft.  | 93          |
| 47            | Relative Displacement, dB, vs Vertical Position for Single Cylinder   | 94          |
| 48            | Farfield Horizontal Beam Pattern - Single Element Section (Free Flooded Inside)                             | 95          |
| 49            | Farfield Horizontal Beam Pattern - Double Element Section (Free Flooded Inside)                             | 96          |
| 50            | Farfield Horizontal Beam Pattern - Triple Element Section (Free Flooded Inside)                             | 97          |



## 1. INTRODUCTION

This report summarizes the results achieved during the past year under Contract N0bsr-95349, Long Range Dome Studies. The report is divided into two volumes. Volume I contains a general description of studies conducted during the past year, including numerical results of the studies and conclusions based on these studies, and a description of tasks to be conducted in the second year of the program. Volume II contains a detailed account of the mathematical models and analytical methods employed to obtain this year's results.

The basic goals of the exploratory development program for sonar domes are (a) to develop guidelines for the sonar dome designer so that he can base his designs on scientific knowledge of the roles played by the system parameters in determining dome-array performance, and (b) to establish realistic models for predicting dome-array performance for the purpose of evaluating existing and contemplated dome-array systems. Many factors must be considered in developing design guidelines and performance prediction models. Among these factors are hydrodynamic and structural requirements, materials, and noise (platform and flow-induced), as well as the effect of dome-transducer interactions on transmit and receive beams. TRACOR's participation in this program has been primarily in the area of dome-transducer interactions. The studies conducted at TRACOR have been principally analytical in nature, although during the past year, the analytical studies have been supported by an experimental program.

As part of a continuing program of the analysis of dome-transducer interactions, the studies conducted during the past year have been directed toward the formulation of mathematical models which represent logical developments of previous efforts. At the beginning of the past year's work, the basic dome-transducer model consisted of a two-dimensional cylindrical transducer surrounded by a concentric shell-type dome. While this model

provided some insight into the importance of various dome-transducer parameters in determining system performance, it had obvious geometrical and structure shortcomings. These shortcomings have been attacked through the development of several new mathematical models, the emphasis being on a model with improved geometry.

Consistent with this goal, work has focused on a two-dimensional model representing a cylindrical transducer surrounded by an elliptical, shell-type dome. In conjunction with this study, an effort has been directed toward mathematical methods which can be applied to the analysis of fairly general dome-transducer configurations. The development of these general analytical methods is essential to the evolution of a realistic dome-transducer model.

As a result of progress on the above tasks, other brief supporting studies were conducted in the past year. These studies are related to comparisons of certain two- and three-dimensional models and to possible methods of treating more complicated types of domes in which structural members are included.

During the past year, the analytical studies have been directly supported by an experimental program, with the principal effort directed toward the development of a scale model of a cylindrical transducer and dome. This support is considered to have three aspects: First, experimental models can furnish validation for the results obtained in the analysis tasks. Second, experimental models can assist in defining the applicability of analytical models to real sonar problems. For example, simplified analytical models such as the two-dimensional elliptical dome model may be adequate for predicting dome-transducer performance for non-tilted transmit operations. The experimental program will assist in supporting such conclusions. Finally, there will undoubtedly be dome configurations, such as are found in the intricate truss work in many dome supporting structures, for which realistic mathematical modeling is difficult, if not impossible. The experimental procedures are expected to assist in revealing legitimate approximations in the analytical work.



6500 TRACOR LANE, AUSTIN TEXAS 78721

The experimental program is not intended to pursue the investigation of exact scale models of existing sonar systems but rather to provide a general facility for complementing the analytical work. In this light, the experimental program is of great value in helping to achieve the goals of the Long Range Dome Studies Program.



## 2. BACKGROUND

The difficulties associated with the exact mathematical modeling of a real dome-transducer system have been discussed many times. One must attempt to solve a boundary value problem for which the boundaries do not permit a solution of the governing partial differential equations by commonly implemented techniques. Further, the exact boundary conditions are difficult to describe. In such a situation the investigator may proceed in either of two ways: (a) he may attempt an approximate solution to an exact model, or (b) he may attempt an exact solution to a simplified model which approximates the geometry and boundary conditions of the real system being analyzed. In the former case one strives for better and better solution techniques until an adequate solution is obtained; in the latter case one strives for ever more realistic geometries and boundary conditions until an adequate model is derived. Due to the highly complex geometry of the dome-transducer one cannot expect to obtain an exact solution for the real system via the route of (b); however, the study of simplified models does offer several distinct advantages.

The chief advantage of analyzing simplified models for which exact solutions are available lies in the ability to isolate the effects of the model parameters on model performance. Once important parameters are recognized in a highly simplified model, the analyst has some insight into what to look for in a more complex model. An example of this point is the character of the normal impedance of a shell-type dome, an important parameter in determining the effects of the dome on transmitted beams. Early analysis, based on a plane wave incident on an infinite plate, demonstrated the essentially mass-like nature of the impedance. Subsequent analyses, of the circular transducer and concentric cylindrical shell, and the spherical transducer and concentric shell, indicate a similar result [1,2]. As another example, analyses of the total radiated power of these models



6500 TRACOR LANE. AUSTIN. TEXAS 78721

have indicated the importance of dome-transducer geometry in determining source level. While these results are qualitative (because of the simplification of the models), they provide a means of upgrading design guidelines since the general influence of some important parameters on system performance has been identified.

While the continuing upgrading of design guidelines logically derives from the analysis of models which can be treated exactly, the long-range thinking at TRACOR is devoted to the development of analysis tools applicable to general dome-transducer configurations. If we seek an approximate solution to the exact problem as stated in (a) above, we foresee two methods of attack. We may proceed directly with the attempt to solve the governing partial differential equation numerically, taking account of the boundary conditions. The finite difference techniques such as relaxation are an example of this approach. Alternatively, we may seek a numerical approximation of an exact integral solution of the boundary value problem. The methods of Chen, Chertock and others typify this procedure [3,4]. We have taken this latter approach, and during the past year have developed techniques which offer a great deal of promise in attacking the general dome-transducer problem.

Finally, it is recognized that in the analysis of a problem as difficult as the dome-transducer, one must rely to a certain extent on experimental support. The experimental phase of the present program is designed to verify the qualitative results of the simplified models and to give help over the "hard spots" of the more realistic models.



### 3. SUMMARY

At the beginning of the previous year's work, the program was divided into three distinct tasks, Task IA - General Analytical Methods, Task IB - Elliptic Dome, and Task II - Experimental Methods. The purpose of Task IA was to initiate development of analytical tools applicable to the analysis of fairly general dome-transducer configurations. Task IB was directed toward an immediate improvement of the dome geometry in the model which existed at that time: namely, the cylindrical transducer and concentric dome. The experimental efforts in Task II were centered around developing a scale dome-transducer and the related measurement and instrumentation techniques necessary for driving the transducer and obtaining transducer displacement profiles and beam patterns.

#### 3.1 TASK IA - GENERAL ANALYTICAL METHODS

The effort in Task IA has been directed toward the application of an integral formulation of the radiation problem. The appealing feature of this approach lies in its versatility, at least as a formalism, in regard to the geometry of the radiating body. Whereas the usual method of seeking a separable solution to the scalar wave equation (describing acoustic radiation) is restricted to a small class of radiator configurations, the integral formulation suffers from no geometrical restraints. The chief difficulty lies in obtaining numerical results from the solution once the problem is formulated. Because of this difficulty, the use of the integral formulation has been restricted in the past to relatively small radiators - much smaller than a modern sonar transducer. In the past year, however, definite progress has been made in applying the integral approach to the dome-transducer problem. Good numerical results have been obtained for radiators comparable in size to the AN/SQS-26 and AN/BQS-6. As a result of these developments, the application of integral methods to the dome-transducer problem appears promising.

### 3.2 TASK IB - ELLIPTIC DOME

While the long range goal of Task IA is to develop general methods of analysis, Task IB, the elliptical dome model, has provided an immediate upgrading of dome-transducer models. Although the model is two-dimensional, the plan view geometry is considerably more realistic than earlier, circular dome models. Conceptually, the elliptical dome model is similar to the circular dome model in that a solution to the scalar wave equation has been obtained through the standard separation of variables technique for boundary conditions specified on the transducer and the mid-surface of the shell-type dome. In the elliptical case, a bit more finesse is required since solutions must be obtained in both cylindrical coordinates (transducer) and elliptical coordinates (dome) and a transformation rule for passing between the two coordinate systems must also be derived. The computed results for the elliptical dome model are more interesting than those for the concentric cylindrical dome because of the lack of symmetry in beam incidence on the dome and the variable dome-transducer spacing. The computed beam pattern structure demonstrates a lack of symmetry for steering angles other than  $0^\circ$  and  $90^\circ$  relative bearing, but the main lobe is not affected appreciably. Although the average side lobe levels for elliptic and circular dome models are about the same, the elliptic dome causes a relatively large side lobe for certain steering angles. Some cavity resonance effects are observed in connection with the computation of transmitted energy; however, the dependence of radiated energy on dome-transducer spacing is not the well-behaved periodic dependence found in models for which the dome and transducer surfaces are uniformly spaced.

### 3.3 RELATED STUDIES

During the course of the above studies several secondary problems were considered from the standpoint of assisting in the isolation of the effects of certain parameters on dome-transducer



interactions. These problems can be classed in three general areas as (1) problems related to the role of dome-transducer geometry in interaction phenomena, (2) problems related to dome construction, and (3) problems related to comparisons of two- and three-dimensional models.

### 3.3.1 Studies of Dome Geometry

The elliptic dome model originally was viewed as the next logical improvement of the concentric, cylindrical dome model. However, the development of relatively straightforward analytical methods for treating a cylindrical transducer and nonconcentric dome led to the possibility of treating an improved model immediately [3]. Consequently, a limited number of numerical results was obtained to determine dome effects on transmitted beams for cases in which the beam axis was not normally incident on the dome surface. The results indicated that for such cases the minor lobe structure was not symmetric about the beam axis; however, the maximum response of the beam pattern was in the steered direction. No beam steering errors resulted from the non-normal incidence of the beam axis on the dome. These results are in qualitative agreement with results subsequently obtained with the elliptic dome model. A brief analysis was conducted for an infinite planar array with a flat dome. The radiated energy of this array was observed to have a periodic dependence on dome-transducer spacing, as was the case with the cylindrical, concentric dome model. In comparison, the radiated energy for the elliptic dome model varies with beam steering direction (along with dome-transducer spacing); however, the dependence is not simple. Finally, a model consisting of a spherical transducer and concentric, shell-type dome was analyzed. Computed beam patterns indicated the effects of the dome for this configuration were similar to those for the cylindrical models: namely, an increase in side lobe level with little effect on the major lobe.



### 3.3.2 Dome Structure

The studies to the beginning of this year's work had assumed the dome behaved as a thin shell. Two brief studies were originated in an effort to generalize this assumption. In the concentric dome model, the thin shell was replaced with a thick shell for which a solution of the linear equations of elasticity were required to specify its response to the acoustic pressure field. (It was necessary to consider boundary conditions on both the inside and outside shell surfaces rather than at the mid-surface only - as with the thin shell). Comparisons based on a limited number of thin and thick shell results indicated that the thin shell theory (a much simpler problem) was adequate for shell thicknesses up to about 0.06 of the transmit wavelength. In addition a concentric dome model which included a number of mass-like inhomogeneities (ribs) was analyzed. Again, only a small number of results have been obtained to date, but these indicate a decrease in source level and a changed lobe structure of the beam pattern as a result of the presence of the ribs. Also of interest was a comparison of the nature of the normal acoustic impedance of the spherical dome and cylindrical dome. It was found that for the parameters used in the study, the normal impedance of the spherical shell was essentially mass-like, as was the case for the cylindrical and planar domes.

### 3.3.3 Comparison of Two- and Three-Dimensional Models

Some modifications to the two-dimensional cylindrical transducer and concentric dome permitted the computation of three-dimensional beam patterns which are of particular interest for tilted beams. The modification entailed replacing the infinitely-long array with a finite-length array. The dome and the baffle in which the array was mounted remained infinitely long. It was found that azimuthal beam patterns computed at  $0^\circ$  tilt with this model were identical to the beam patterns computed with the two-



dimensional model. Further, a simple rule was discovered for relating the azimuthal beam pattern for depressed beams with the azimuthal beam patterns computed with the two-dimensional model. Another interesting comparison was made between the mutual radiation forces existing between transducer elements in the cylindrical model and elements in the spherical model. It was found that for equal frequencies, transducer radii, and element sizes the magnitude and variation of the interaction forces with element separation were very similar for the two configurations.

#### 3.4 TASK II - EXPERIMENTAL PROGRAM

The requirements for the experimental program included the development of instrumentation and measuring techniques suitable for obtaining velocity profiles and beam patterns for a small cylindrical transducer, and the construction of a sound source (transducer) which was tractable from a mathematical standpoint. This latter feature imposed fairly severe constraints on the source; for example, uniform azimuthal and vertical velocity profiles on the transducer surface. The problems associated with instrumentation and measuring techniques were overcome successfully. However, the constraints placed on the transducer have resulted in a great deal of difficulty in developing an acceptable design. As a result, experiments which were to be performed in the first year of studies have not yet been conducted. The problems with an acceptable source are expected to be overcome with a design presently under evaluation, and the experimental program should proceed in a more normal course during the second year of studies.

## DISCLAIMER NOTICE

THIS DOCUMENT IS BEST QUALITY PRACTICABLE. THE COPY FURNISHED TO DTIC CONTAINED A SIGNIFICANT NUMBER OF PAGES WHICH DO NOT REPRODUCE LEGIBLY.

OR ARE  
Blank pgs.  
that have  
Been Removed

**BEST  
AVAILABLE COPY**

## 4. GENERAL METHODS

4.1 INTRODUCTION

This section summarizes studies conducted under Task IA of the past year's program. The objective of Task IA is to develop analytical techniques which are applicable to a larger class of dome-transducer geometries than can be treated by classical methods. The past year's effort under this task was concerned with the applicability of the integral equation formulation of radiation acoustics to dome-transducer problems. During this feasibility study, the basic equations of the integral formulation have been modified to include the capability of treating a dome. Two techniques aimed at increasing the size of dome-transducer geometry which can be treated have been tested for no-dome cases. The procedure followed in applying the integral formulation will be summarized in sufficient detail so that the techniques which have been considered can be discussed. Conclusions, supported by a limited number of numerical results, are presented, and recommendations for future work are made.

The integral equation formulation of acoustics is derived from the wave equation. The integral form relates the acoustic pressure within a fluid to a distribution of pressure sources at the boundaries of the fluid. The strength of these sources is related to the acoustic field variables evaluated at the boundaries, the particular relation depending on which integral formulation is employed. For the two most common formulations, the integral equation has the form [4,5]

$$p(\vec{q}) = \int_S \varphi(\vec{q}|\vec{q}') dS(\vec{q}') - f(\vec{q}) . \quad (1)$$

In Eq. (1)  $\vec{q}$  is the field point, i.e., the position vector at which the pressure  $p$  is to be computed. The source point  $\vec{q}'$  is the position on the surface  $S$  at which the source strength  $\varphi$  is evaluated, and  $S$  is comprised of both the transducer surface and the surface

of the dome. The kernel,  $K(\vec{q}|\vec{q}')$ , is a measure of how strongly the source at  $\vec{q}'$  on  $S$  is felt at  $\vec{q}$ . The inhomogeneity function  $f(\vec{q})$  is completely determined by the boundary conditions, and is assumed to be known for any given problem. Explicit forms for the terms in Eq. (1) are given in Volume II. It should be noted here that the generality of the integral equation formulation is due to the fact that the surface  $S$  in Eq. (1) can have any shape. Thus, the method is applicable, in principle, to any dome-transducer geometry.

The procedure employed in the integral equation approach is as follows: First, in Eq. (1) the field point  $\vec{q}$  is allowed to approach the surface of integration, resulting in an expression for  $p$  on the surface in terms of an integral of  $\varphi$ , an expression involving  $p$ . If  $p$  is then written in terms of  $\varphi$ , an integral equation for  $\varphi$  results. This integral equation is then solved for  $\varphi(\vec{q}')$  on the surface. Finally,  $\varphi(\vec{q}')$  is substituted into Eq. (1) to obtain  $p(q)$  at points in the fluid. The second step, the solution of the integral equation, is the most difficult part of the procedure. For most problems the integral equation cannot be solved analytically, so a numerical solution technique must be used. The use of high-speed computers to obtain a numerical solution to this integral equation is a subject of much recent interest among acousticians [6-11]. The usual method of obtaining a numerical solution to the integral equation is discussed in the references cited above. The procedure is initiated by subdividing the radiating surface into a finite number of patches which are small enough that the variation in the unknown source strength over an individual patch can be assumed to be negligible. On the basis of the assumption, the integral equation reduces to a system of algebraic equations for the unknown source strengths. The number of these equations is equal to the number of patches into which the surface has been divided. Moreover, the above assumption implies that there is one unknown associated with each patch: namely, the source strength on the patch; therefore, the number of algebraic equations exactly



equals the number of unknown quantities. Once the system of equations has been formulated for the particular geometry of interest, existing computer algorithms can be used to obtain a numerical solution for the source strengths. This numerical approach has the desirable feature of being extremely general in the types of geometrical configurations to which it can be applied. Moreover, the assumptions made in obtaining the approximate equations are not restrictive in the sense that they preclude analysis of a physical problem; rather they impose a requirement on how the radiator is to be subdivided in order for the results of the analysis to be physically meaningful.

On the other hand, the requirement that the surface of the radiator be subdivided finely enough that variations in the source strength over individual surface elements are negligible means that the total number,  $N$ , of algebraic equations which must be solved to analyze a realistic-sized radiator becomes quite large. For example, Chen [6] used subdivisions corresponding to  $N = 80$  and  $N = 320$  to analyze a spherical radiator having a circumference of two wavelengths. To analyze a spherical radiator having a circumference of 36 wavelengths, using surface elements having areas the same as those used by Chen in the above example, would require values of  $N$  equal to 25,920 and 103,680, respectively. Even with the largest computer available today, the simultaneous solution of systems of equations of these orders of magnitude would be impracticable. From the above example it seems evident that the application of the numerical scheme described above to arbitrary radiators is possible from a practical point of view only when a characteristic length of the radiator is of the order of a few wavelengths. Moreover, the size of a dome-transducer system which can be analyzed is correspondingly reduced because it is necessary to subdivide the surfaces on both the transducer and the dome.

## 4.2 OUTLINE OF PRESENT TECHNIQUE

In view of the large number of algebraic equations which arise from applying Eq. (1) to a realistic-sized radiator it is clear that, to be able to apply this technique to a dome-transducer system, it is necessary to look for ways of reducing the number of equations required to analyze a given sized radiator. Two devices which allow a reduction of the number of simultaneous equations that must be solved have been considered.

The first is based on the following observations. The reason such a large number of equations are required is that the kernel,  $K$  in Eq. (1), is two-dimensional, i.e., a given point on the surface is determined by specifying two coordinates. It is shown in Volume II that, for certain special shapes, it is possible to replace the two-dimensional kernel by a family of one-dimensional kernels, and, for geometrical configurations which belong to this special class, a solution of Eq. (1) is equivalent to solving a set of one-dimensional integral equations. There are two classes of geometrical shapes for which the above decomposition is possible, and these two classes contain a large variety of configurations of interest in acoustic radiation studies. Included in these two classes are (a) cylindrical configurations of arbitrary cross section having infinite height (all two-dimensional configurations are a special case of this class<sup>+</sup>), and (b) axi-symmetric configurations; i.e., those geometrical shapes which are generated by revolving one or more plane curves about a common axis\*. Problems of each type are presented in the next section.

---

<sup>+</sup>An application of the integral formulation to radiators of this class is given in Banaugh and Goldsmith [9].

\*An application of the integral formulation to radiators of this class is given in Chertock [8].

The decomposition of the kernel,  $K(\vec{q}|\vec{q}')$  gives rise to a set of one-dimensional integral equations which can be written in the form

$$\varphi_a(u) = \int \varphi_a(u') K_a(u, u') du' - f_a(u) . \quad (2)$$

The quantities appearing in Eq. (2) have the same interpretations as discussed previously. The subscript,  $a$ , appearing on all quantities in Eq. (2), distinguishes the different equations involved in the set. The integral in Eq. (2) is a definite integral rather than a surface integral as in Eq. (1). The interpretation of the variable,  $u$ , depends on the class of problems one is considering. The limits of integration have been left unspecified since they depend on the parametric representation of the geometry.

After a solution to Eq. (2) has been obtained for each value of "a" for which the inhomogeneous term,  $f_a(u)$ , is non-zero, the final solution for the source distribution is obtained by summing the contributions from all the  $\varphi_a$  involved in the given problem<sup>#</sup>.

The second device which allows a reduction of the number of simultaneous equations for a given radiator and frequency is based on the following considerations: One may consider the process of approximating the integral equation by a set of algebraic equations as being equivalent to constructing a table of values to define the unknown function in the entire interval of integration. The number of equations corresponds to the number of entries in the table. The assumption described in the preceding section implies that the values of the function must be tabulated closely enough that no interpolation is necessary to determine the function at values of the independent variable

---

<sup>#</sup>The sum for the infinite cylinder case is actually a Fourier Integral since the subscript "a" takes on continuous values. The sum for the axi-symmetric case is an ordinary Fourier series.

which are between the tabulated entries. Fewer entries would be required if a physically meaningful interpolation process were used to evaluate the tabulated function at points other than the table entries. The interpolation scheme used here is based on the fact that the function to be tabulated varies smoothly throughout the range of integration.

The interpolating procedure can be implemented by specifying an  $n$ th order polynomial (interpolating function) to pass through  $(n+1)$  entries in the table. An interpolating function which satisfies the physical smoothness constraint is then uniquely determined. Once a set of interpolating functions is determined for the entire range of integration the tabulated function can be evaluated at any point within that range.

#### 4.3 NUMERICAL RESULTS

Computational algorithms which incorporate the methods and restrictions outlined above have been devised to calculate source distributions and farfield directivity patterns for several radiators in the absence of a dome. These algorithms were designed primarily to determine whether the numerical approach outlined could in fact be used to analyze a radiator of realistic size with a reasonable amount of computational effort, and to determine some guidelines concerning the relationship between the boundary conditions imposed on the radiator and the manner in which the radiator must be subdivided to obtain meaningful results. Consequently all of the results which are presented are for geometrical shapes for which predictions can be made readily by eigenfunction expansions.

Figure 1 shows the farfield patterns obtained by two methods, eigenfunction expansion and numerical solution, for a plane-wave phased circular radiator with a circumference of 18 wavelengths ( $ka = 18$ , where  $a$  is cylinder radius) having four active staves  $7.5^\circ$  wide. The solid line is the result

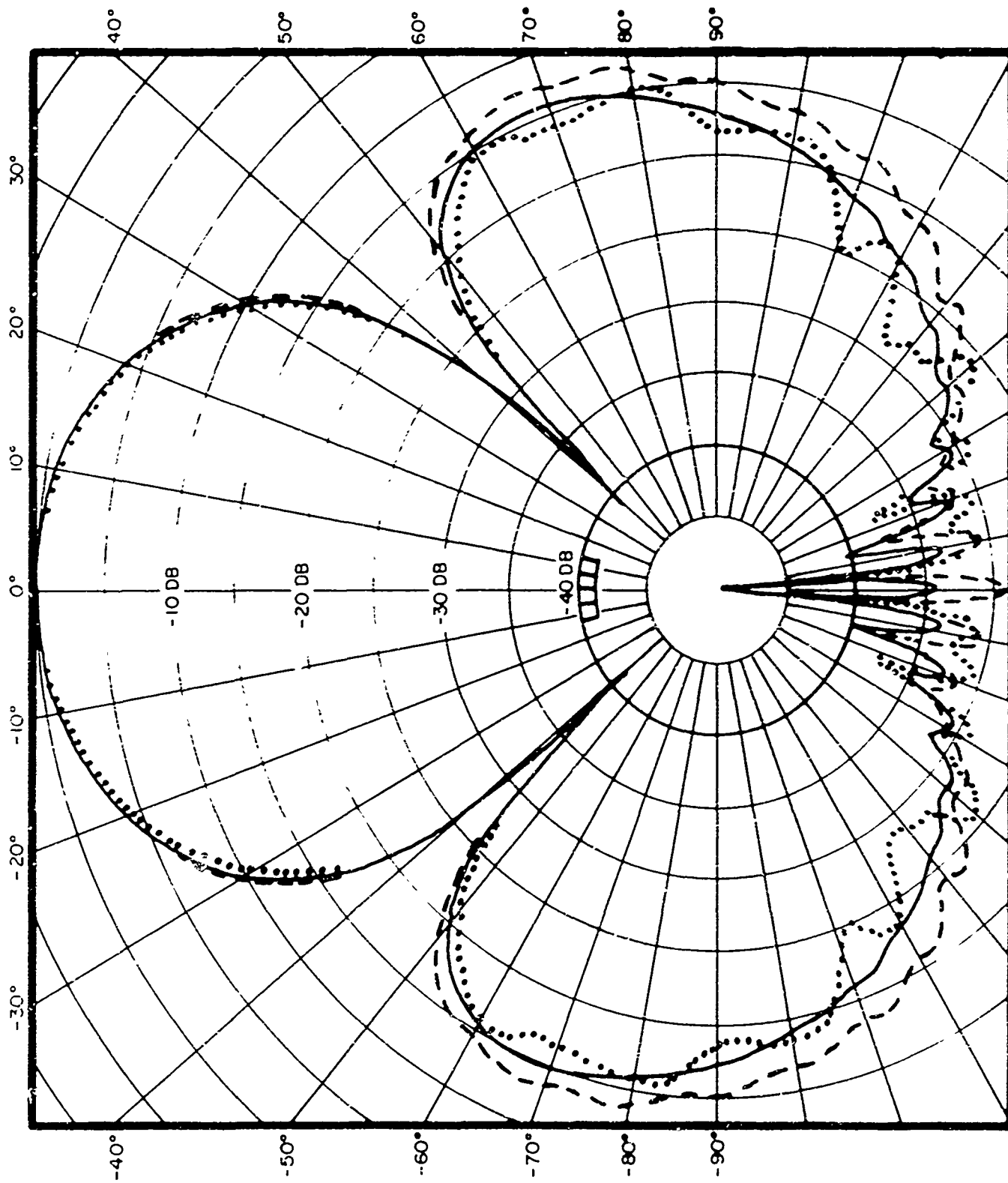
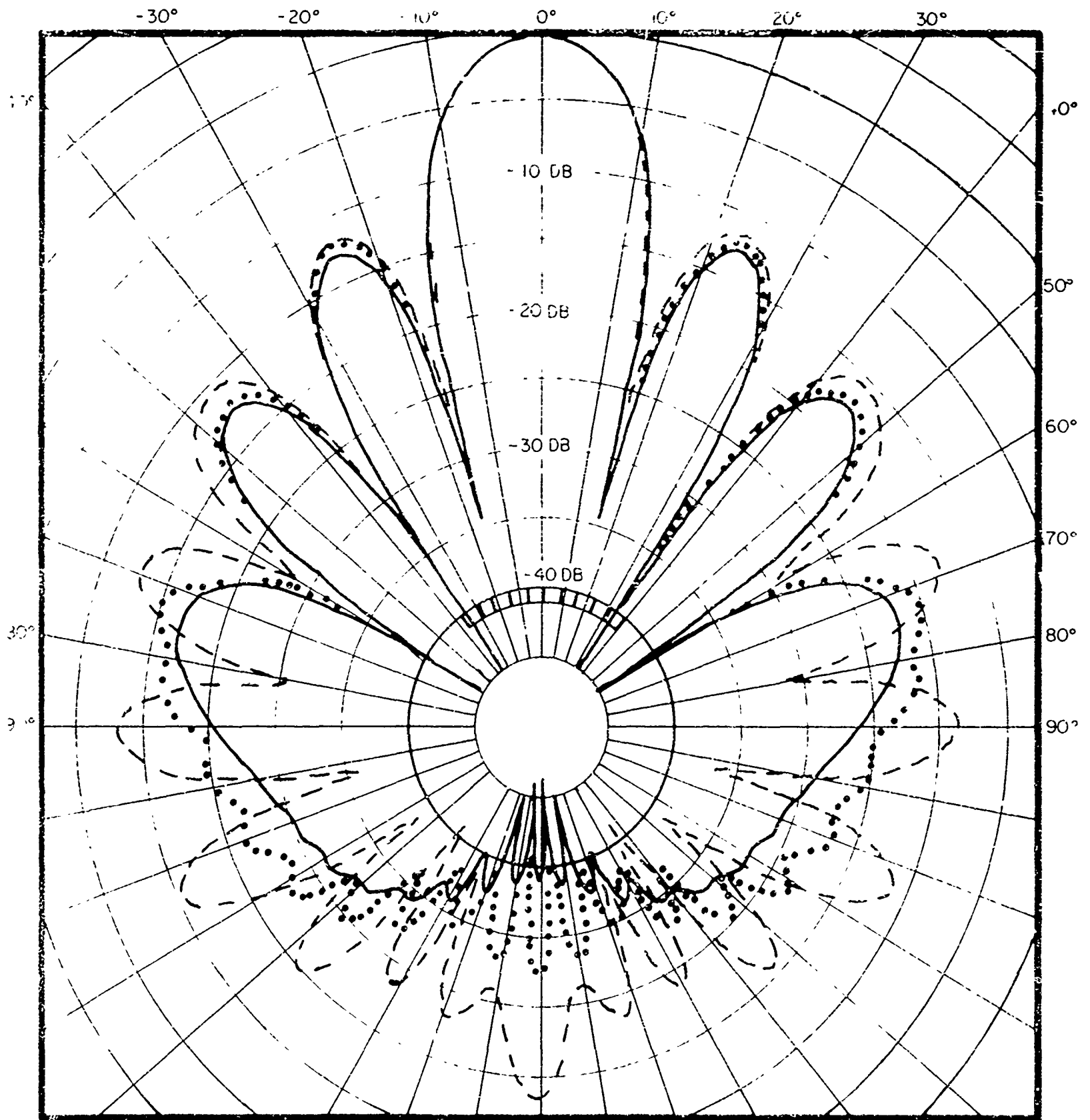


FIG.1 - FARFIELD BEAM PATTERN FOR A CIRCULAR TRANSDUCER



obtained from an eigenfunction expansion. The dashed line is the numerical solution obtained using a parabolic interpolation function and an equidistant mesh point spacing of  $3/8$  wavelength. This results in an algebraic system of 48 equations with complex coefficients. The dotted line is the numerical solution obtained by adding mesh points at the edges of the outer staves in addition to the 48 equidistant points, and defining the velocity at these points as the average of left and right values. The agreement between the latter numerical solution and the eigenfunction solution is seen to be better in the forward portion, but it has been found that, within the limits of these numerical experiments, the quality of predicted patterns from numerical results depends more strongly on the total number of mesh points rather than their specific location.

Figure 2 shows results for the same transducer with a larger active portion. The solid line is the eigenfunction expansion; the dotted line is the result of using a parabolic interpolating function with  $3/8$  wavelength spacing as explained for Fig. 1. The dashed line is the numerical result from using  $3/8$  wavelength spacing and a constant interpolating function (i.e., a step function). This figure shows the superiority of a higher order interpolating function over that of a lower order function. Also, a comparison between the eigenfunction solutions and equivalent numerical solutions (the dashed line of Fig. 1 and the dotted line of Fig. 2) shows that the pattern of a radiator is easier to predict when the active portion is large than when it is small. This is a result of the numerical approximations used to solve Eq. (2). It is shown in Volume II that the accuracy of an approximate solution is better for a slowly varying velocity distribution, as is the case for the results of Fig. 2.



ka = 18  
75° ACTIVE (10 STAVES)

————— - EIGENFUNCTION EXPANSION  
 ..... - 3/8 λ SPACING, PARABOLIC INTERPOLATING FUNCTION  
 - - - - - 3/8 λ SPACING, CONSTANT INTERPOLATING FUNCTION

FIG. 2 - FARFIELD BEAM PATTERN FOR A CIRCULAR TRANSDUCER

Figure 3 corresponds to a cylindrical radiator having a size and a velocity distribution representative of the AN/SQS-26; i.e., it has a circumference of 36 wavelengths ( $ka = 36$ ) with a plane-wave phased velocity distribution resulting from 24 staves, each staff being  $5^\circ$  wide. Again the solid line is the eigenfunction expansion. The dotted line corresponds to a numerical solution using a parabolic interpolating function and a mesh point spacing of  $1/4$  wavelength, while the dashed line results from a constant interpolating function and  $1/4$  wavelength mesh point spacing. This radiator represents the largest body to which the present technique has been applied and was obtained by solving a system of 72 equations<sup>+</sup>.

Figures 4 and 5 show the results of applying this technique to an array of 16 quarter-wavelength staves centered on an elliptical baffle whose major to minor axis ratio is 10. The dashed line shows numerical results obtained with a parabolic interpolating function using 60 mesh points which are spaced equidistantly along the parametric variable  $u$ , where

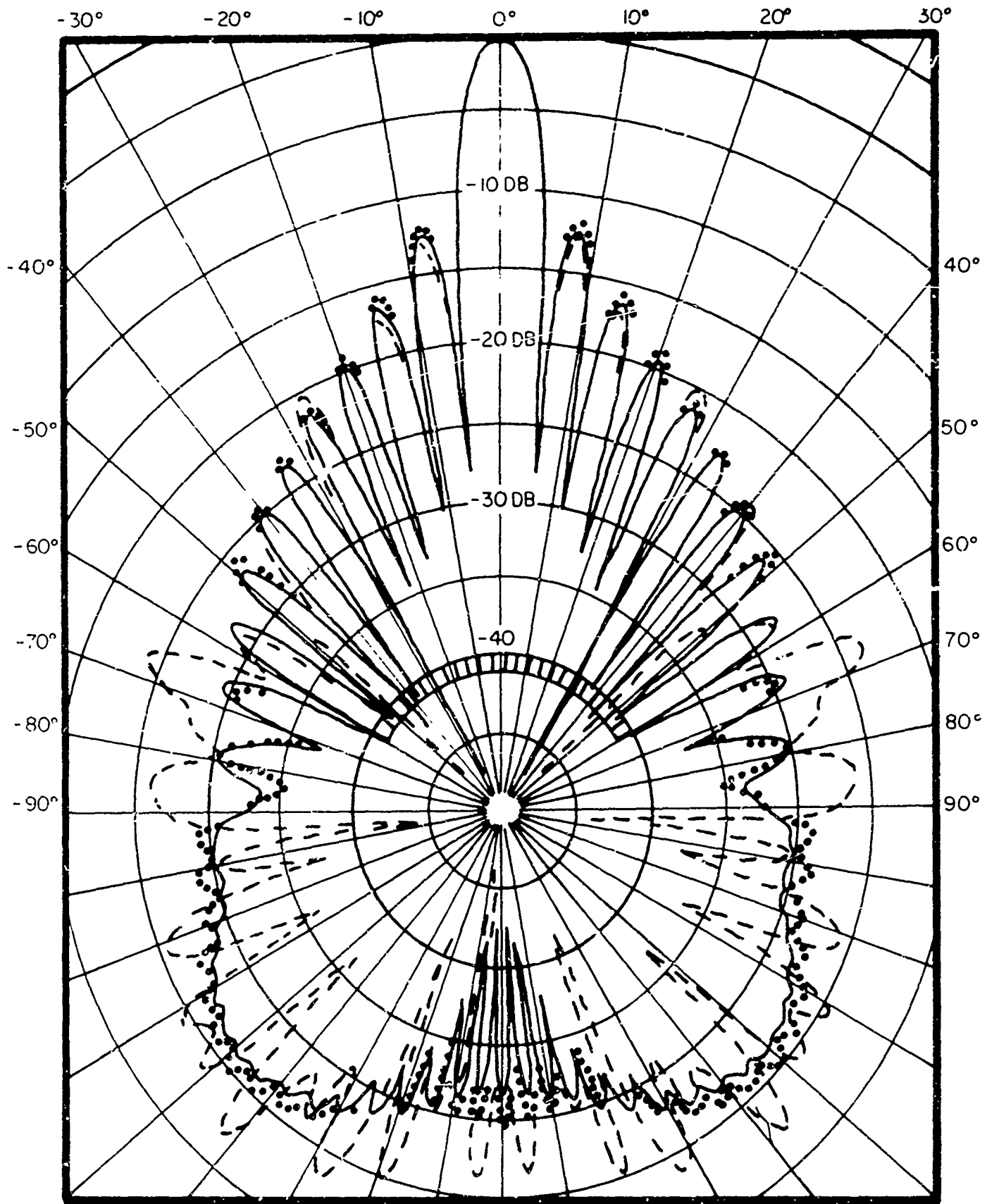
$$x = a \cos u, \text{ and}$$

$$y = b \sin u,$$

denote points on the elliptical circumference. The solid line represents an eigenfunction expansion solution [12] for a planar strip baffle the same width as the elliptical baffle. This width corresponds to 4.5 wavelengths. Figure 4 is for the array steered to broadside and Fig. 5 corresponds to endfire steering. Since the present computer program is not set up to handle a strip, the thin ellipse was used. The deviation, however, between the results for the endfire case seems to be in the direction one would expect on the basis of the different

---

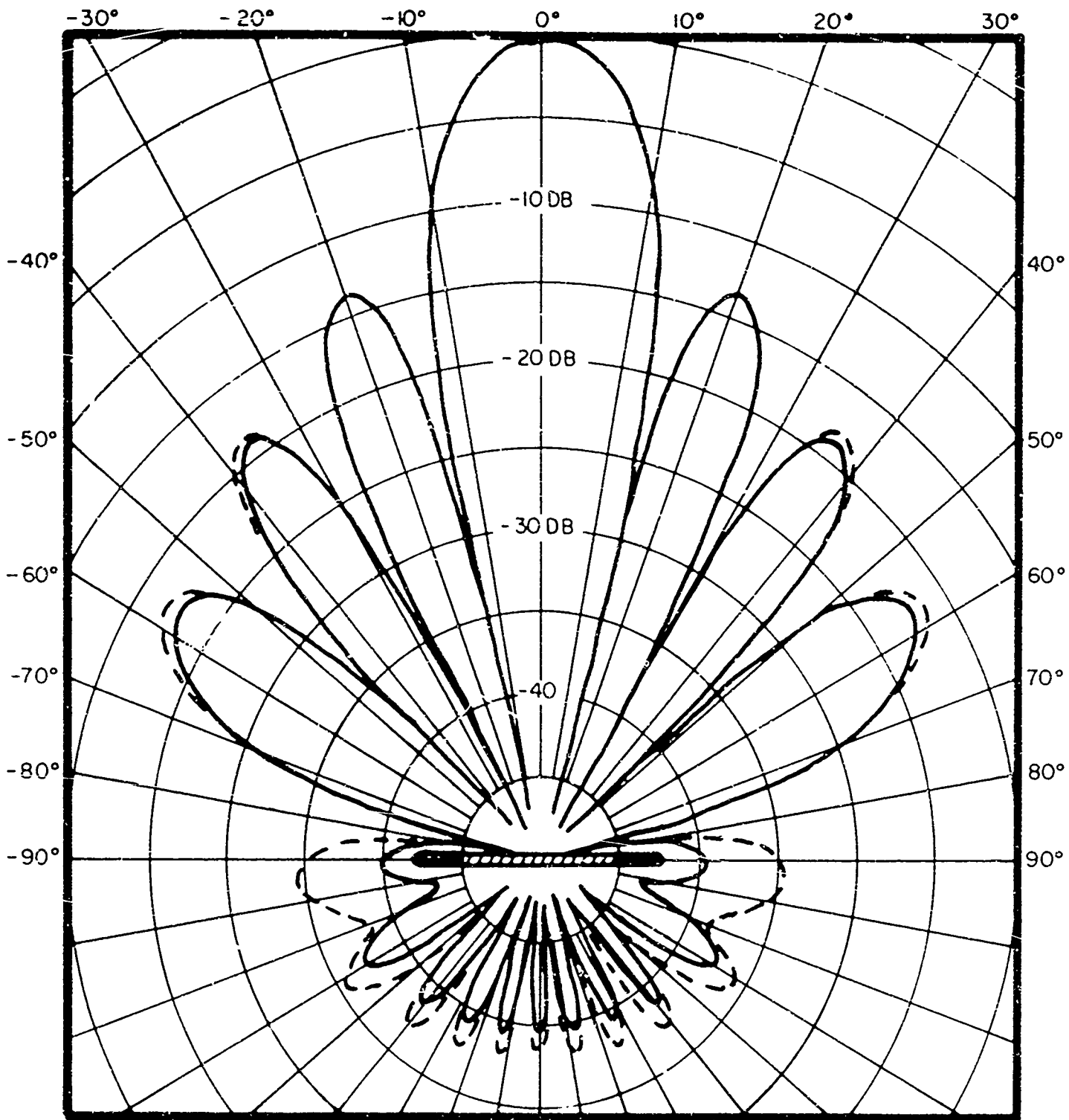
<sup>+</sup>The radiator has a symmetry plane which allows the number of required mesh points to be distributed over only half the radiator.



$ka = 36$   
 120° ACTIVE (24 STAVES)

- EIGEN FUNCTION EXPANSION
- ..... 1/4  $\lambda$  SPACING; PARABOLIC INTERPOLATING FUNCTION
- - - - - 1/4  $\lambda$  SPACING, CONSTANT INTERPOLATING FUNCTION

FIG. 3 - FARFIELD BEAM PATTERN FOR A CIRCULAR TRANSDUCER



$ka = 14.4$   
 $kb = 1.44$

— PLANAR BAFFLE EIGENFUNCTION SOLUTION

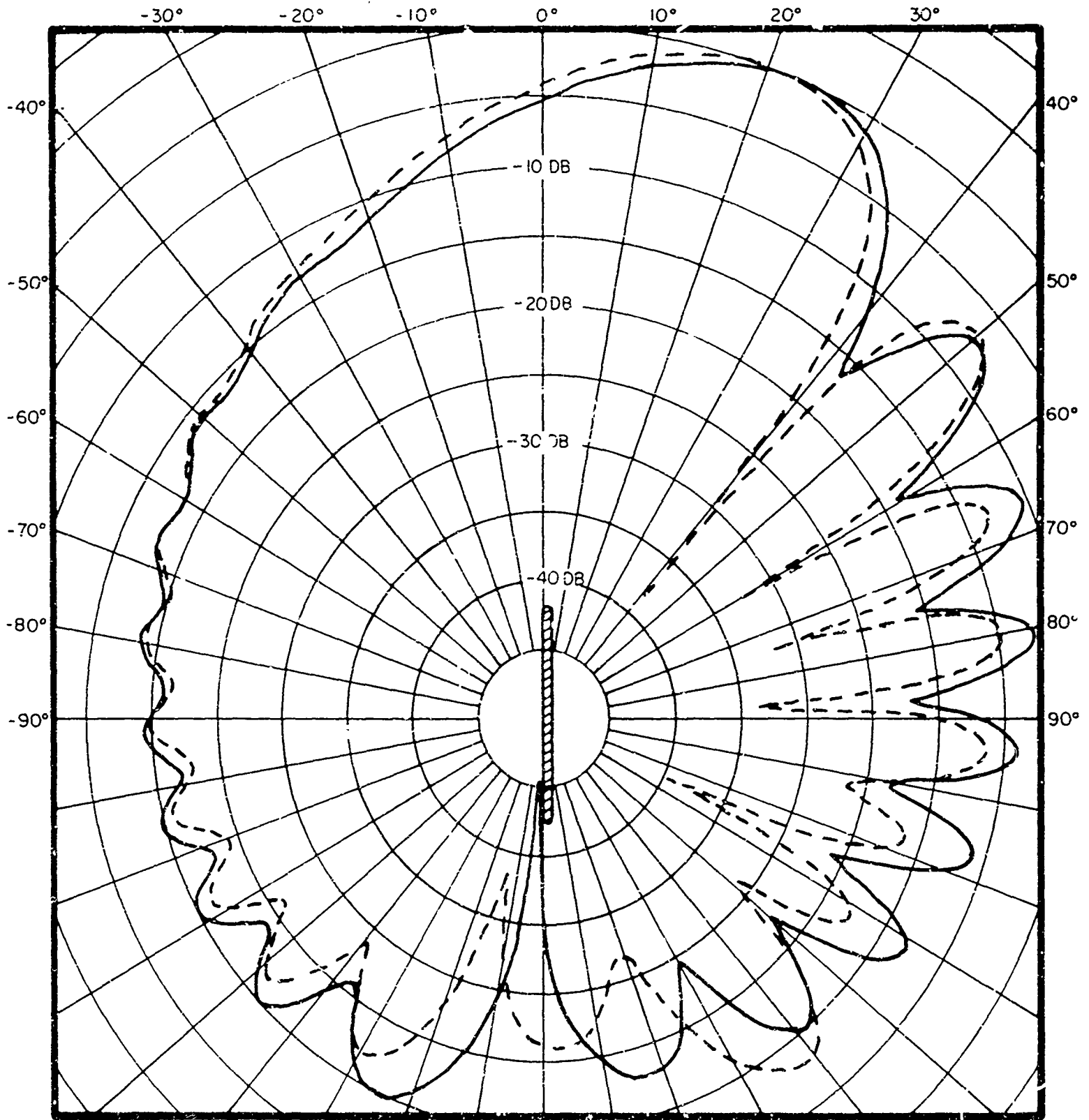
- - - ELLIPTICAL BAFFLE NUMERICAL SOLUTION

PARABOLIC INTERPOLATING FUNCTION

MESH POINTS ·  $X_i = a \cos t_i$ ,  $Y_i = b \cos t_i$

$t_{i+1} - t_i = \pi/60$

FIG. 4 - BROADSIDE BEAM PATTERN FOR AN ELLIPTICAL BAFFLE  
16 QUARTER WAVE-LENGTH STAVES ACTIVE



ka = 14.4  
kb = 1.44

— — — — — PLANAR BAFFLE EIGENFUNCTION SOLUTION  
 - - - - - ELLIPTICAL BAFFLE NUMERICAL SOLUTION  
 PARABOLIC INTERPOLATING FUNCTION  
 MESH POINTS  $X_1 = a \cos t_1, Y_1 = b \sin t_1, t_{i+1} - t_i = \pi/60$

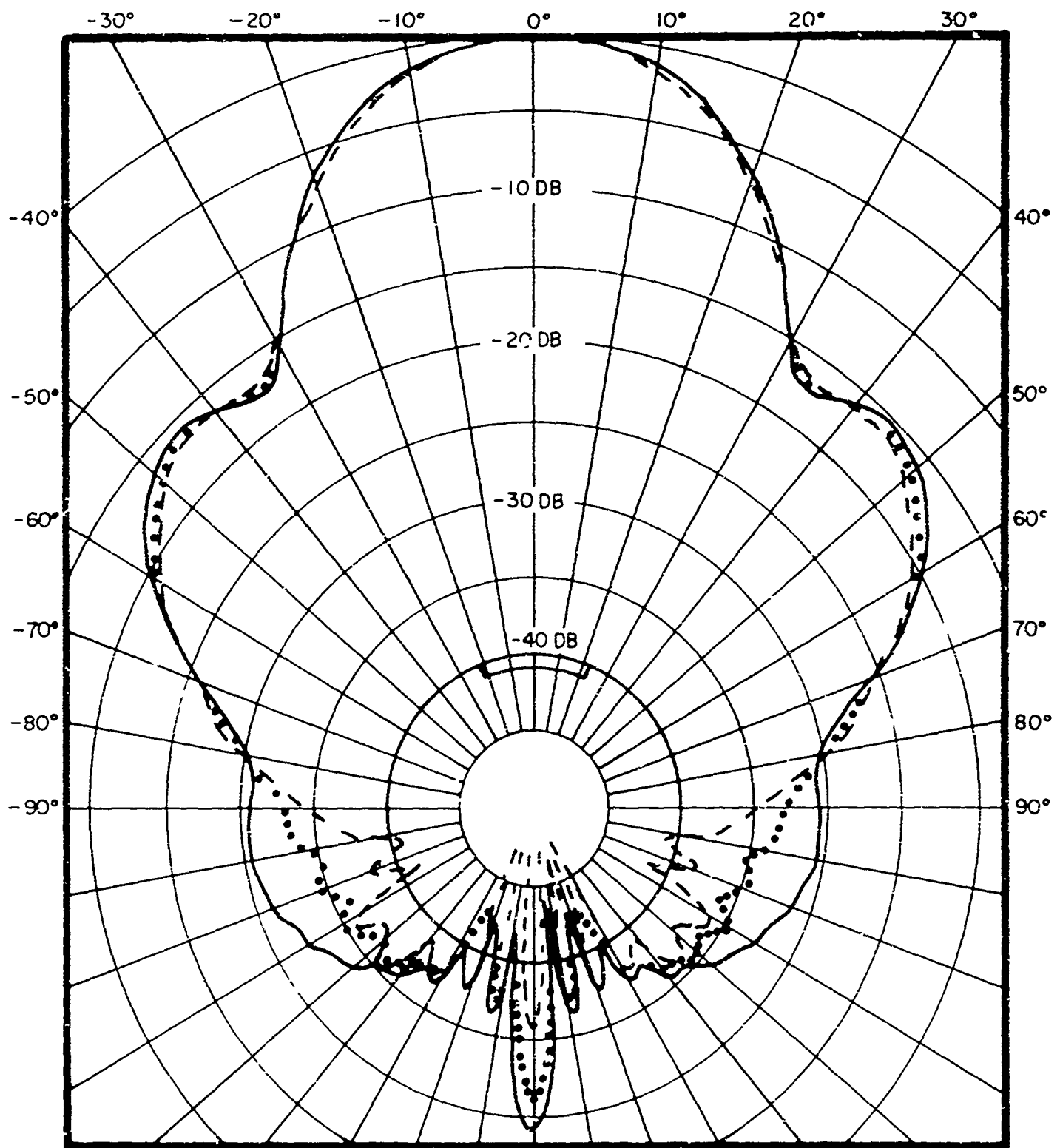
FIG. 5 — ENDFIRE BEAM PATTERN FOR AN ELLIPTICAL RADIATOR  
 16 QUARTER WAVE-LENGTH STAVES ACTIVE

geometry. For example, one would expect the ellipse to be more efficient in steering a beam to endfire because of the slight curvature of the baffle, and this is indicated by the results.

Figures 1-5 have shown typical results from application of the numerical technique to two-dimensional radiators. Figure 6 shows the result of applying the technique to a three-dimensional spherical transducer with a radiating spherical cap. The circumference of a great circle of the sphere is 18 wavelengths, and the angular half-width of the cap is  $22.5^\circ$ . The solid line shows the directivity pattern from an eigenfunction expansion discussed elsewhere in this report. The dashed line is the result of a numerical solution using 25 equidistant mesh points, while the dotted line results from using 33 equidistant mesh points. Both numerical solutions used a parabolic interpolation scheme. The numerical solutions are essentially the same for the forward portion of the pattern, but the solution with 33 points shows closer agreement with analytical results for the backside.

#### 4.4 SUMMARY

In the development of general analytical methods the emphasis, up to this point, has been centered on implementing the integral formulation as a means of predicting radiation patterns. The advantage of this formulation over classical methods of analysis results from the fact that it applies, in principle, to any dome-transducer geometry. The integral formulation relies on the solution of a system of simultaneous algebraic equations. The number of these equations increases with the size of the radiating system so that computational ability places a restriction on the size of the radiating system which can be analyzed by this method.



$ka = 18$   
 $45^\circ$  ACTIVE (1 CAP)

- EIGENFUNCTION EXPANSION
- .....  $9/32 \lambda$  SPACING, PARABOLIC INTERPOLATING FUNCTION
- - -  $3/8 \lambda$  SPACING, PARABOLIC INTERPOLATING FUNCTION

FIG. 6 - FARFIELD BEAM PATTERN FOR A SPHERICAL TRANSDUCER



By specializing the formulation to cylindrical and axi-symmetric configurations, and by using higher order interpolating functions, the size capability of the integral formulation can be increased. An application of these ideas to the analysis of several simple radiators shows good agreement with directivity patterns obtained by methods discussed elsewhere in this report.

The primary conclusion evident from the results presented above is that a numerical solution to the integral formulation is a feasible approach to the problem of predicting directivity patterns for radiators of realistic size. Moreover, within the framework of the methods summarized in the preceding sections and described more fully in Volume II, the method is also practical in the sense that it allows an analysis of realistic-sized radiators by means of a system of equations which is not unduly large by present-day computer standards. This fact is of utmost importance for a practical analysis of a coupled dome-transducer system since the introduction of a dome increases the number of equations which must be solved simultaneously.

## 5. ELLIPTIC DOME

### 5.1 INTRODUCTION

The elliptic dome, circular transducer model provides a significant upgrading of dome-transducer models with respect to geometry, since the plan view geometry is considerably more realistic than the earlier, circular dome models. Only a limited number of results have been obtained to date. However, a complete study of this model should permit the formulation of design guidelines concerning the effects of non-constant dome-transducer spacing.

The geometry of the elliptic dome and circular transducer is shown in Fig. 7. The problem is two-dimensional; all physical quantities are independent of the axial coordinate. To simplify the analysis, the dome is assumed to behave as a mass-like impedance discontinuity. This assumption is supported by the results of studies with the circular dome. The analysis is further simplified by allowing the surface mass density (product of dome thickness and mass density) to vary slightly with position. This surface density variation is indicated as a variation in thickness in Fig. 7. The pressure field in the fluid, interior and exterior to the dome, obeys the scalar wave equation. At any point at the transducer surface the normal component of the fluid particle velocity is equal to the velocity of the transducer element at that point. For the portion of the study described herein, the transducer elements are phased to a plane and have a uniform amplitude distribution. By use of the mathematical techniques outlined below and described in detail in Volume II, the farfield beam pattern can be computed for various dome eccentricities and array steering angles.

The general solutions for the pressure fields in the neighborhood of circular and elliptic boundaries are well-known infinite series of eigenfunctions. Each term in the series is

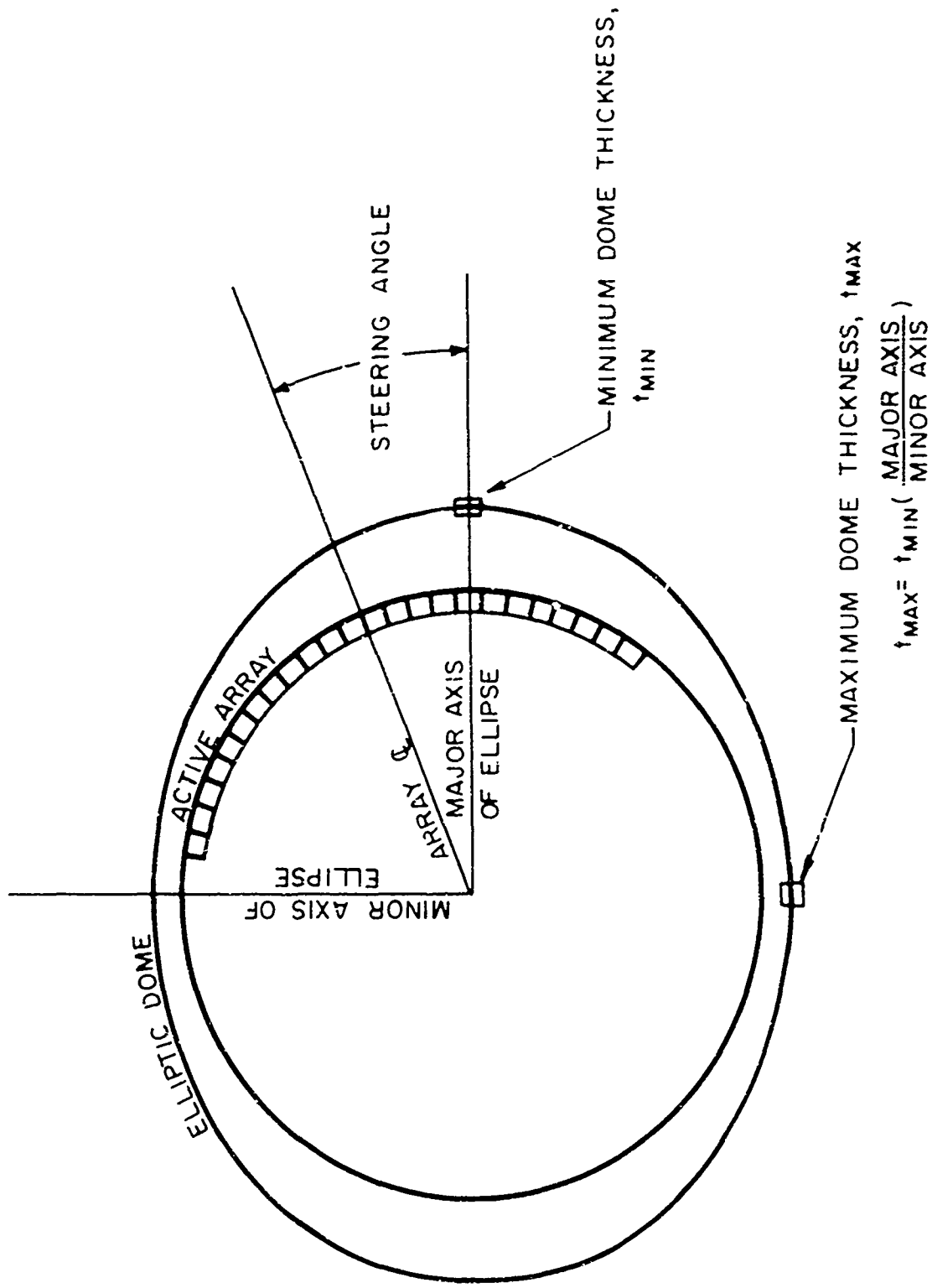


FIG. 7 - GEOMETRY OF ELLIPTIC DOME AND CIRCULAR TRANSDUCER

a product of an arbitrary constant and known functions of the independent radial, angular, and time variables. The pressure field between the transducer and the dome can be expressed in terms of either the elliptic geometry solution or the circular geometry solution. By requiring the two representations of the pressure field to match at all points between the dome and transducer, the constants in the solutions can be evaluated, and thus the pressure field can be determined.

## 5.2 NUMERICAL RESULTS

The results obtained to date are for the dome-transducer geometry shown to rough scale in Fig. 7. The cylindrical array has a radius of 5.6 wavelengths ( $ka = 35.2$ , "a" being cylinder radius) and has 24 active half-wavelength staves. The staves are phased to a plane and are given uniform velocity amplitudes. The dome has semi-major and semi-minor axes of 7.6 wavelengths and 6.4 wavelengths, respectively. The dome surface density varies from  $1.35 \text{ gm/cm}^2$  at  $0.0^\circ$  to  $1.59 \text{ gm/cm}^2$  at  $90.0^\circ$ . Were the dome composed of rubber of specific gravity 1.7, the thickness would vary from 3.68 cm to 4.35 cm (1.45 in. to 1.71 in.). For a steel dome the thickness variation would be from 0.80 cm to 0.94 cm (0.31 in. to 0.37 in.). Beam patterns have been computed for steering angles of  $0.0^\circ$ ,  $11.0^\circ$ ,  $22.5^\circ$ ,  $34.0^\circ$ ,  $45.0^\circ$ ,  $56.0^\circ$ ,  $67.5^\circ$ ,  $79.0^\circ$ , and  $90.0^\circ$ . These are shown in Figs. 8 to 16. Although the model does not permit the computation of absolute source level, it is possible to evaluate the peak intensity in dB relative to the intensity at  $0.0^\circ$  steering. This quantity is plotted as a function of steering angle in Fig. 17. Finally, the beam patterns for two concentric circular domes were computed for comparison with those for the elliptic dome. The beam pattern for a circular dome of radius 7.6 wavelength and surface density  $1.35 \text{ gm/cm}^2$  is shown in dashed lines in Fig. 8 for comparison with the elliptic dome beam pattern with  $0.0^\circ$  steering. Figure 16 compares the beam pattern for a

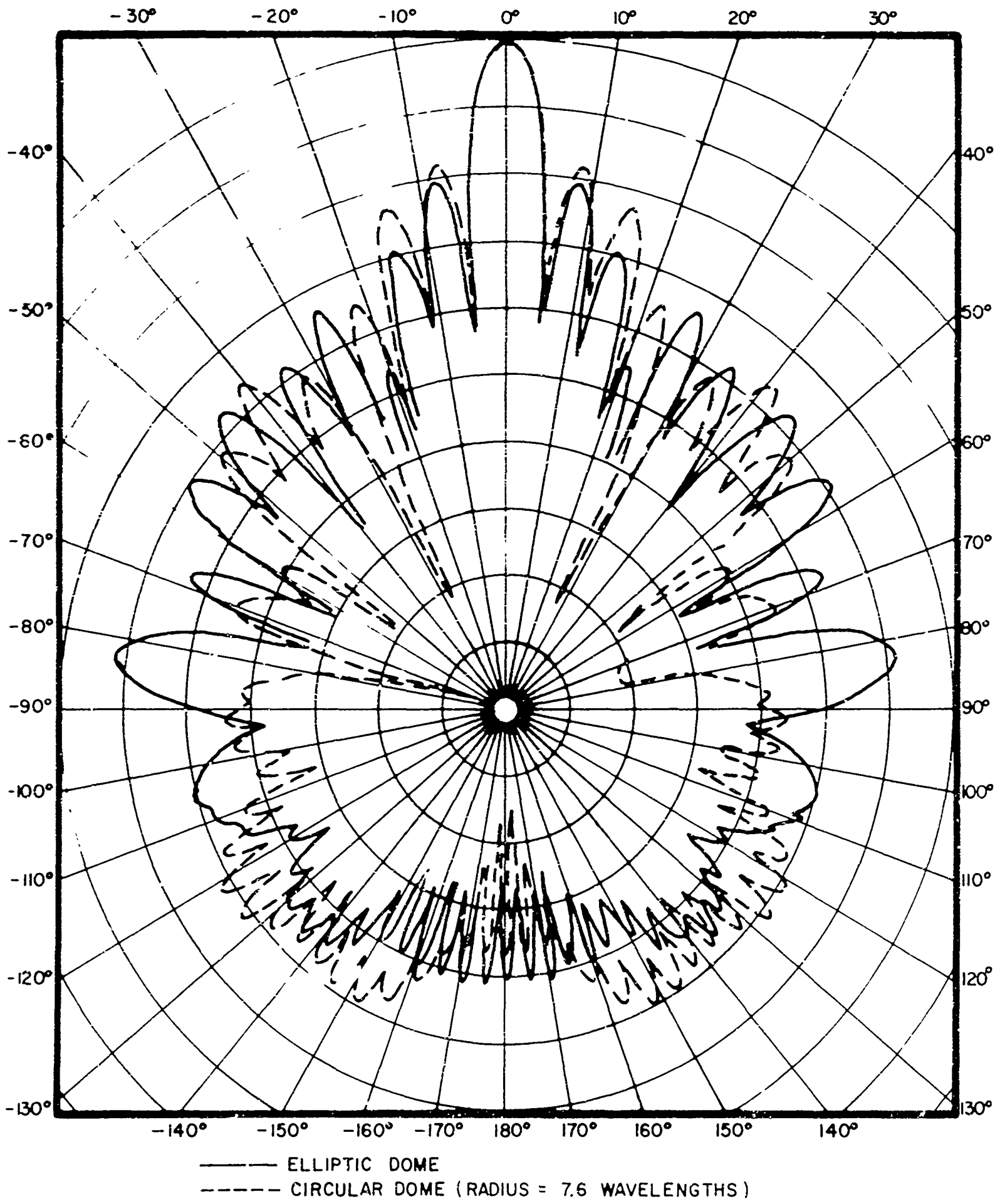


FIG. 8 - BEAM PATTERN FOR ELLIPTIC DOME - CIRCULAR TRANSDUCER, 0.0° STEERING

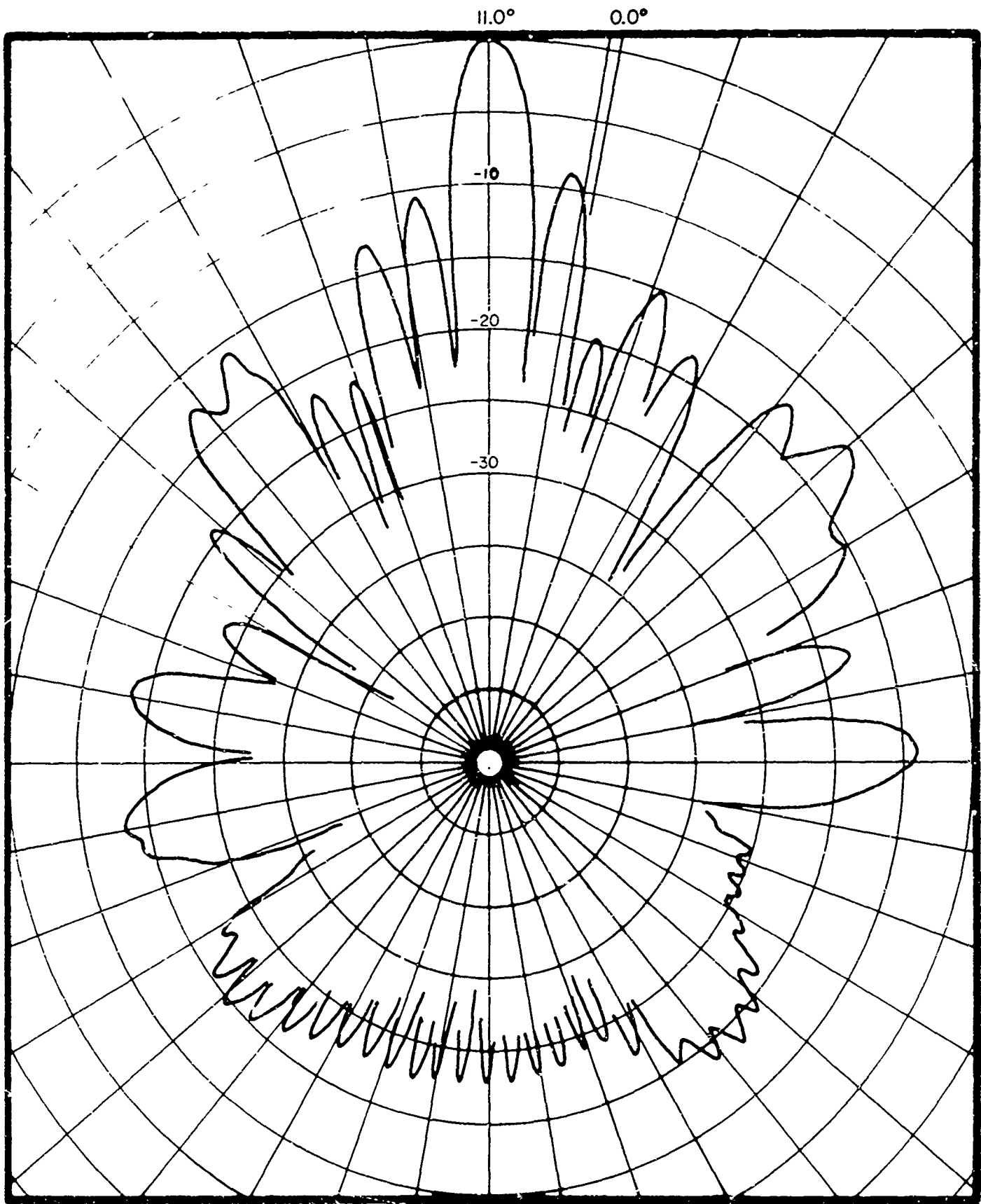


FIG. 9 - BEAM PATTERN FOR ELLIPTIC DOME - CIRCULAR  
TRANSDUCER, 11.0° STEERING

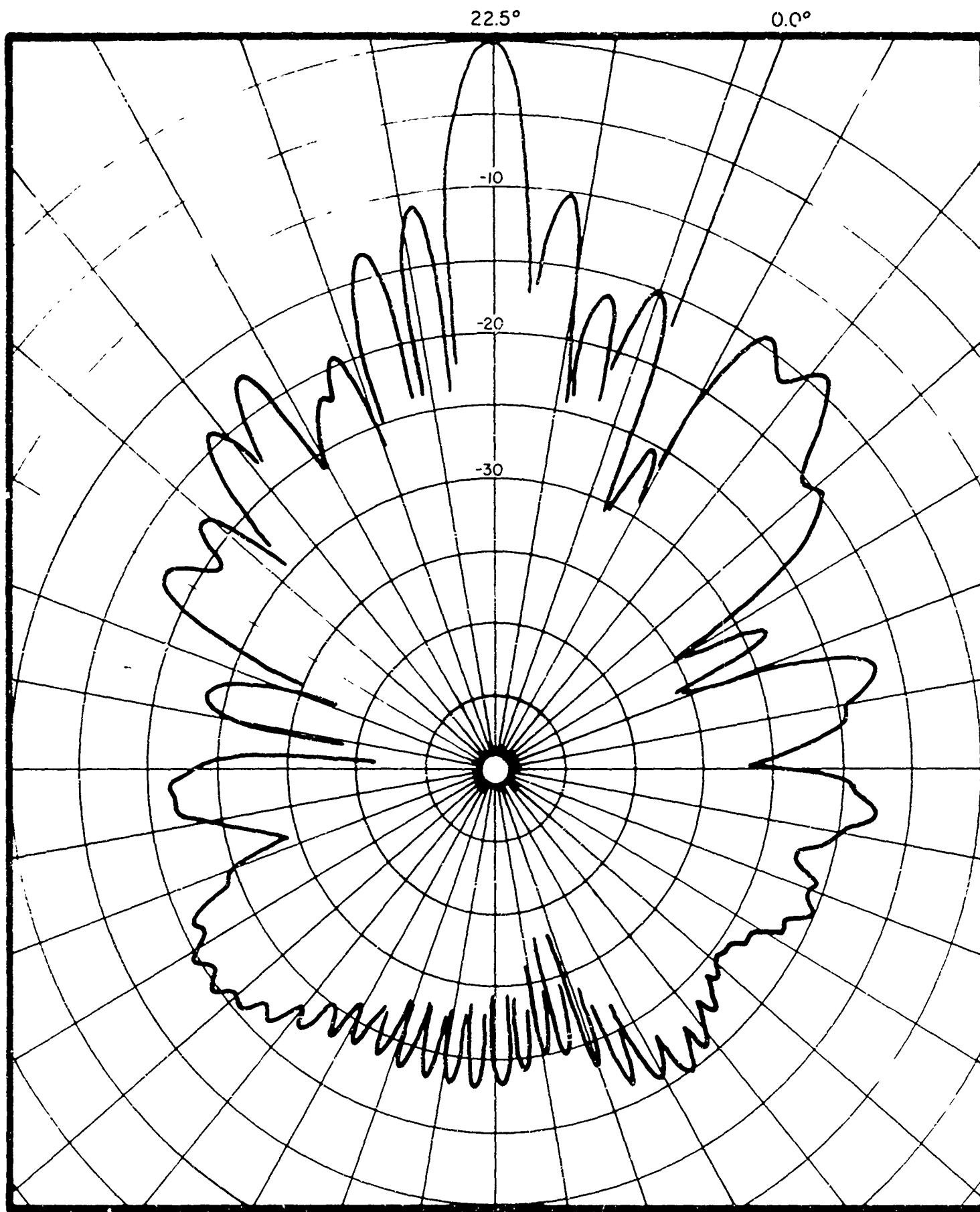


FIG. 10 - BEAM PATTERN FOR ELLIPTIC DOME - CIRCULAR TRANSDUCER, 22.5° STEERING

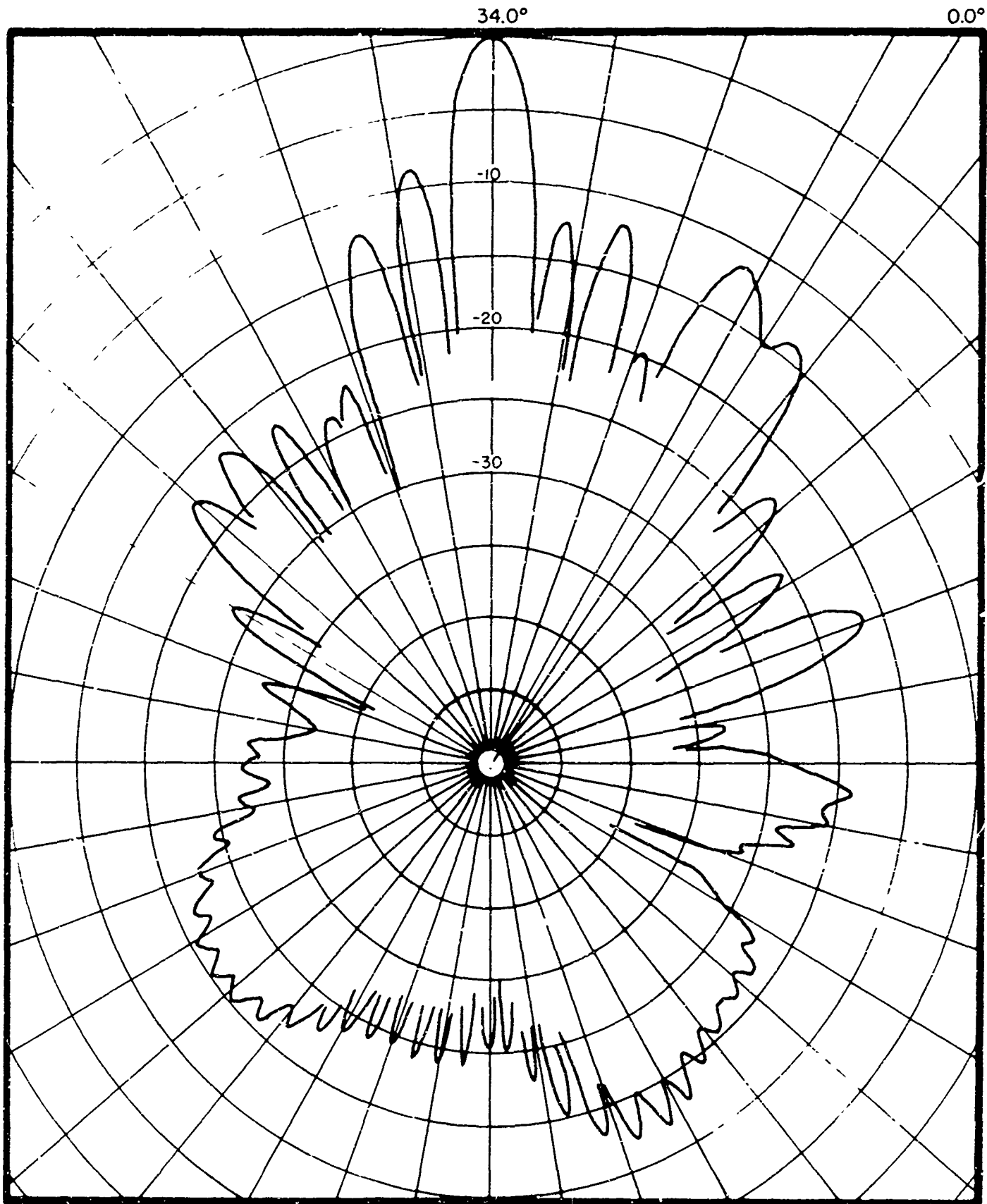


FIG. II - BEAM PATTERN FOR ELLIPTIC DOME - CIRCULAR  
 TRANSDUCER, 34.0° STEERING

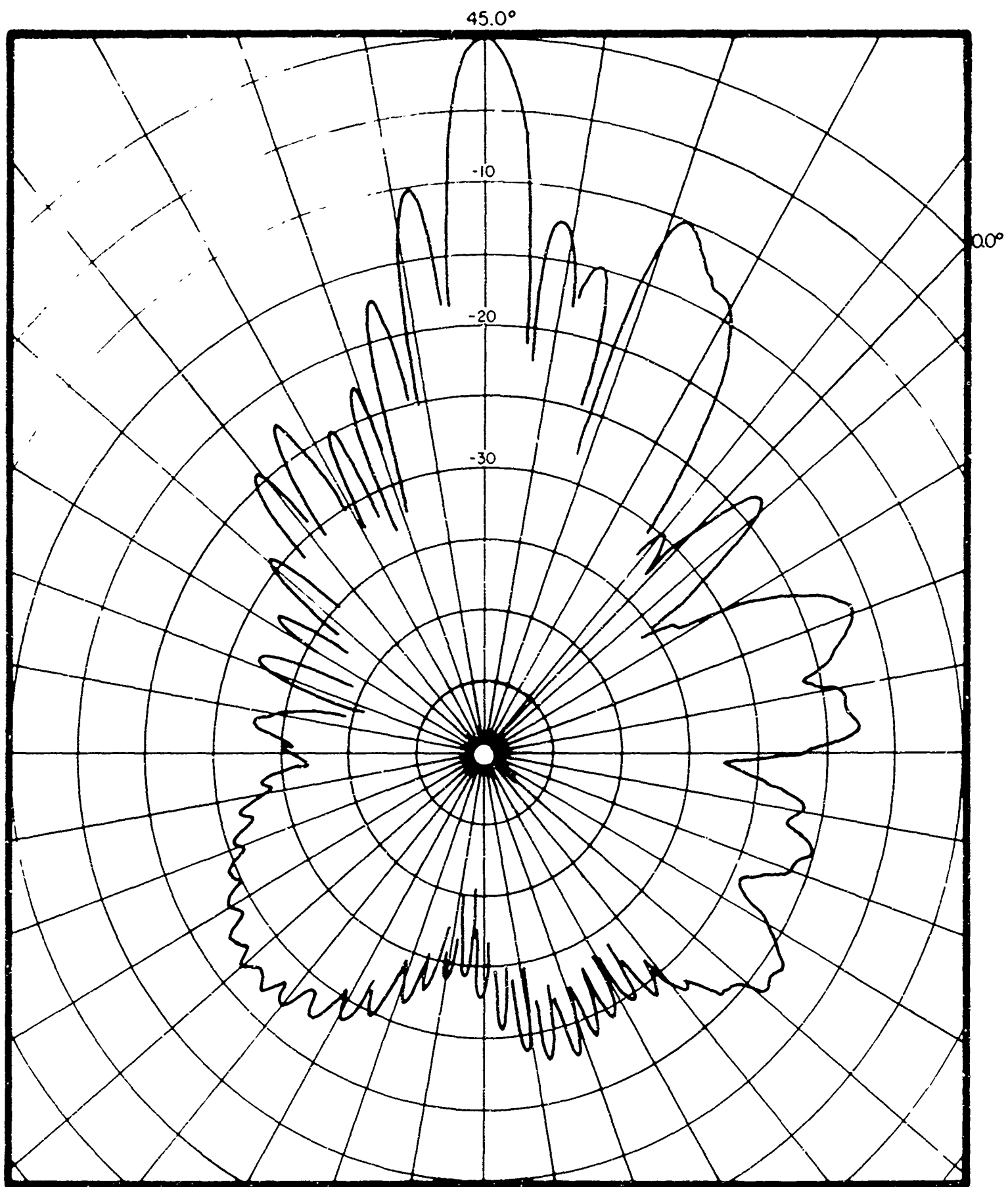


FIG. 12 - BEAM PATTERN FOR ELLIPTIC DOME - CIRCULAR  
TRANSDUCER, 45.0° STEERING

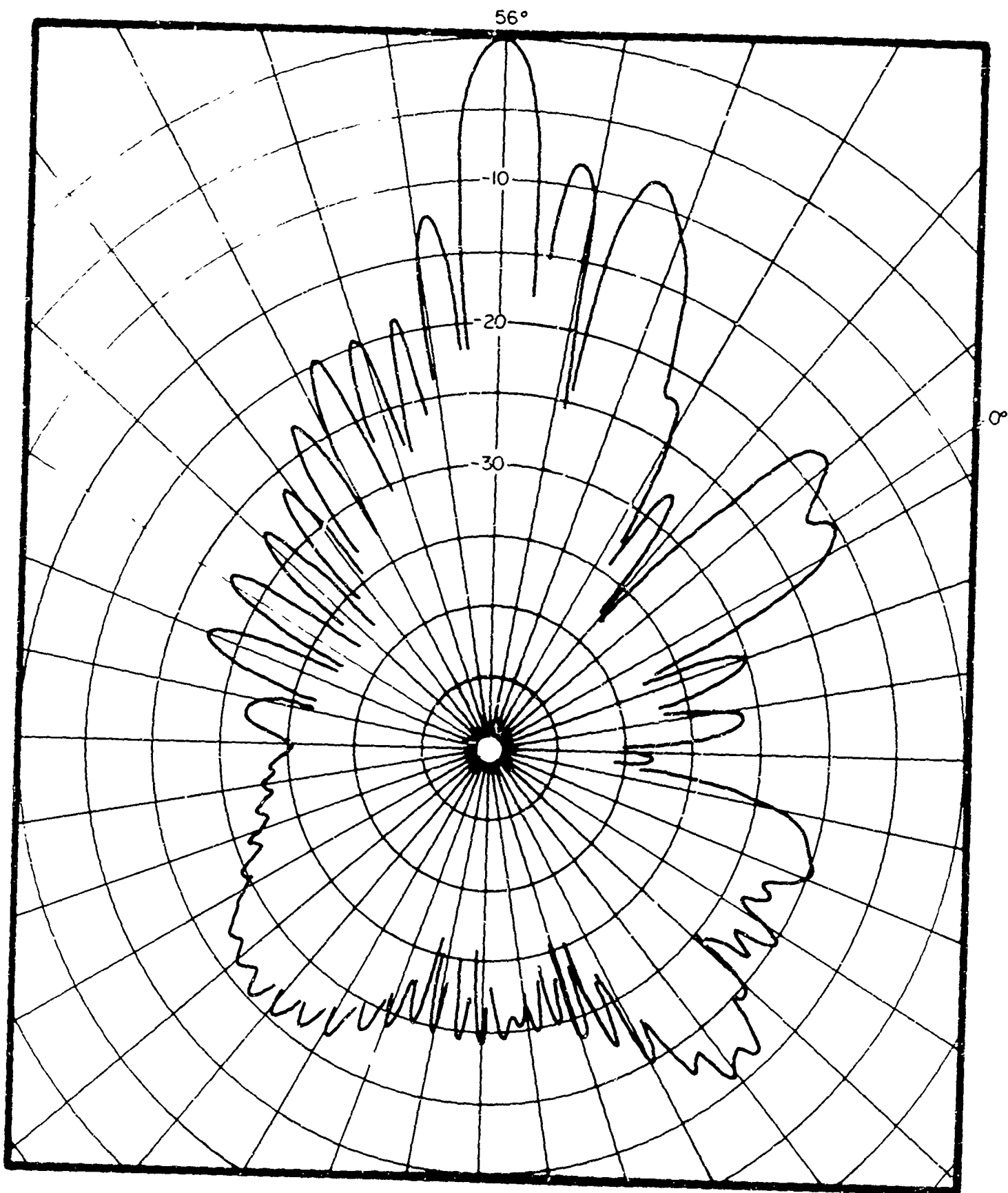


FIG. 13 - BEAM PATTERN FOR ELLIPTIC DOME-CIRCULAR TRANSDUCER,  
56.0° STEERING

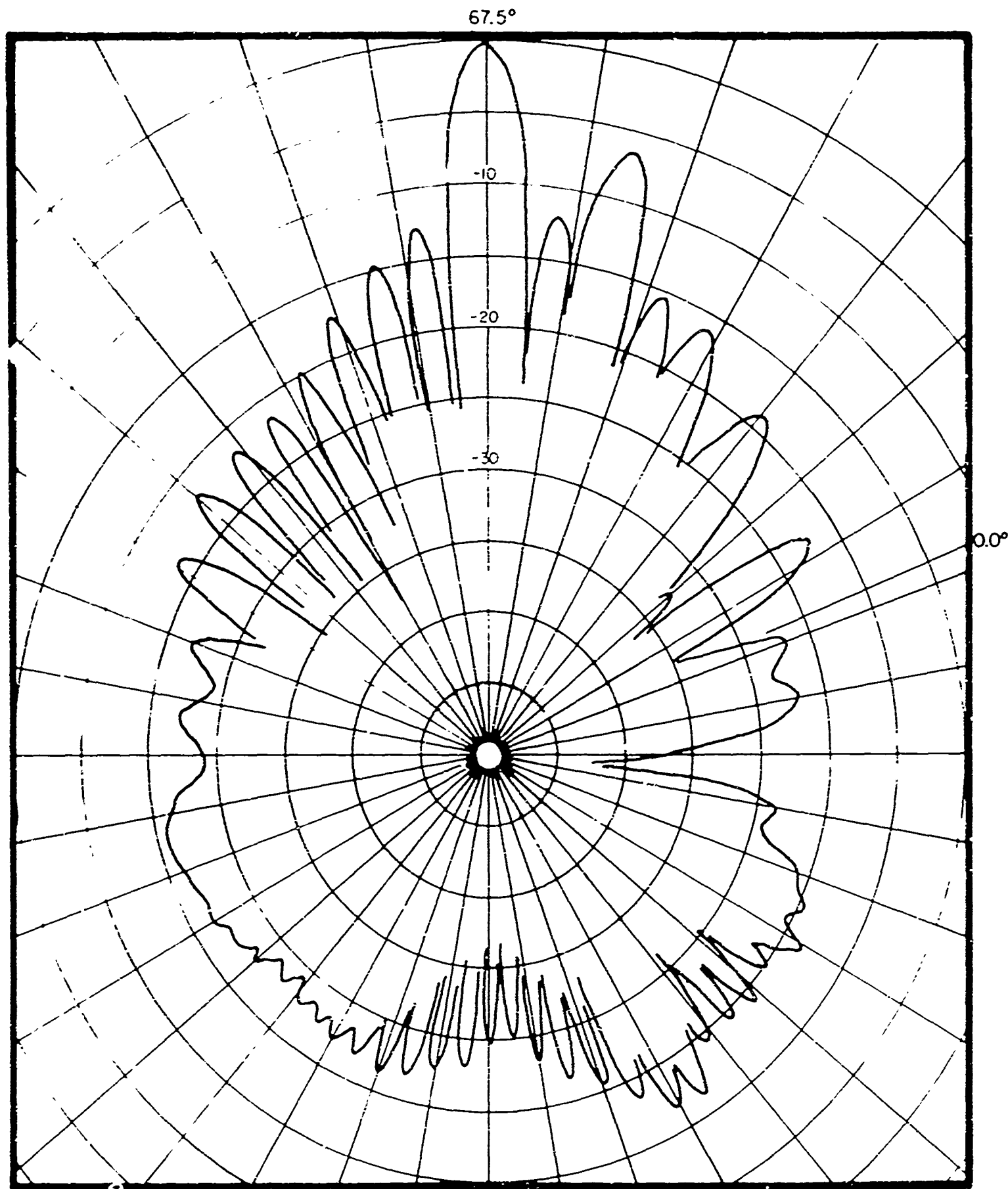


FIG. 14 - BEAM PATTERN FOR ELLIPTIC DOME - CIRCULAR  
 TRANSDUCER, 67.5° STEERING

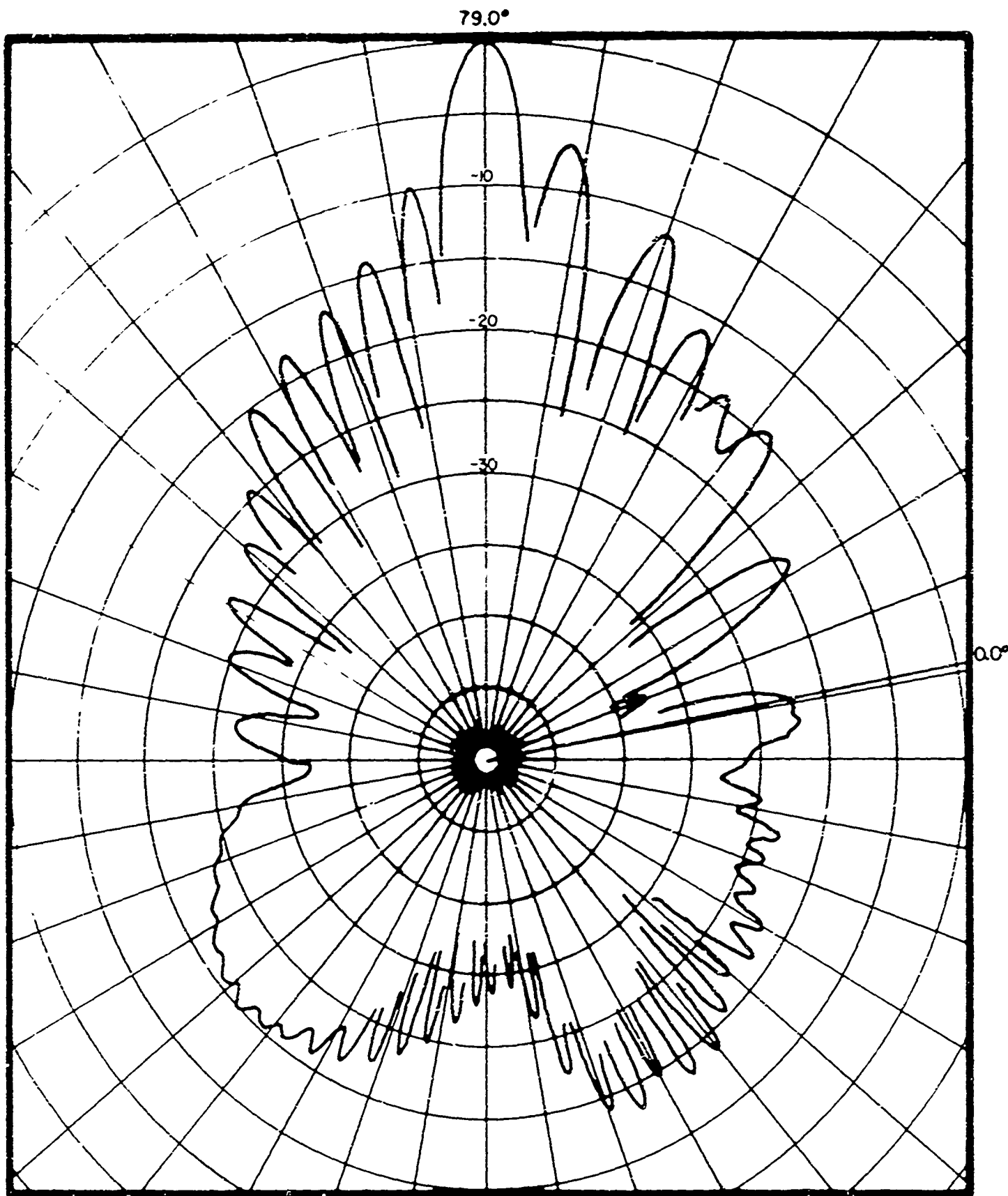
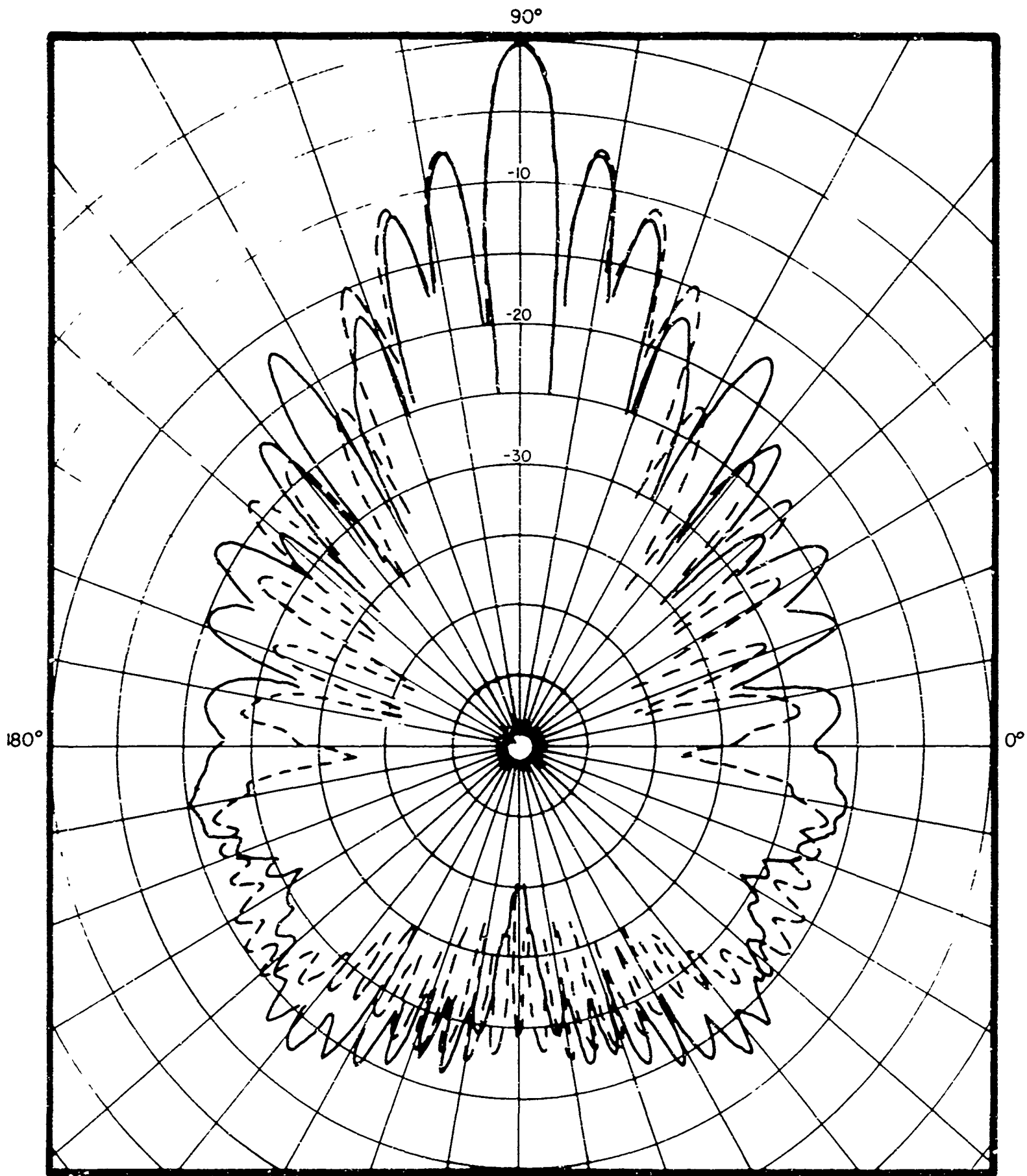


FIG. 15 - BEAM PATTERN FOR ELLIPTIC DOME - CIRCULAR  
TRANSDUCER, 79.0° STEERING



——— ELLIPTIC DOME  
 - - - - - CIRCULAR DOME (RADIUS = 6.4 WAVELENGTHS)

FIG. 16 — BEAM PATTERN FOR ELLIPTIC DOME — CIRCULAR  
 TRANSDUCER, 90.0° STEERING

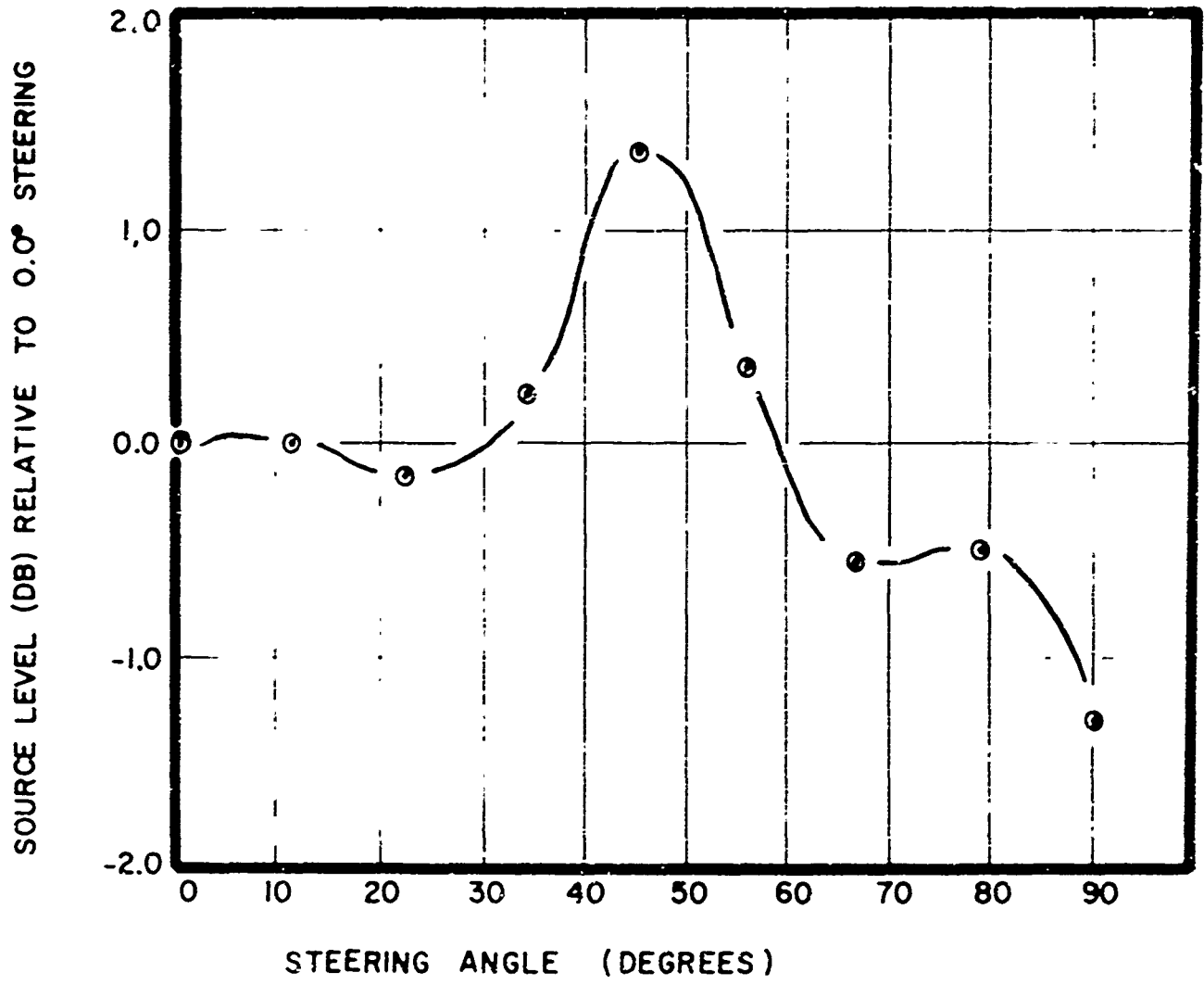


FIG. 17 - SOURCE LEVEL VERSUS STEERING ANGLE

circular dome of radius 6.4 wavelengths and surface density 1.59 gm/cm<sup>3</sup> with the pattern for the elliptic dome with 90.0° steering.

### 5.3 DISCUSSION OF RESULTS

Several observations can be made about the behavior of the beam pattern as the beam steering is changed from 0.0° to 90.0°. The main lobe does not change with steering, and its peak intensity is always in the desired direction. The first side lobes vary from about -8 dB to -12 dB as steering is changed. For 0.0° steering the first side lobes are about the same as those for a circular dome of radius 7.6 wavelengths and surface density 1.35 gm/cm<sup>2</sup>. For 90.0° steering they are about the same as those for a circular dome of radius 6.4 wavelengths and surface density 1.59 gm/cm<sup>2</sup>. The average minor lobe level for the elliptic dome is about the same as that for a circular dome. For the elliptic dome, however, isolated lobes, which can be as large as the first side lobe, begin to appear as the steering angle increases. For a steering angle as small as 34.0° a -11 dB lobe has developed (at about 6.0° in Fig. 11). This lobe increases in magnitude with increasing steering angle, and its direction of peak intensity approaches that of the main lobe from the direction of maximum dome-transducer spacing. The phenomenon of a large lobe structure appearing between the main lobe and the direction of maximum dome-transducer spacing was noticed in the study of the non-concentric cylinder dome model.

The plot of source level versus steering angle does not display any obvious trend of behavior. The source level data have been plotted as a function of various parameters, such as dome-transducer separation along the active array center-line, for the various steering angles. None of these attempts has succeeded in isolating a simple behavior pattern such as that for the infinite planar geometry described in Section 4.5 for the concentric dome models treated in earlier work.



6500 TRACOR LANE AUSTIN, TEXAS 78721

#### 5.4 SUMMARY

The results obtained to date from the elliptic dome model should be regarded as preliminary to a complete study of that model. Hopefully, a parametric analysis based on the elliptic dome model will provide certain information about the effects observed in the beam patterns presented in this section. It may be possible to isolate the physical mechanism which causes the large side lobes in these beam patterns. It would be desirable to find a simple rule for estimating the location and amplitude of these lobes for given values of maximum and minimum dome-transducer spacing and steering angle. A thorough study of the elliptic dome model may yet yield an explanation for the variation of source level with steering angle in terms of the simple model described in Section 4.5.

It is also of interest to see how sensitive the far-field beam patterns are to small changes in the elliptic dome geometry and surface density.

## DISCLAIMER NOTICE

THIS DOCUMENT IS BEST QUALITY PRACTICABLE. THE COPY FURNISHED TO DTIC CONTAINED A SIGNIFICANT NUMBER OF PAGES WHICH DO NOT REPRODUCE LEGIBLY.

OR ARE  
Blank pgs.  
that have  
Been Removed

**BEST  
AVAILABLE COPY**

## 6. OTHER DOME-TRANSDUCER MODELS

### 6.1 THREE-DIMENSIONAL CONCENTRIC DOME MODEL

The three-dimensional concentric dome model is geometrically similar to the earlier, two-dimensional model, but the infinitely-long staves are replaced by an active array having finite dimensions. The array, shown in Fig. 18, is composed of an arbitrary number of rectangular elements each having a prescribed velocity amplitude and phase. Present use of the model is limited to farfield computations because of certain difficulties associated with the numerical evaluation of the solution in the nearfield. (These problems are discussed in Volume II.) The model does represent an extension of the two-dimensional model, however, since three-dimensional beam patterns, including patterns for tilted beams, can be computed.

One interesting result obtained from the solution is the relation between the horizontal beam pattern for a tilted beam and that for a particular two-dimensional problem. Suppose a beam is depressed to an angle  $\theta$  by assigning constant phase delays between adjacent layers of the transducer. The horizontal beam pattern computed at that depression angle (that is, the beam pattern computed on the cone making constant angle  $\theta$  with the horizontal) will be nearly the same as that for a two-dimensional (zero tilt) problem with the wave number ( $2\pi/\text{wavelength}$ ) multiplied by  $\cos \theta$ . The comparison becomes more exact as the stiffness effects in the dome become less important, and, as mentioned previously, stiffness effects are small in the models studied to date. To examine this comparison, beam patterns were computed for three-dimensional and two-dimensional cases which were related as described above. For the three-dimensional case an array of twenty-four staves and eight layers was phased to a plane to produce a narrow beam, tilted  $42^\circ$  relative to the horizontal. The radius of the cylindrical array was 5.6 wavelengths ( $ka = 35.2$ , where  $a$  is the cylinder radius and  $k$  the

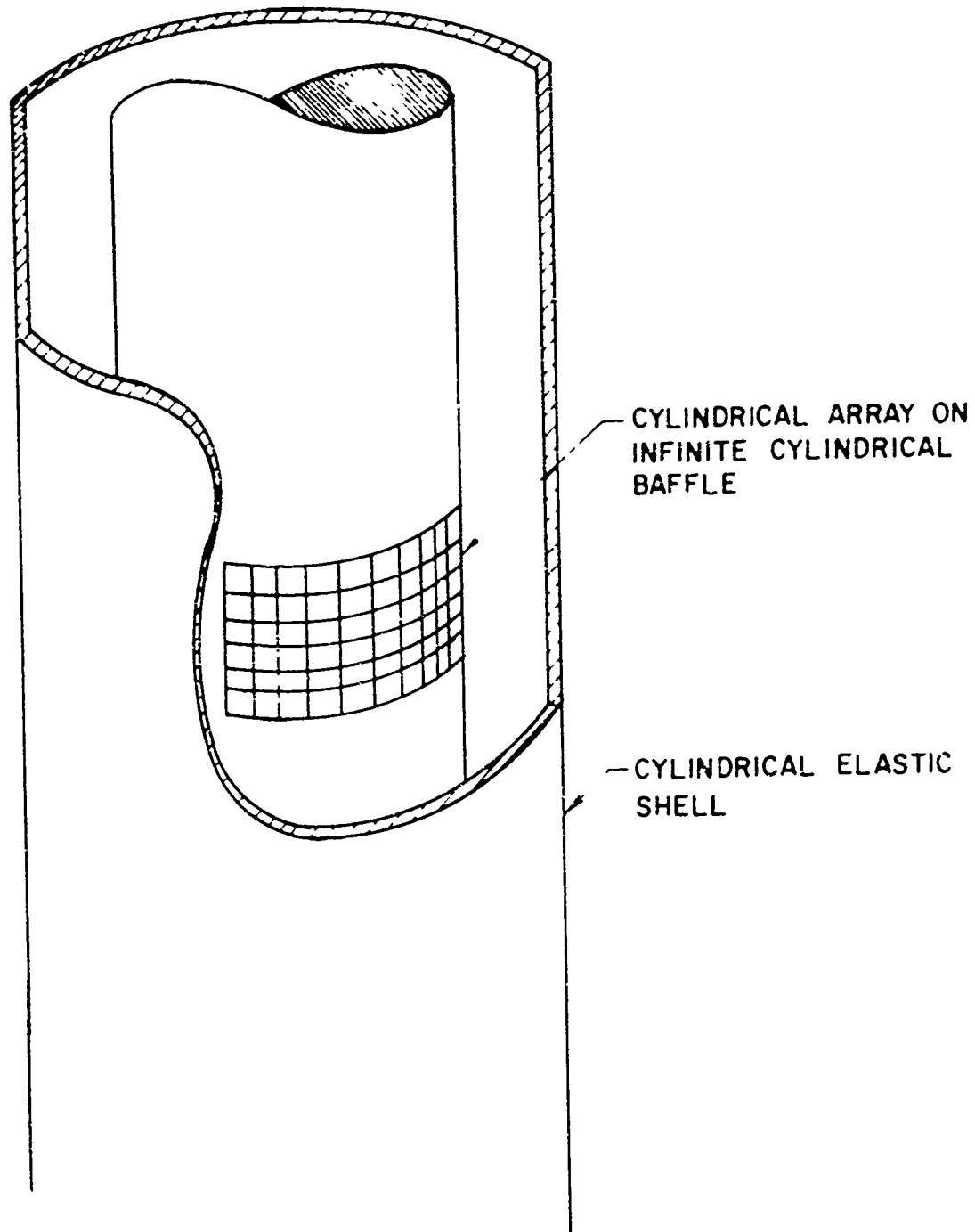
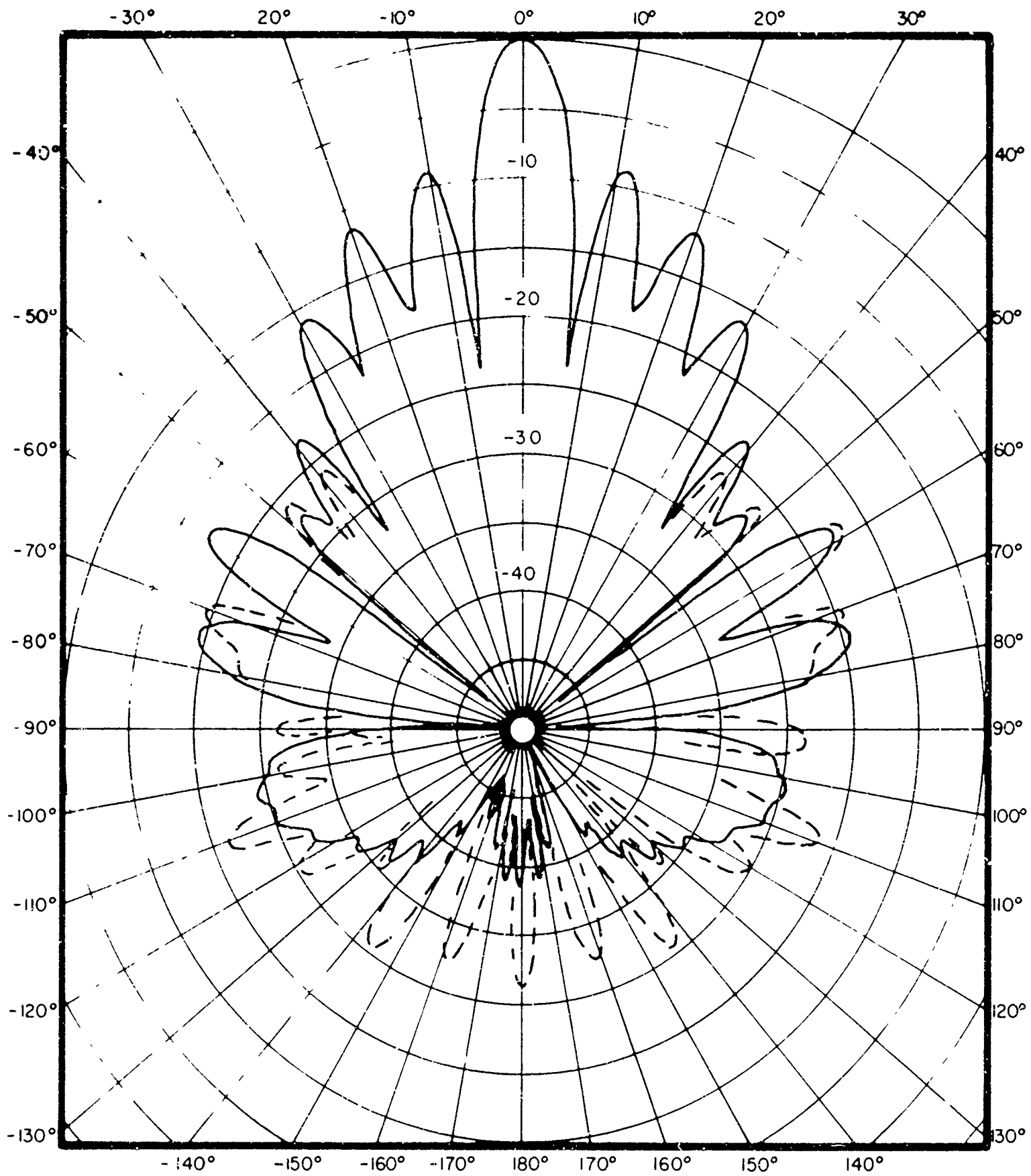


FIG. 18 - GEOMETRY OF CYLINDRICAL DOME  
TRANSDUCER MODEL

wave number) and the radius of the dome was 7.6 wavelengths. The array was composed of close-packed half-wavelength square elements. The dome was 0.018 wavelength thick steel for this case. In the two-dimensional case, twenty-four half-wavelength wide (infinitely long) staves were phased to direct a narrow beam. The array and dome parameters were the same as for the three-dimensional case, but the wave number was reduced by a factor  $\cos 42.0^\circ$ . The beam patterns for these two cases are plotted in Fig. 19. The agreement is seen to be rather good, the discrepancies being caused by small stiffness effects.

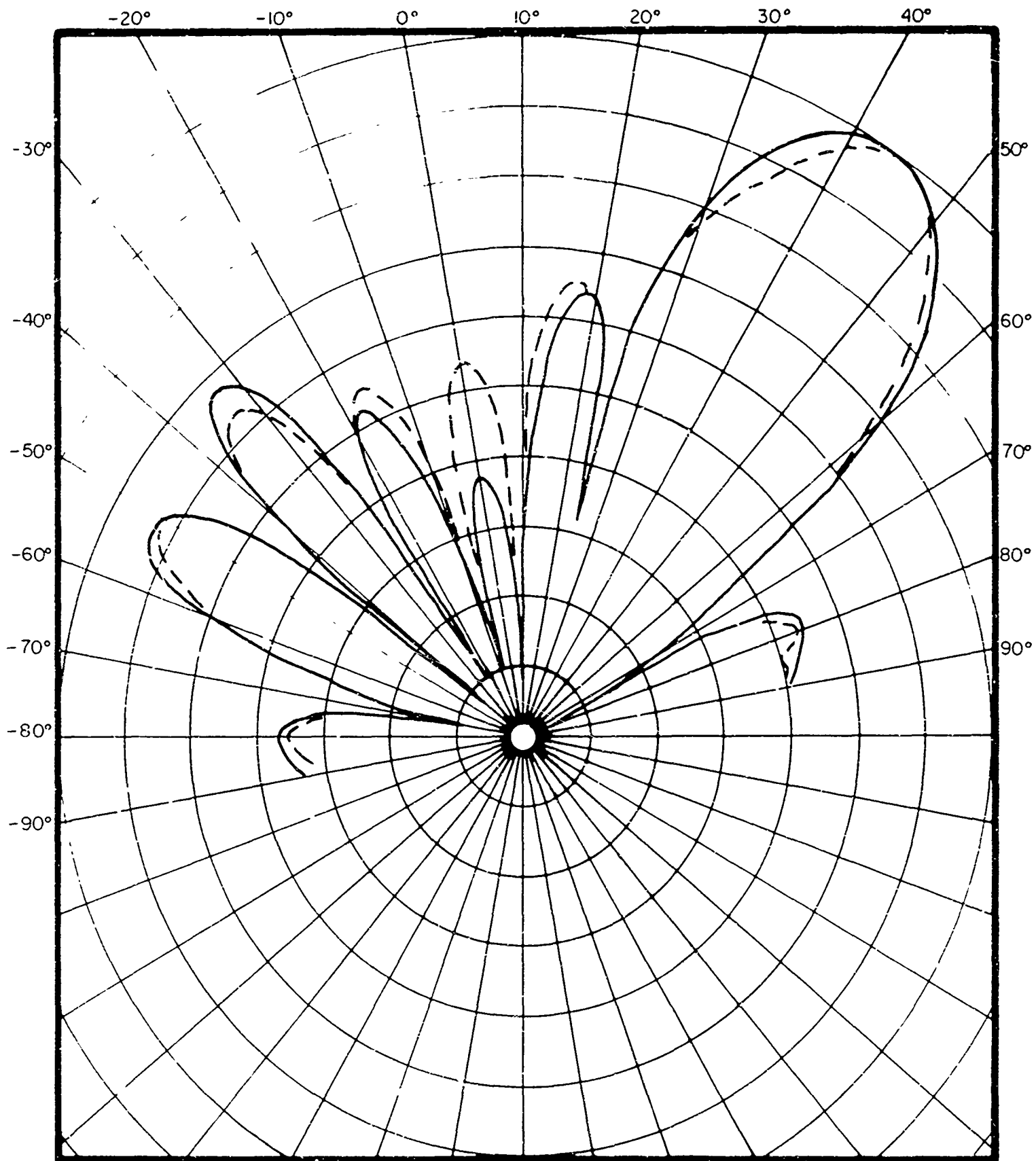
There is one particularly important result which can be derived from the form of the solution for the farfield pressure. When all of the elements of any stave are given the same shading and phasing, the resultant horizontal beam pattern is identically equal to that of the two-dimensional model. Thus the two-dimensional model is as valid as the three-dimensional cylinder model for computing horizontal beam patterns. Of course, a three-dimensional model must be used to compute beam patterns for depressed beams (with the exception of the approximation described above).

While the effect of a cylindrical dome on horizontal beam patterns of cylindrical arrays has been analyzed extensively in studies based on two-dimensional dome models, the three-dimensional cylinder model is the first model that permits an estimation of the effect of a dome on vertical beam patterns and directivity indices of cylindrical arrays. Extensive studies have not been performed with the three-dimensional model; however, several beam patterns have been computed to estimate dome effects and to compare with the results of other models. In Fig. 20, vertical beam patterns for the 8 x 24 array described previously are shown for both dome and no-dome cases. It is seen that the addition of the dome has modified the lobe structure to some



——— 8x24 ARRAY, 42° DEPRESSION  
 - - - - - 2-DIMENSIONAL, 24 STAVE ARRAY (WAVE NUMBER REDUCED BY  $\cos 42^\circ$ )

FIG. 19 - HORIZONTAL BEAM PATTERN FOR CYLINDRICAL ARRAY AND CONCENTRIC DOME, 42.0° DEPRESSED BEAM



——— - WITH DOME  
 - - - - - WITHOUT DOME

FIG. 20 - VERTICAL BEAM PATTERN FOR CYLINDRICAL ARRAY AND CONCENTRIC DOME, 42.0° DEPRESSED BEAM

extent and has broadened the main lobe. The directivity index has changed from 25.3 dB to 24.2 dB and the peak intensity is reduced by 1.1 dB.

From a computational point of view, the cylindrical dome model is ideal for computing farfield quantities. The computer programs for predicting horizontal and vertical beam patterns, source levels, and directivity indices are relatively inexpensive to run. The analytical model is a rather accurate representation of the transducer, even though the dome model is not quite so realistic. Unfortunately, it is difficult to obtain nearfield acoustic quantities from this model. On the other hand, the spherical array-dome model described in the next section is suitable for both nearfield and farfield computations. However, the computer programs based on the spherical model are somewhat more expensive to use than those for the cylindrical model. In some active arrays the horizontal dimension (number of staves) is several times larger than the vertical dimension (number of layers). For such arrays, it may be a reasonably accurate procedure to compute farfield quantities as if the array were on a cylindrical baffle, within a cylindrical dome, and to compute nearfield quantities as if the array were on a spherical baffle, within a spherical dome. The accuracies of these approximations are treated in the next section.

## 6.2 SPHERICAL DOME MODEL

The analysis of the spherical transducer array within a concentric spherical dome was presented in an earlier memorandum [2]. Several new results have been obtained from this model, and the analysis has been extended to include the capability to compute acoustic interaction forces among the array elements. Before the results for the interaction coefficients are presented, the earlier work will be briefly reviewed and several new results will be given for comparison with those of the three-dimensional cylindrical model.

The dome-transducer geometry is shown in Fig. 21. The dome is modeled by a thin elastic shell whose dynamic properties are described by the strain energy expressions derived by Love (see Volume II). Results obtained from this model are qualitatively the same as those of the earlier cylindrical model. That is, the main lobe of a narrow beam is not changed by the addition of the dome, but the side lobe levels are raised. Even with the doubly curved dome, the dome surface density is more important than the stiffness parameters in determining the modal impedance of the dome and, consequently, the effect of the dome on transmitted beams.

To study the effects of dome curvature on a depressed beam, an array consisting of eight layers and twenty-four staves was positioned on the spherical baffle. Although the elements were circular, they were given the same area and center-to-center spacing as the rectangular elements of the cylindrical array, discussed in Section 6.1. The elements were phased to a plane in order to depress a narrow beam to  $42^\circ$ . A spherical  $0.018\lambda$  thick steel dome of radius  $7.6\lambda$  was positioned about the array, and vertical and horizontal beam patterns were computed to compare with those of the three-dimensional cylindrical model. ( $\lambda$  is the wavelength of the transmit frequency). The horizontal beam patterns for the two models are shown in Fig. 22 and the vertical beam patterns are in Fig. 23. It is seen that, even for this large depression angle, there is good agreement between the main lobes and first side lobes of the horizontal beam patterns, and fair agreement of the major lobes of the vertical pattern. The agreement should improve for smaller depression angles since, for small depression angles, the ensonified regions of the two models are geometrically similar. For comparison, the bare-transducer vertical beam patterns are shown in Fig. 24, and for this case the agreement is seen to be very good.

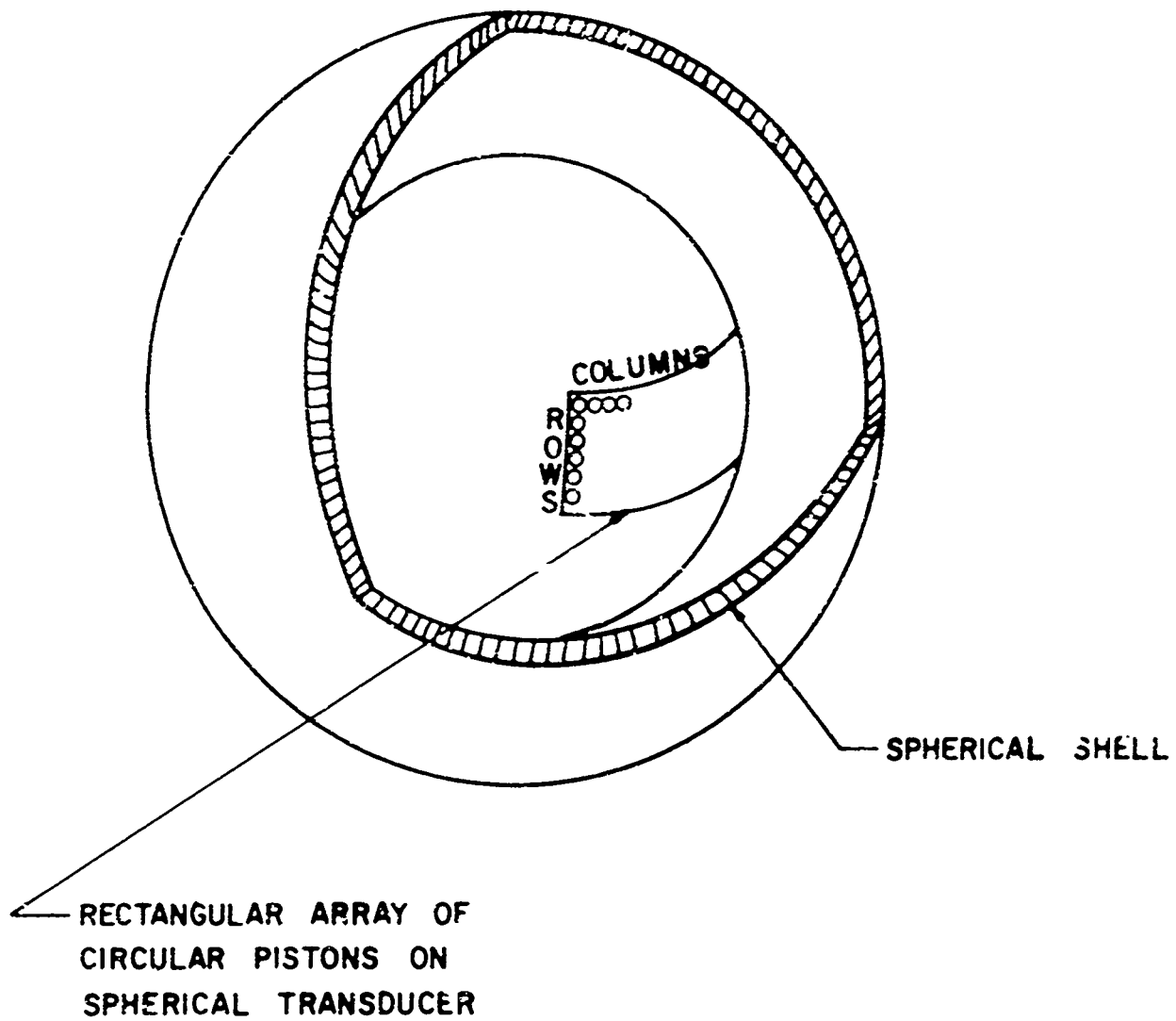


FIG. 21- GEOMETRY OF SPHERICAL DOME - TRANSDUCER  
MODEL

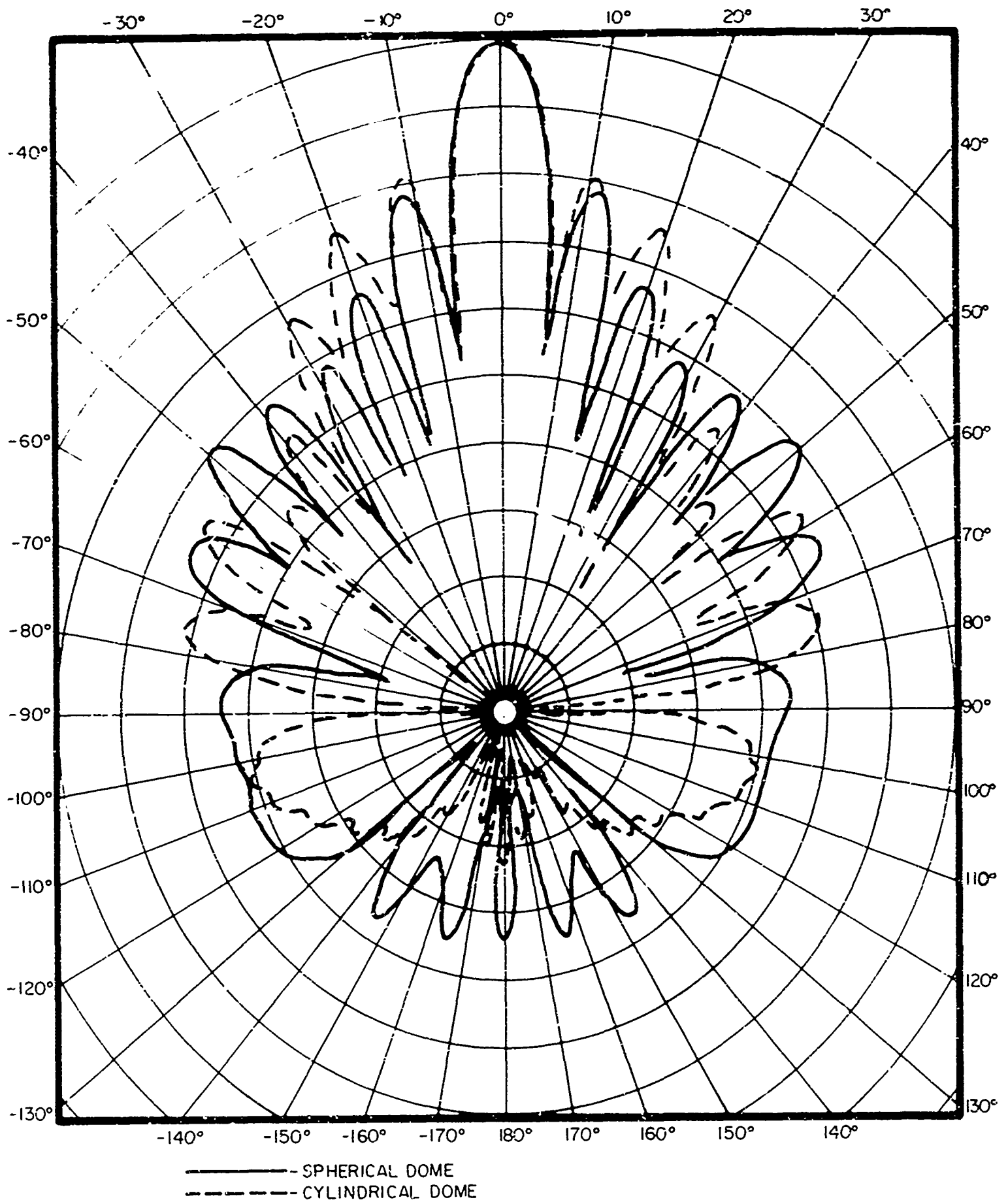
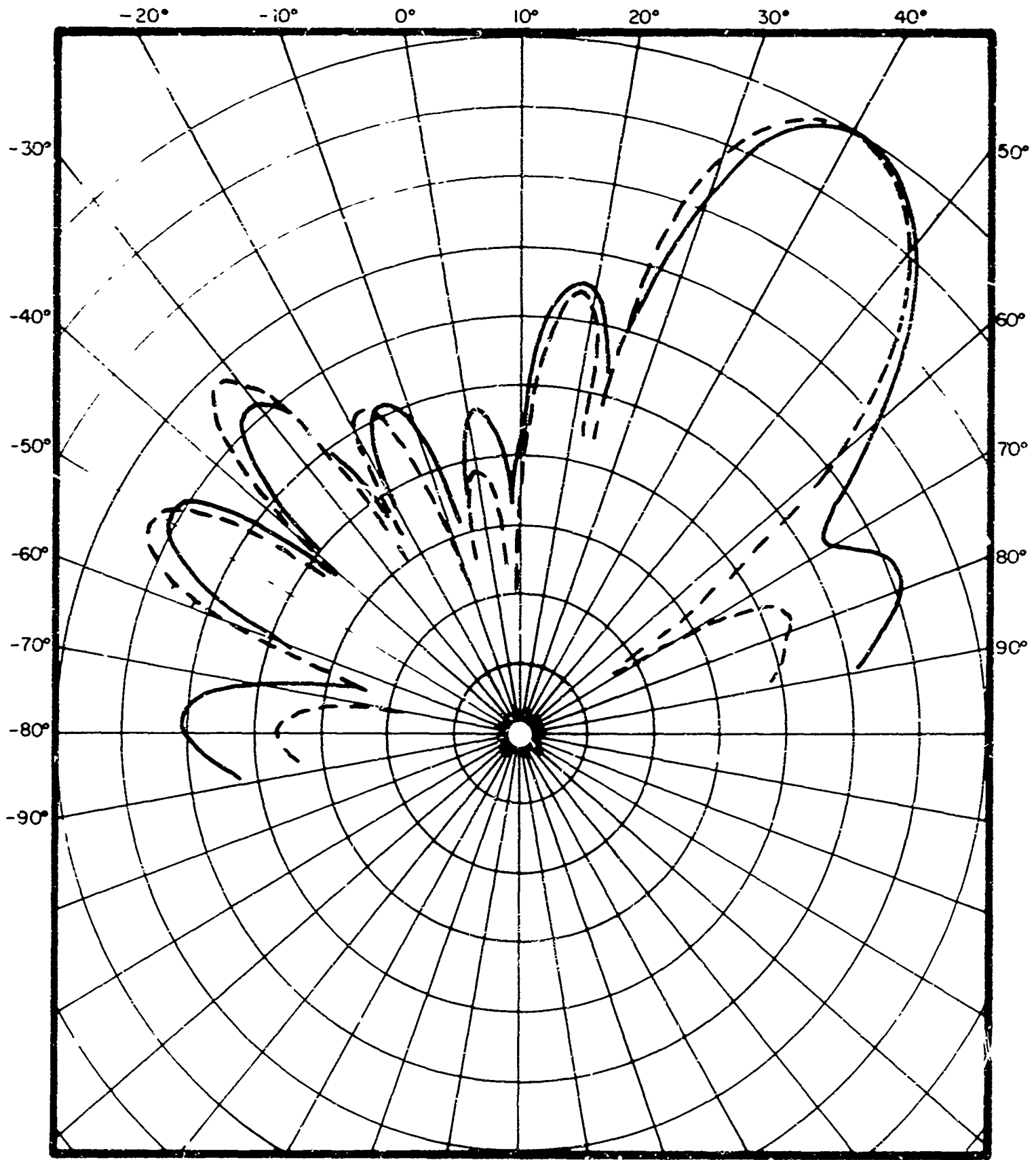


FIG. 22 - HORIZONTAL BEAM PATTERN FOR SPHERICAL AND CYLINDRICAL ARRAYS, WITH DOMES, 42.0° DEPRESSED BEAM



——— SPHERICAL ARRAY  
 - - - - - CYLINDRICAL ARRAY

FIG. 23 - VERTICAL BEAM PATTERN FOR SPHERICAL AND CYLINDRICAL ARRAYS WITH DOMES, 42.0° DEPRESSED BEAM

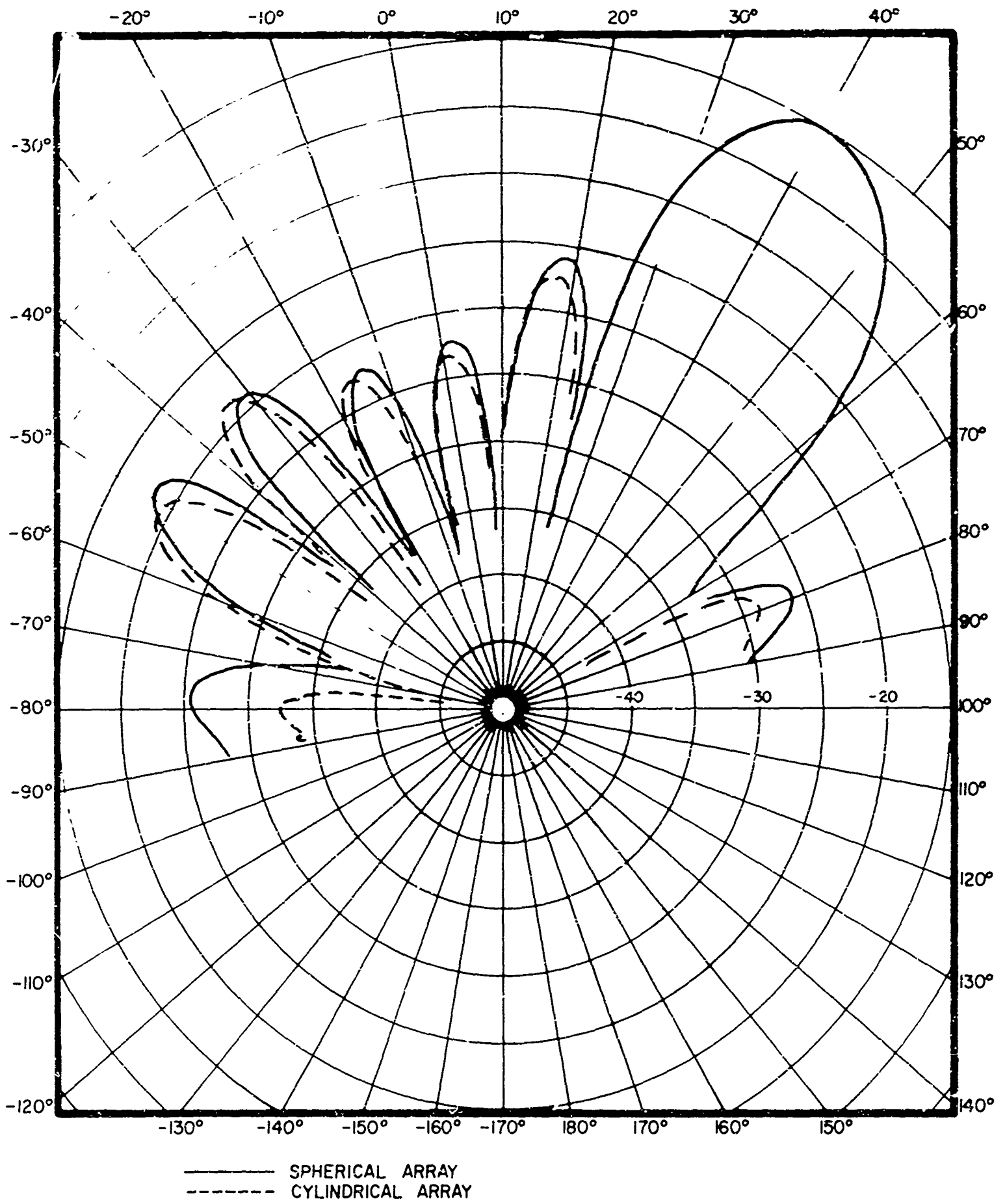


FIG. 24 - VERTICAL BEAM PATTERNS FOR SPHERICAL AND CYLINDRICAL ARRAYS WITHOUT DOMES

While the spherical dome-array model permits the computation of nearfield pressure distributions, the only nearfield quantity which has so far been programmed for computation is the acoustic interaction coefficient  $Z_{ij}$ . The coefficient  $Z_{ij}$  is defined as the acoustic force produced on the  $j^{\text{th}}$  array element when the  $i^{\text{th}}$  element vibrates with unit velocity amplitude and zero phase, and all the elements except the  $i^{\text{th}}$  are fixed. (The use of these quantities to take element interaction into account in computing beam patterns will be discussed in a later technical note.) The analytical expression for the  $Z_{ij}$  is derived in Volume II. All of the interaction coefficients presented here are normalized to  $\rho c A$  (product of fluid density, speed of sound, and area of element).

Interaction coefficients have been computed for circular elements of area  $0.217\lambda^2$  on a spherical baffle of radius 5.6 wavelength ( $ka = 35.2$ ). One set of coefficients has been computed for the no-dome case to compare with those for rectangular elements of the same area on a cylindrical baffle of the same radius [13]. In Figs. 25 and 26, the real and imaginary parts of the interaction coefficients for no dome are plotted as continuous functions of the center-to-center separation in degrees. For  $0.0^\circ$  separation the interaction coefficient is the self impedance. In fact, for separation angles less than about  $5^\circ$  the elements are physically overlapping. The small triangles in these figures are for the rectangular elements on the cylindrical baffle. It is seen that the  $Z_{ij}$  for the cylindrical baffle lie very close to those for the spherical baffle.

In Figs. 27 and 28 the real and imaginary parts of the interaction coefficient are presented for three different spherical domes. All of the domes were steel shells of thickness 0.018 wavelength, but three different values of dome radius were used. It is seen that the curves for the no-dome case and the three cases with domes are similar. They are decaying oscillatory

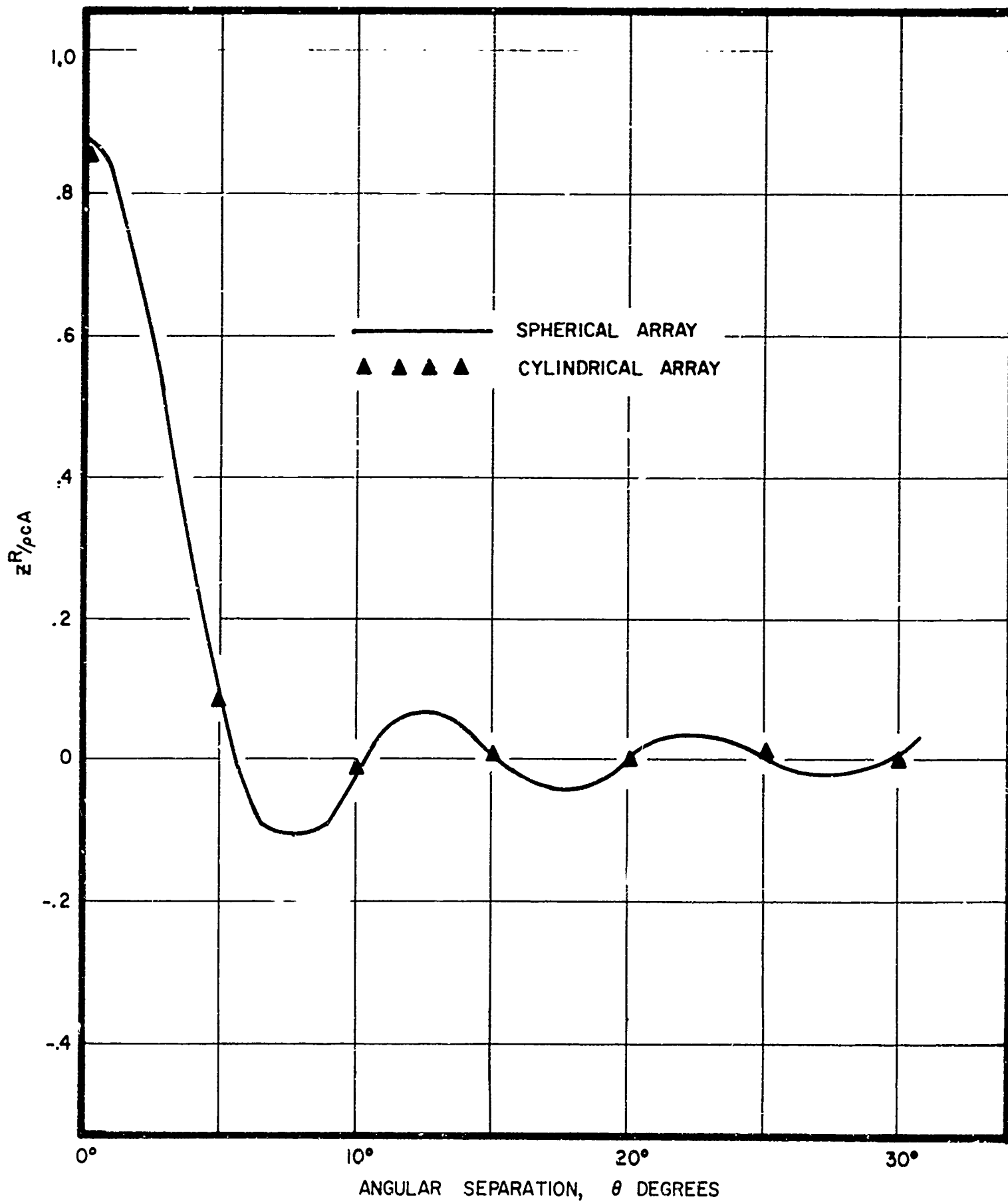


FIG. 25 REAL PART OF NORMALIZED MUTUAL ACOUSTIC IMPEDANCE ( $Z^R/\rho cA$ ) FOR ELEMENTS ON BARE TRANSDUCER

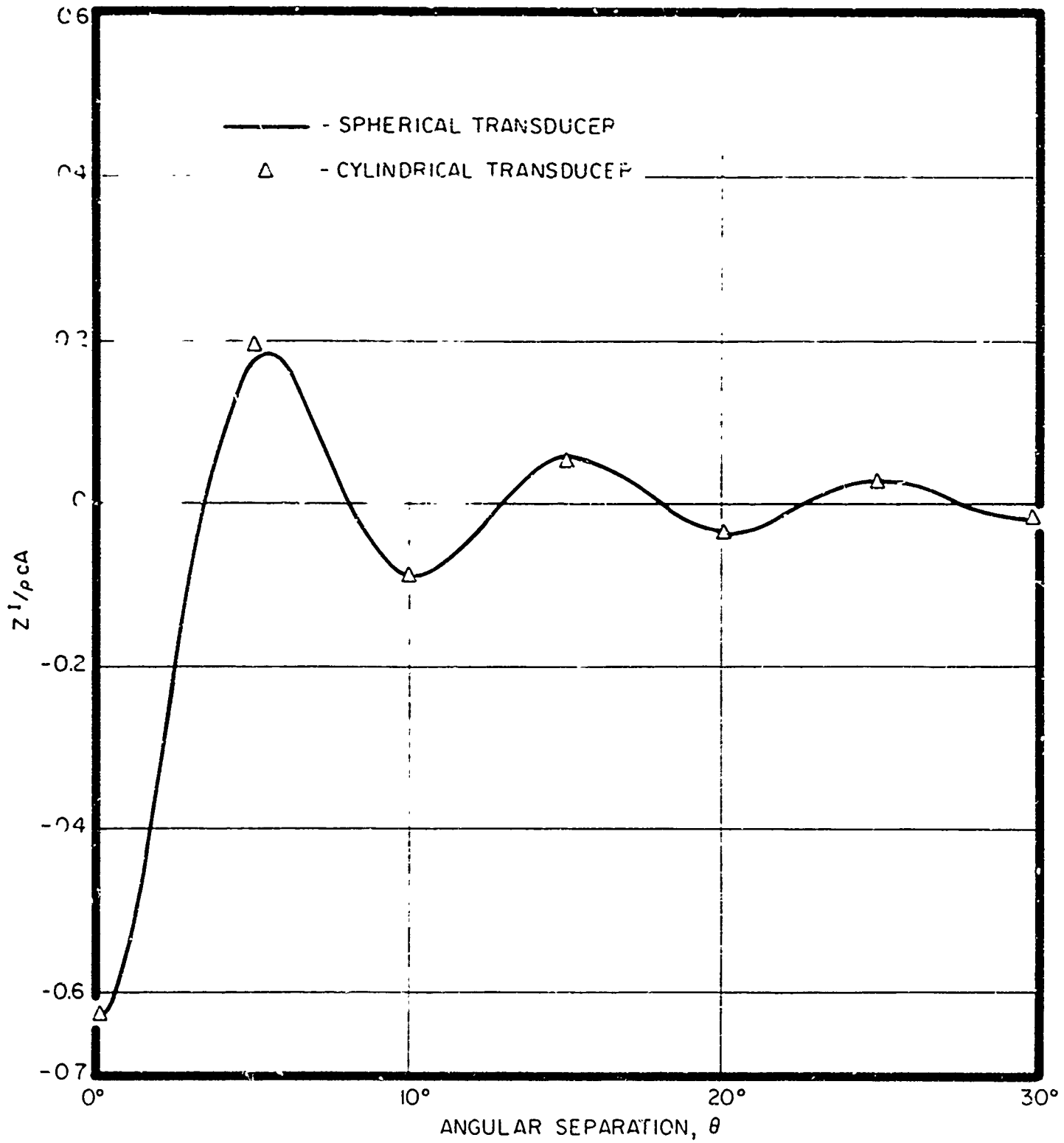


FIG. 26 - IMAGINARY PART OF NORMALIZED MUTUAL ACOUSTIC IMPEDANCE ( $Z / \rho c A$ ) FOR ELEMENTS ON BARE TRANSDUCER

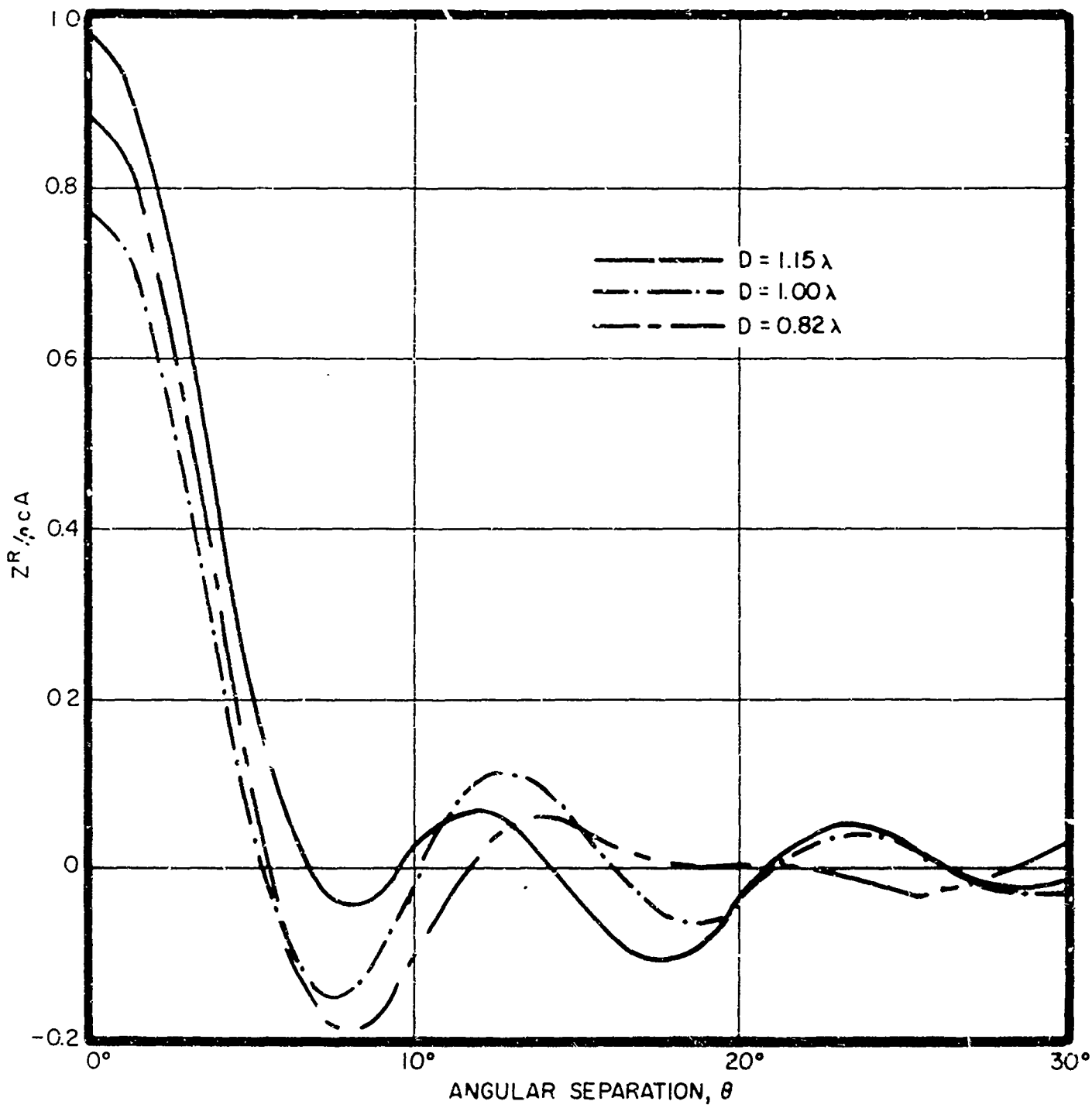


FIG. 27 — REAL PART OF NORMALIZED MUTUAL ACOUSTIC IMPEDANCE ( $Z^R / \rho c A$ ) FOR ELEMENTS UNDER DOME FOR VARIOUS DOME-TRANSDUCER SPACINGS ( $D$ )

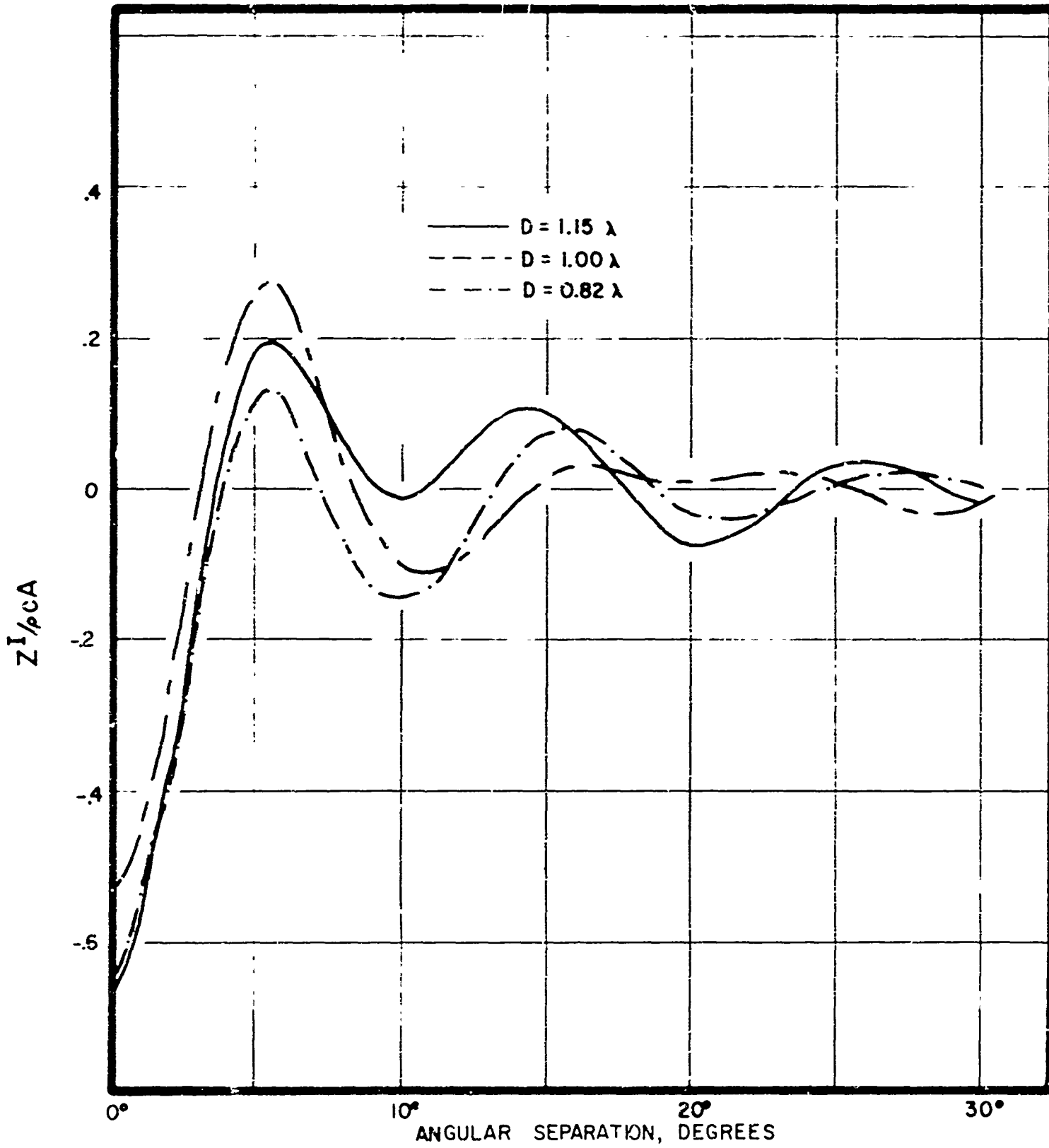


FIG. 28— IMAGINARY PART OF NORMALIZED MUTUAL ACOUSTIC IMPEDANCE ( $Z^I/\rho c A$ ) FOR ELEMENTS FOR VARIOUS DOME TRANSDUCER SPACINGS ( $D$ )

functions of angle and differ mainly in the magnitude of oscillation. Since the self impedance seems to serve as a measure of the difference among the  $Z_{ij}$  curves, it was decided to compute the self impedance as a function of dome-transducer separation for the steel dome. These curves are shown in Fig. 29. The self impedance oscillates with decaying amplitude about the no-dome self impedance as the dome-transducer spacing increases.

### 6.3 THICK DOME MODEL

The thick shell model for the dome was formulated to determine how well the thin shell model approximated the dynamic behavior of the dome in the computation of beam patterns. However, the thick shell model will also permit a study of elastic wave effects within the dome. Because of the limited time available for analyzing this model, the computer program for evaluating the solution to the model was not as general as might be desired. For this reason, only a limited amount of computation was performed to compare the thick shell model results with those of the thin shell model.

The model geometry is identical to the two-dimensional cylinder model used in previous studies, with the exception of the dome thickness. In the thick dome model the boundary conditions at the inner and outer surfaces of the dome are actually satisfied at these surfaces, rather than at the dome middle surface. Further, the dome itself is considered as a region of elastic material in which it is necessary to solve for the velocity field. The velocity field within the dome material obeys the equations of linear elasticity, which can be decomposed into a pair of wave equations, one for compression waves and one for shear waves. A description of the solution of these equations, along with the solution for the pressure field in the fluid, is given in Volume II.

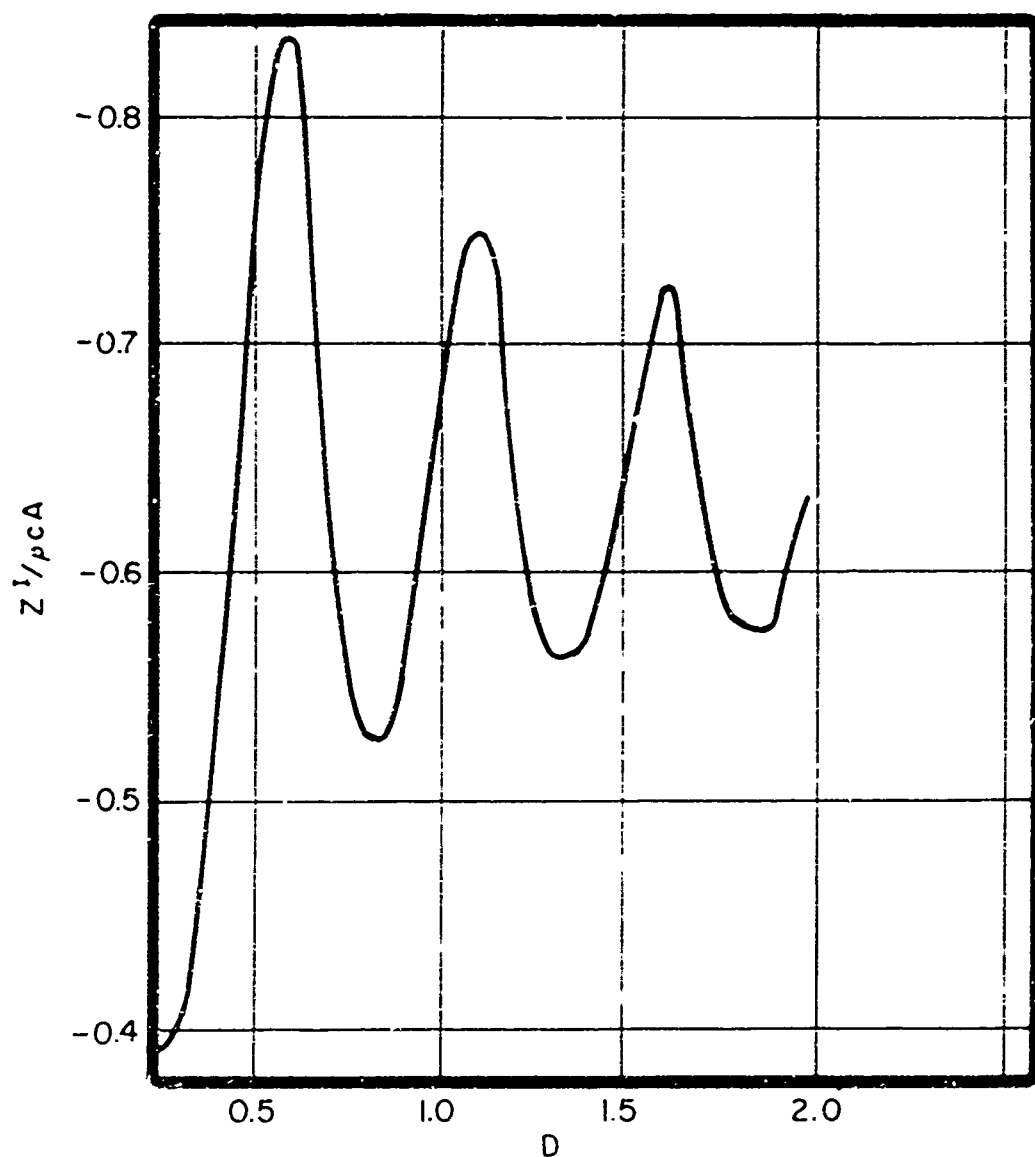
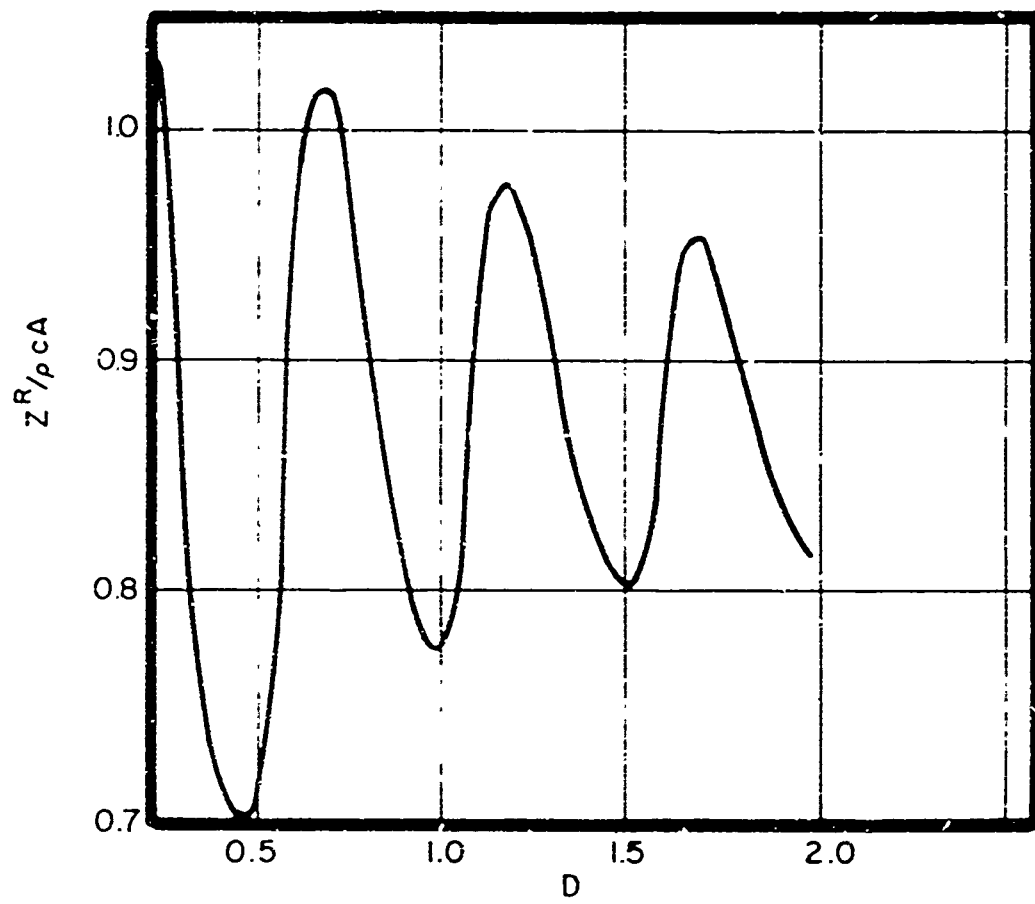


FIG. 29 - NORMALIZED SELF IMPEDANCE ( $Z/\rho c A$ ) VS DOME TRANSDUCER SPACING ( $D$  IN WAVE LENGTHS)

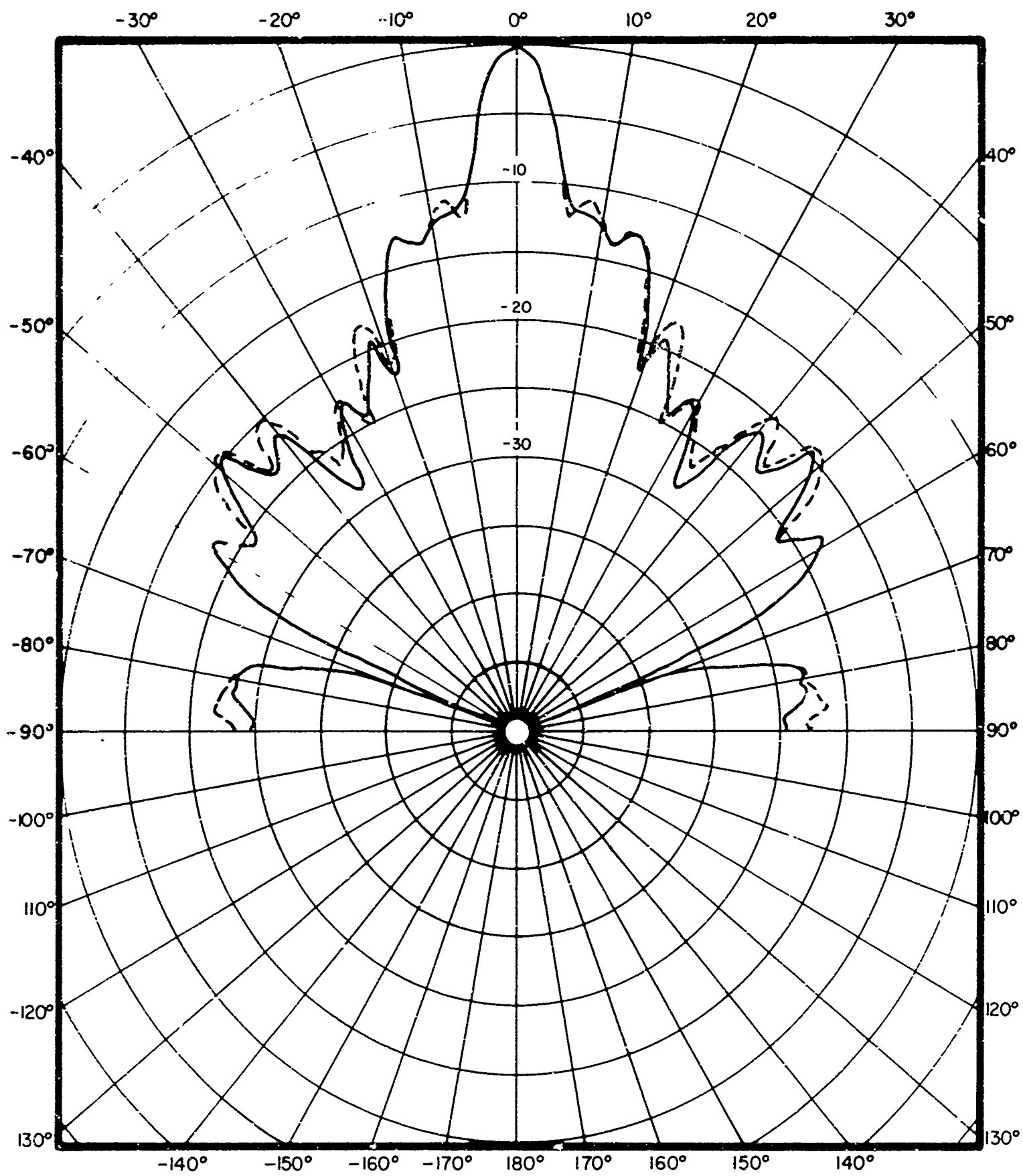


Beam patterns for several thicknesses of steel domes have been computed using both the thick shell model and the thin shell model. For all cases the transducer had a radius of 5.6 wavelengths ( $ka = 35.2$ ) and contained 24 half-wavelength staves. The staves were phased to a plane and given cosine shading. The radius of the middle surface of the dome for both thick shell and thin shell models was  $7.6\lambda$ . The results presented here are for dome thicknesses of  $0.029\lambda$ ,  $0.058\lambda$ , and  $0.116\lambda$ . The beam patterns predicted for these cases by the two models are compared in Figs. 30, 31, and 32. While the discrepancies between the predictions of the two models increase as the dome thickness increases, it should be noted that the average side lobe levels of the beam patterns predicted by the two models are about the same.

Hopefully, the computer program based on the thick dome model can be made more efficient and more general, so that further studies can be made. In particular, it would be desirable to modify the program to include the capability to treat thick rubber domes, since wave effects in such domes might increase the energy absorption above the estimates based on a thin shell model.

#### 6.4 STRUCTURE MODEL

The analytical model described here is the first to permit an estimate of the effect of the supporting structure of a sonar dome on transmit beam patterns and source level, although an earlier study [14] investigated amplitude build-up in the dome skin and transmission loss due to structure. While the present model has been simplified to make the mathematics tractable, it still has the ability to predict mode coupling and standing waves between structure members.



——— THIN DOME MODEL  
 - - - THICK DOME MODEL  
 THICKNESS OF DOME = 0.033 WAVELENGTHS

FIG. 30 - BEAM PATTERNS FOR CYLINDRICAL TRANSDUCER,  
 THICK DOME AND THIN DOME MODELS

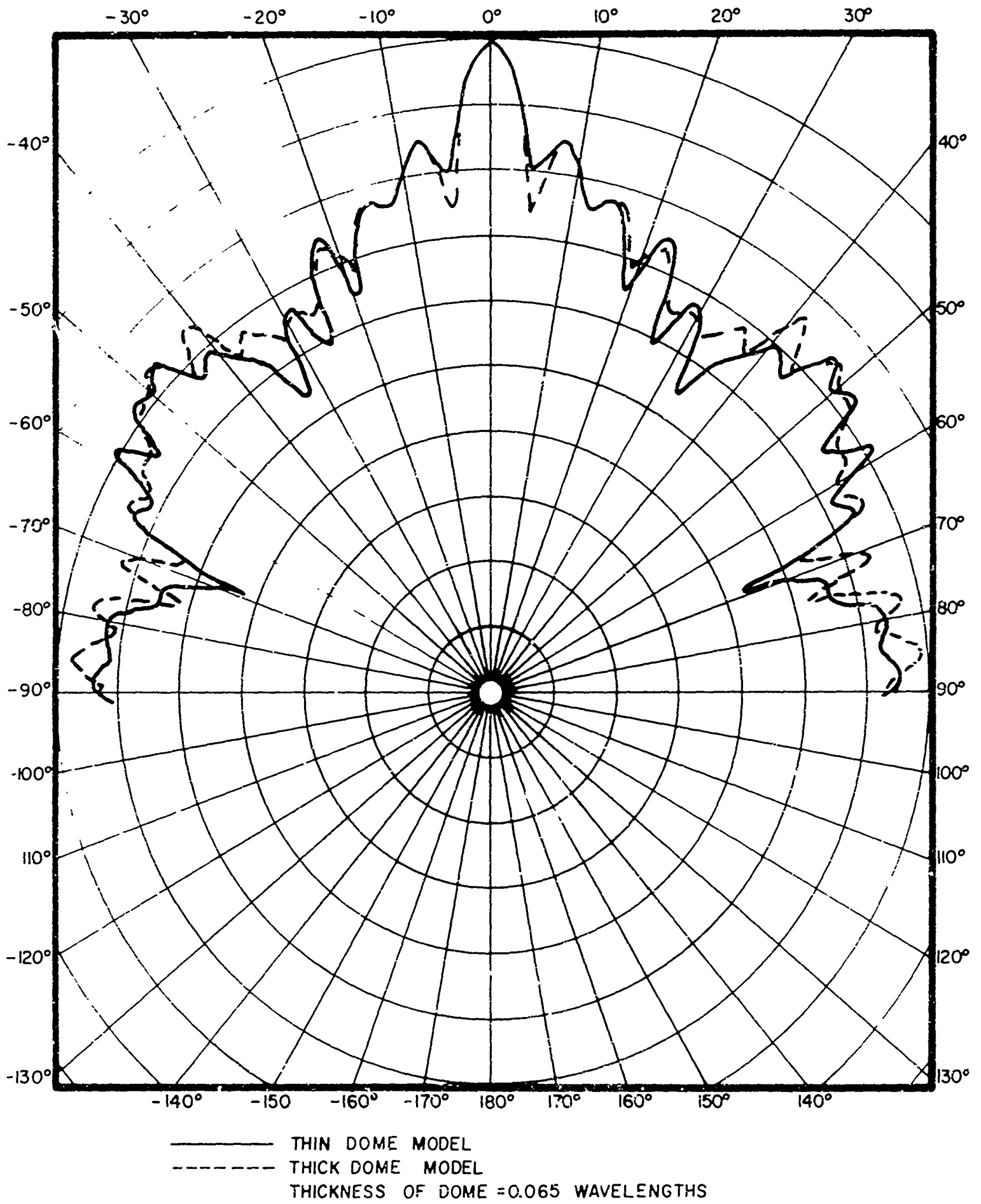
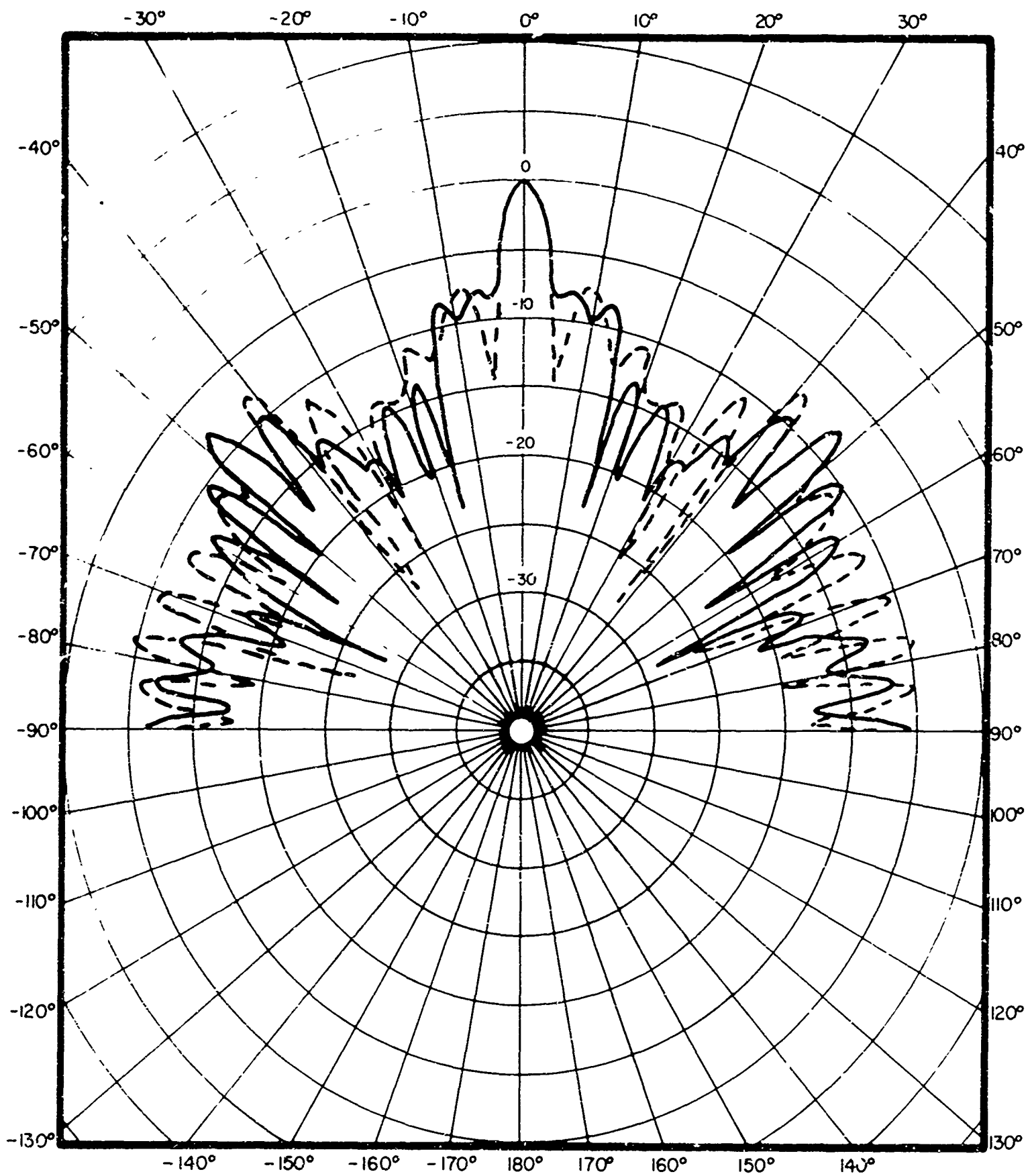


FIG. 31 - BEAM PATTERNS FOR CYLINDRICAL TRANSDUCER,  
THICK DOME AND THIN DOME MODELS



——— THIN DOME MODEL  
 - - - THICK DOME MODEL  
 THICKNESS OF DOME = 0.12 WAVELENGTHS

FIG. 32 - BEAM PATTERNS FOR CYLINDRICAL TRANSDUCER, THICK DOME AND THIN DOME MODELS



The analytical model consists of a circular transducer within a concentric circular shell whose dynamic properties are described by the Flügge thin shell equations. The properties of the structure are included by specifying the point driving impedance of a structure element at the location on the shell where it is attached. Since the model is two-dimensional, the attachments must be considered to be ribs which extend indefinitely in the axial direction. It is assumed that the width of a rib is small relative to the wavelength and that its effect is due to the added mass which must be driven by the shell. The analysis of the structure model is described in detail in Volume II.

This model has been used to predict the beam pattern for one structure configuration to date. A number of structure elements whose mass per unit length is equivalent to a 1 in<sup>2</sup> steel rod were attached to a steel dome of thickness 0.018 wavelength and radius 7.6 wavelengths. The transducer had a radius of 5.6 wavelengths and had 24 active half-wavelength staves. The staves were phased to a plane to direct a narrow beam, and 40 structure elements were located at 0.65 wavelength intervals on the dome so that they were symmetrical about the beam direction. The structure extended over an angular range of 200 degrees in front of the active array, which subtended 120°. The 0.65 wavelength spacing corresponds to two flexural wavelengths in the shell at the frequency of interest. The beam pattern for this structure configuration is shown in Fig. 33 in solid lines. The dashed curve in that figure is for the same dome with no structure.

While Fig. 33 shows the small change in the beam pattern due to the addition of structure, it does not show the change in peak intensity. The peak intensity has been decreased 1 dB relative to the no dome peak intensity. This small difference seems more significant when one realizes that it is caused by an amount of structure which, were it averaged or "smeared out" over 120° of the dome, would increase the dome thickness by only

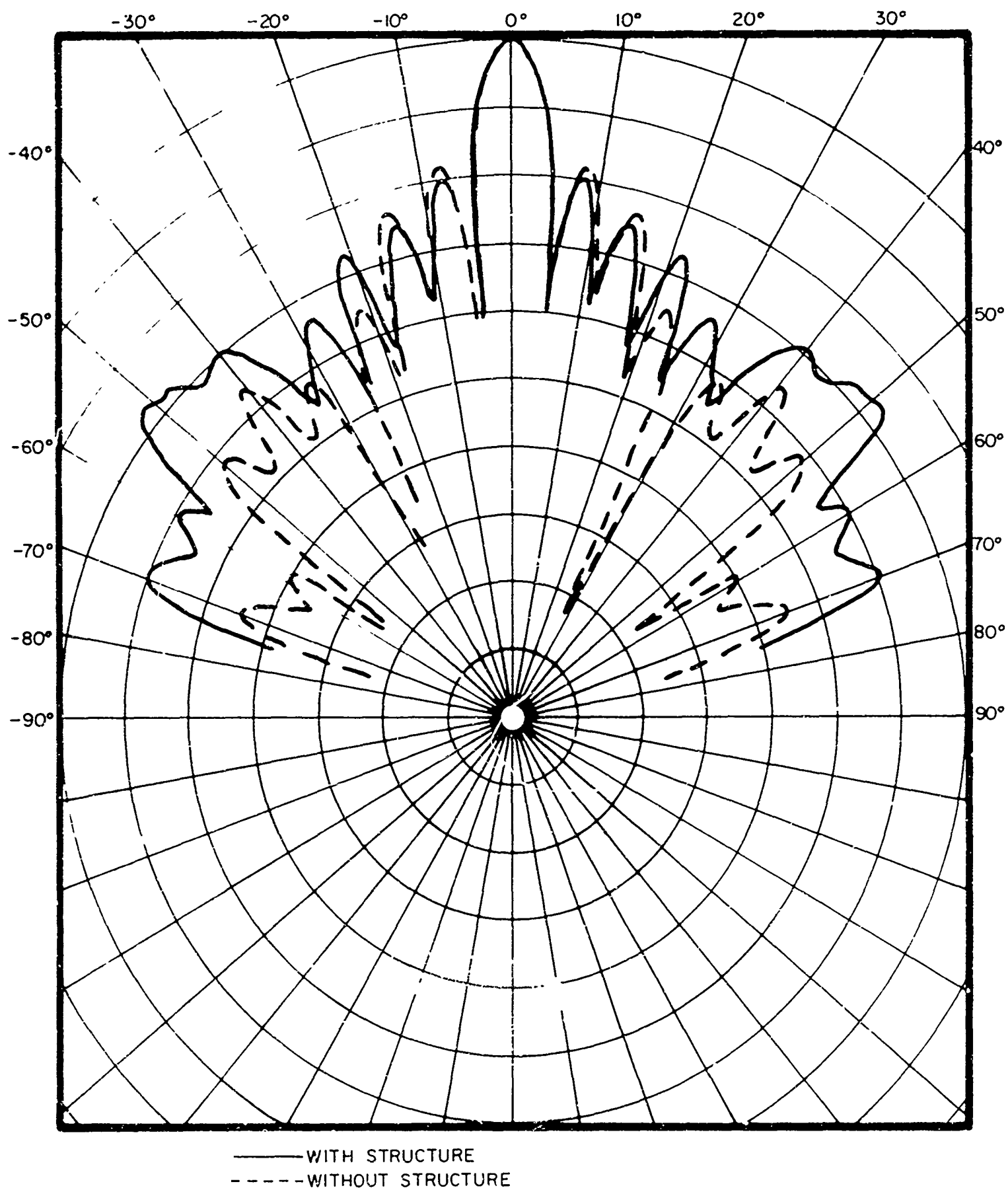


FIG. 33 - BEAM PATTERN FOR CYLINDRICAL TRANSDUCER AND CONCENTRIC DOME, WITH STRUCTURE



0.4%. The effect of the structure may have been enhanced by the spacing, which was an integral number of flexural wavelengths in the shell.

There are a number of further studies which should be conducted with the structure model. First, the velocity distribution on the shell should be computed for enough cases to determine the existence of standing wave resonances between structure elements. Also, it would be of interest to see how the structure changes the modal density of, say, the farfield beam pattern. Finally, it will be useful in the formulation of new dome analyses to determine an acoustic performance trade-off between a few large ribs and many small ribs.

#### 6.5 NONCONCENTRIC CIRCULAR DOME MODEL

The nonconcentric circular dome model was developed prior to completion of the elliptic dome model to provide an immediate analysis of transmit beams nonsymmetrically incident on a dome. Details of the analysis conducted with this model are reported in an earlier technical memorandum [3]. The dome-transducer geometry is shown in Fig. 34. The dome is modeled by a thin elastic shell positioned eccentrically with respect to a cylindrical transducer.

A typical beam pattern predicted by the nonconcentric dome-transducer model is shown in Fig. 35. For this data, the transducer radius was 5.6 wavelengths. As usual, 24 half-wavelength staves were phased to a plane to produce the beam. The eccentricity of the dome-transducer-active array configuration is shown to scale in the inset in Fig. 35. The beam pattern predicted by the elliptic dome model for a comparable case is shown in dashed lines in the figure and the geometry is indicated in the inset. It is seen that the beam patterns show qualitative agreement.

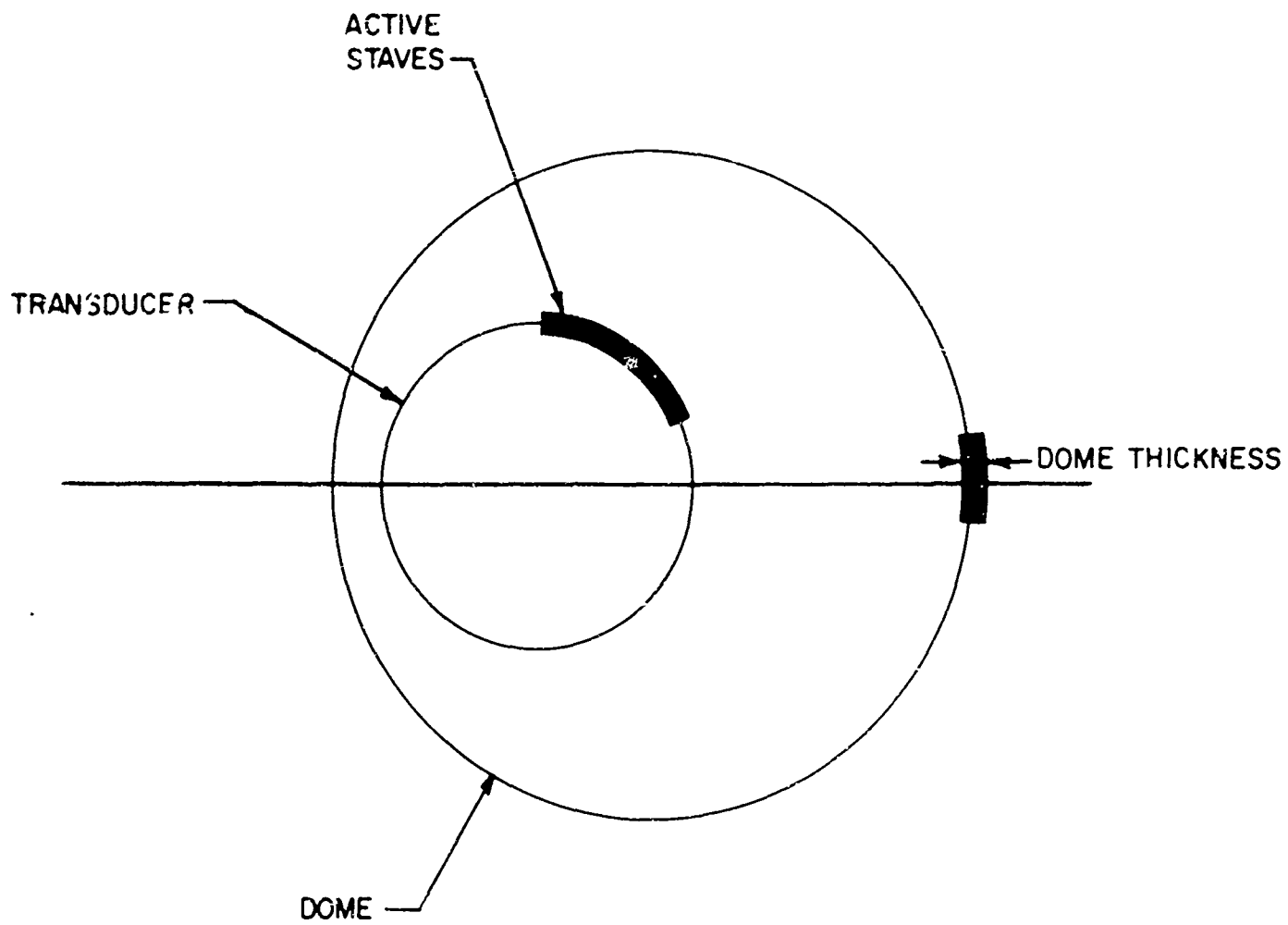
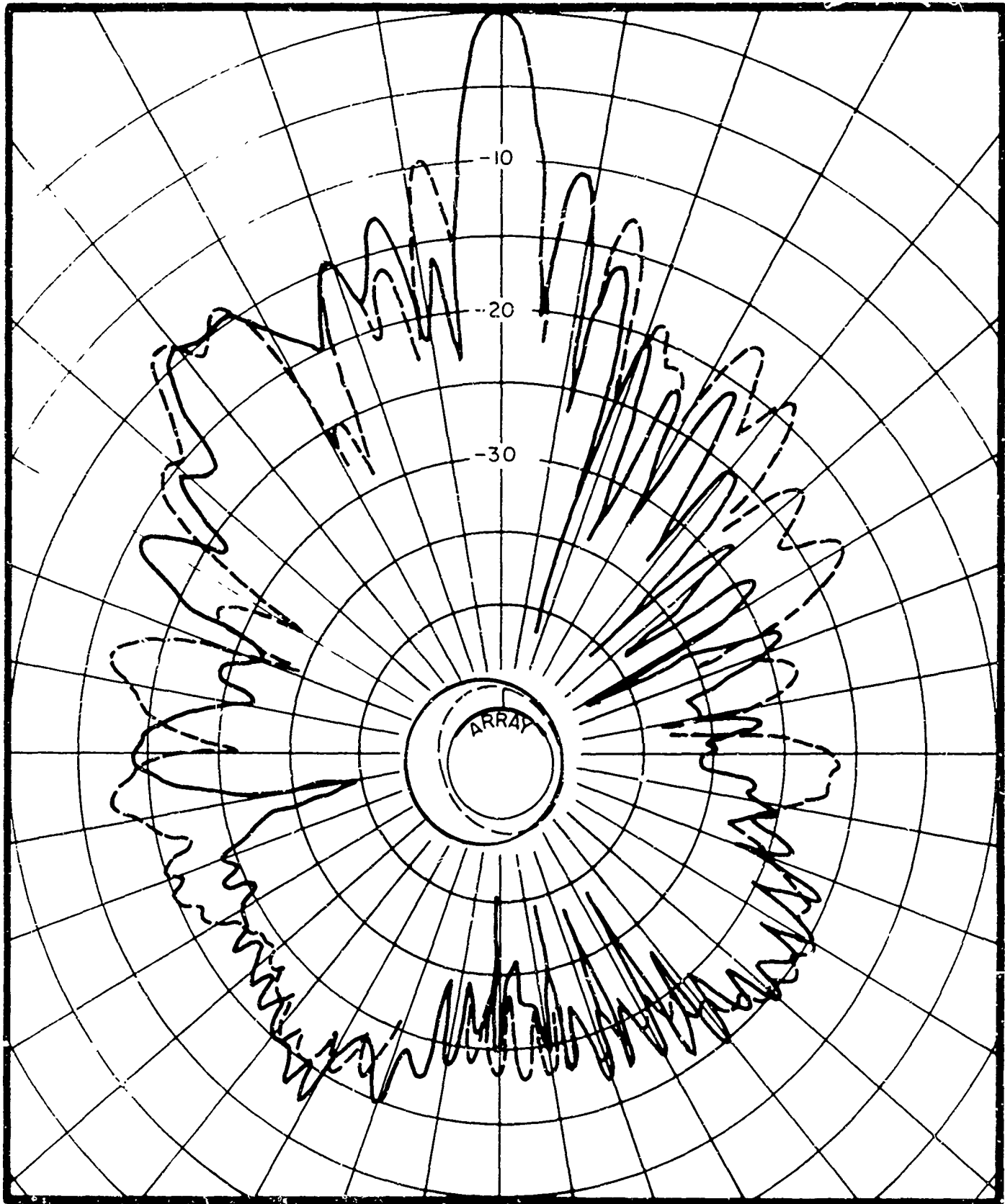


FIG. 34 - NONCONCENTRIC DOME - TRANSDUCER GEOMETRY



———— - NON CONCENTRIC DOME  
 - - - - - ELLIPTIC DOME

FIG. 35 - BEAM PATTERN FOR NONCONCENTRIC DOME - CIRCULAR TRANSDUCER MODEL AND ELLIPTIC DOME MODEL

The results obtained from this model led to several interesting conclusions. First, the main lobe of the beam pattern was not altered by the nonconcentric dome. Second, the minor lobe structure became unsymmetrical about the steering direction for steering angles other than  $0^\circ$  and  $180^\circ$ . Finally, a relatively high intensity region appeared in a direction between the main lobe and the direction of maximum dome-transducer spacing. Qualitatively, the same conclusions were subsequently obtained from the elliptic dome model. The latter results are of course more realistic; however, the similar nature of results of the two models indicate the effect of dome geometry on beam patterns.

#### 6.6 INFINITE PLANAR DOME-TRANSDUCER MODEL

In a previous investigation [1] of the concentric cylindrical dome model, the transmitted power was observed to have a periodic dependence on dome-transducer spacing. This dependence is readily explained in terms of the interference of the waves reflected from the dome with the waves emanating from the transducer face. In the more complicated geometry of the elliptic dome, the transmitted power varies as a function of steering angle, as do the dome-transducer spacing and the angle of beam incidence on the dome. In an effort to gain some insight into the dependence of transmitted power on dome-transducer spacing for beams non-normally incident on the dome, the simple model of the infinite planar transducer and planar dome was analyzed. While the infinite planar dome-transducer model is not capable of predicting beam patterns and source levels, it clearly displays the dependence of transmitted power on both steering angle and dome-transducer spacing. Further, the mathematical form of the solution for the pressure field is readily analyzed to separate the standing wave between the dome and transducer and the wave which is transmitted through the dome.

The model is shown in Fig. 36. The "transducer" is an infinite plane with a continuous normal velocity distribution which simulates the particle velocity of a plane wave steered in the direction making an angle  $\theta$  with the normal to the plane. The wave outside the dome is just such a plane wave; however, the dome modifies its amplitude and phase. Inside the dome the pressure field consists of a plane wave traveling in the  $\theta$  direction and a reflected wave traveling in the  $\pi - \theta$  direction. These two waves include the direct transmission and all of the multiply-reflected components. The sum of all these components add to yield a net transmitted wave plus a standing wave. The dome is simply an elastic plate, whose dynamic properties are described by the classical plate equation. The analysis of this model indicates that, for frequencies of interest, the plate presents a mass-like impedance discontinuity. In this case the time average intensity transmitted through the plate is a periodic function of  $kd \cos \theta$ , where  $k = 2\pi/\lambda$  and  $d$  is the dome-transducer spacing. This function is plotted in Fig. 37 for a steel dome, 0.018 wavelength thick, for three values of  $\theta$ . The abscissa in these plots is  $kd \cos \theta$  and the ordinate is the intensity, normalized to the no-dome intensity. The behavior of these curves is exactly as predicted in the analysis given in Volume II. They all are periodic functions, whose amplitude of oscillation decreases with increasing  $\theta$ .

It was originally hoped that the behavior of the transmitted power as a function of steering in the elliptic dome model could be interpreted in terms of the results of the infinite planar dome-transducer model. The fact that no such interpretation is readily apparent is probably due to the wide angular extent of the array in the elliptic dome model. For most cases of interest the dome-transducer spacing varies significantly over the face of the array. It may yet be possible to explain the behavior of the elliptic dome model in terms of the planar model

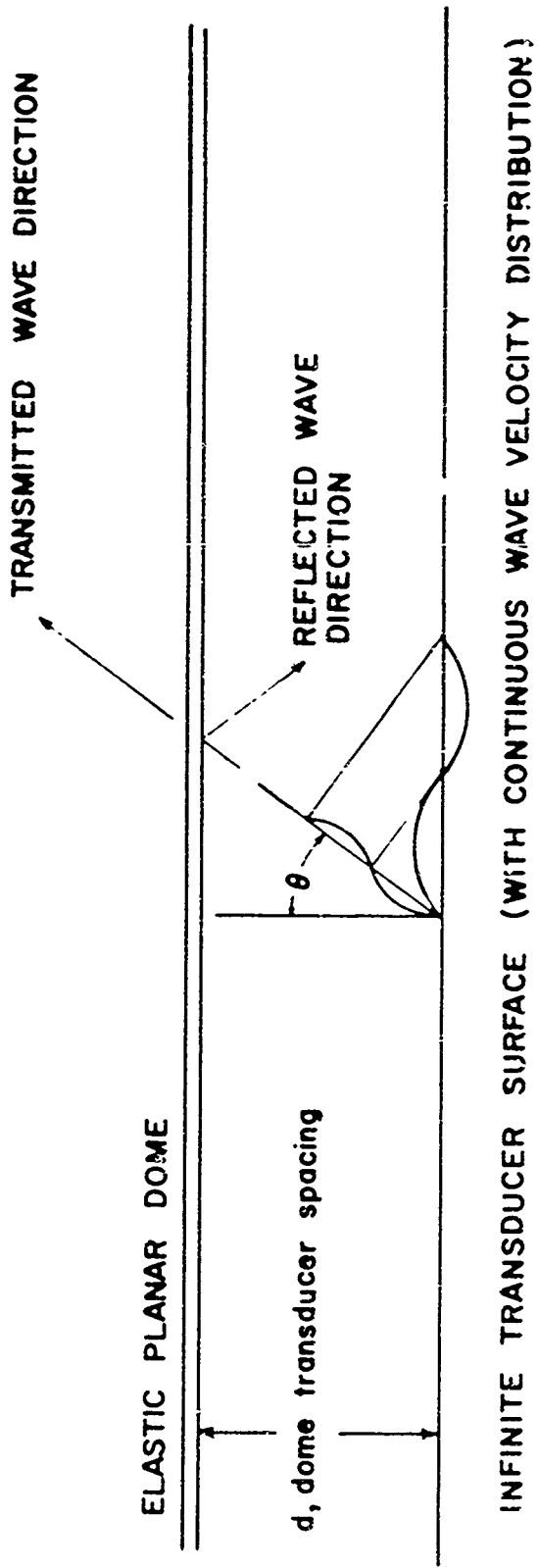


FIG. 36 GEOMETRY OF INFINITE PLANAR DOME -- TRANSDUCER MODEL

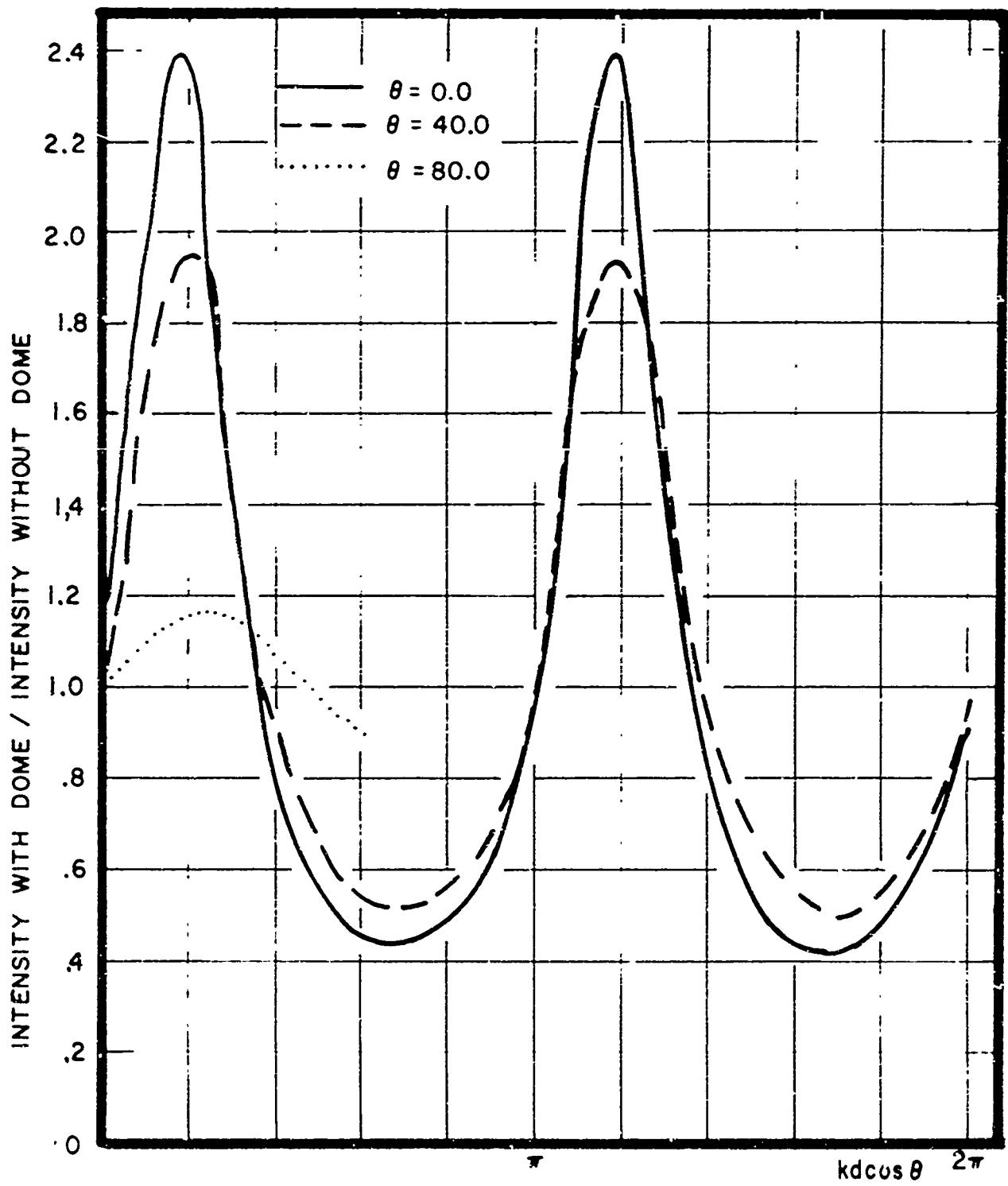


FIG. 37 RADIATED INTENSITY OF PLANAR DOME-  
TRANSDUCER MODEL VERSUS  $kd \cos \theta$



6500 TRACOR LANE AUSTIN TEXAS 78721

by employing some device, such as dividing the elliptic dome model into regions over which the dome-transducer spacing is effectively constant.



## 7. EXPERIMENTAL PROGRAM

### 7.1 INTRODUCTION

The goals of the experimental program during the past year have been (a) to establish measurement techniques, appropriate to the TRACOR test facility and experimental models, for radiated beam patterns and dome and transducer displacements, (b) to develop a sound source (transducer) with well-defined radiation characteristics, and (c) to perform two experiments with a dome-transducer model. The first experiment was performed to determine the dependence of azimuthal beam patterns on the axial length of a cylindrical dome-transducer (this experiment relates to the applicability of two-dimensional analytical models to three-dimensional problems). The second experiment was performed to validate results predicted with the concentric dome-transducer model (homogeneous dome) and to obtain measured beam patterns for a concentric dome containing a simple supporting structure.

### 7.2 MEASUREMENT TECHNIQUES

Requirements for the experimental program include instrumentation for both displacement and sound pressure measurements. Displacement measurements are necessary to determine the velocity profiles across the sound source, and to determine the dome response. Sound pressure measurements are required to obtain beam patterns. The displacement measurements correspond to the "inputs" (transducer boundary conditions) for the analytical models and the beam patterns correspond to the "response" of the models.

Initial experimental requirements called for very detailed measurements of displacement amplitude over the sound source area in order to establish the acceptability of several sound sources. Initial emphasis was, therefore, directed towards displacement measurements in air, with a parallel evaluation of

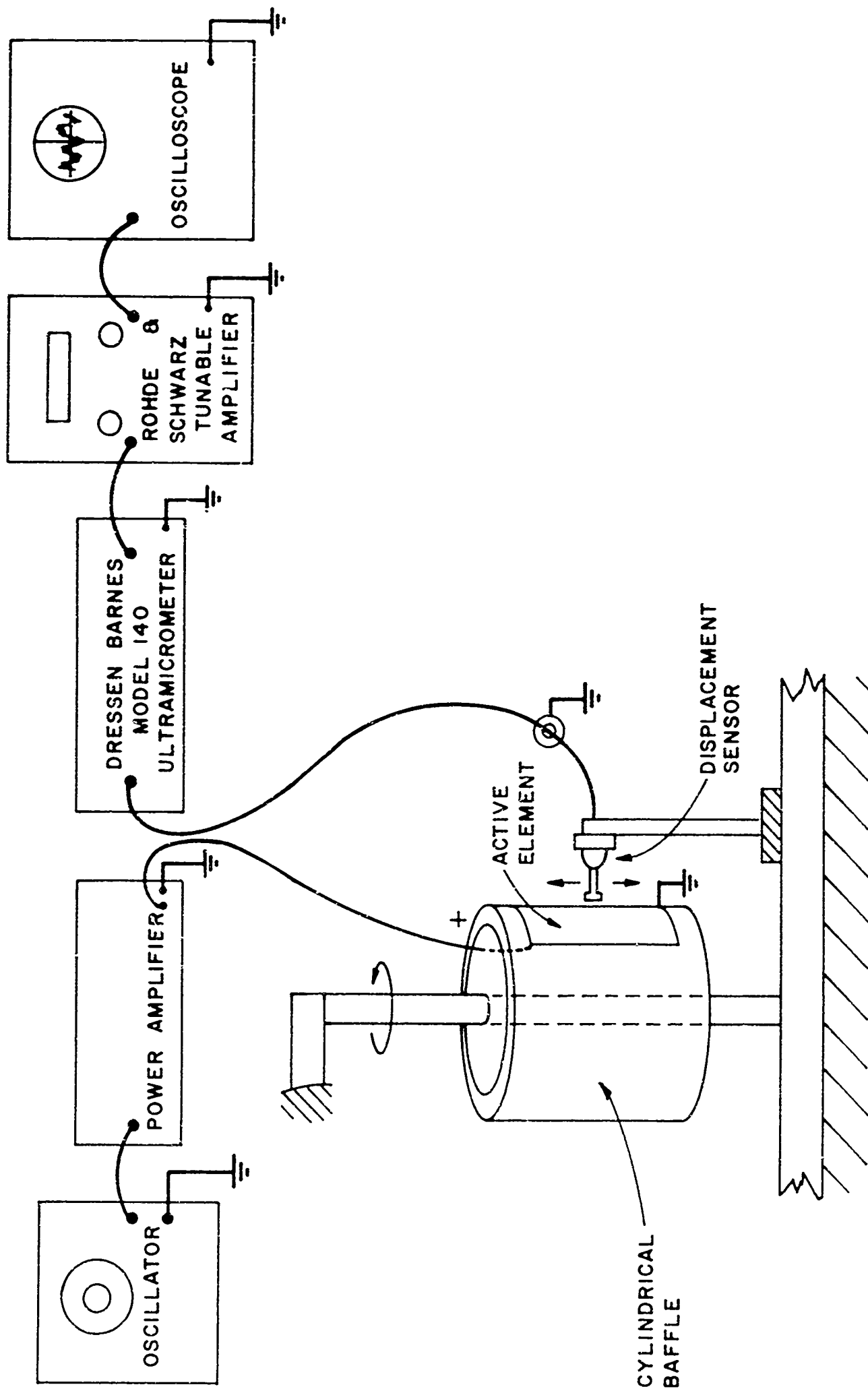


FIGURE 38 - EXPERIMENTAL APPARATUS FOR MEASURING THE DISPLACEMENT PROFILE OF A MODEL SOUND SOURCE

techniques for future measurements underwater. The frequency modulation capacitance probe technique (commonly referred to as the "ultracrometer") was selected for the displacement measurements in air. A typical arrangement of experimental apparatus is shown in Fig. 38. The technique relies upon the capacitance between a sensing probe and any electrically grounded surface to form part of an oscillator resonant circuit. When the grounded surface is an active part of a vibrating system, variations in capacitance, caused by changes in the probe-surface separation, produce frequency modulation in the oscillator. The output of the oscillator is coupled to an IF amplifier and FM discriminator where the signal is detected. The system is aligned to provide a large linear region on the discriminator curve, as shown in Fig. 39A. In practice, the displacement sensing probe is positioned approximately 2-4 thousandths of an inch from the vibrating surface of interest. The tuning controls on the oscillator are adjusted to the operating point on the discriminator curve (Fig. 39A) by observing the deflection of a d.c. coupled oscilloscope trace. Once tuned to the operating point, the zero displacement reference is also established for the probe-surface separation in use (Fig. 39B). The ultramicrometer calibration curve of Fig. 39B is obtained by altering the probe-surface separation by known increments about zero, and observing the corresponding d.c. voltage deflection on an oscilloscope. Measurements of displacement amplitudes as small as 20 Å, at frequencies up to about 500 kHz are readily detected using this technique. In addition, random changes due to heating or spurious vibration are readily detected by monitoring the zero voltage reference on a d.c. coupled oscilloscope. Those changes can be compensated for by altering the probe-surface separation. The Rohde and Schwarz tunable amplifier shown in Fig. 38 is used as an active filter to "clean up" the displacement signal, and thus provide a higher degree of resolution.

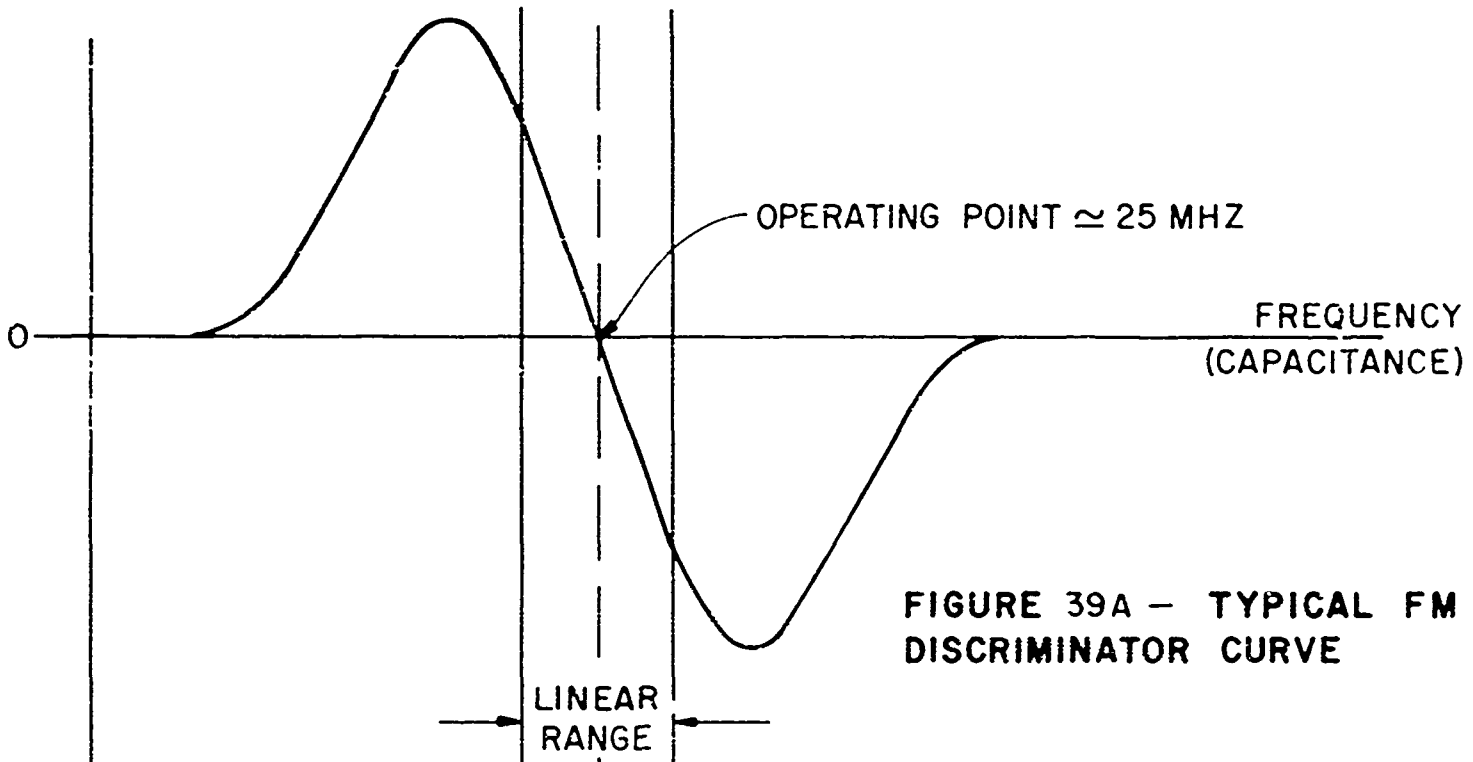


FIGURE 39A - TYPICAL FM DISCRIMINATOR CURVE

DISCRIMINATOR OUTPUT VOLTAGE

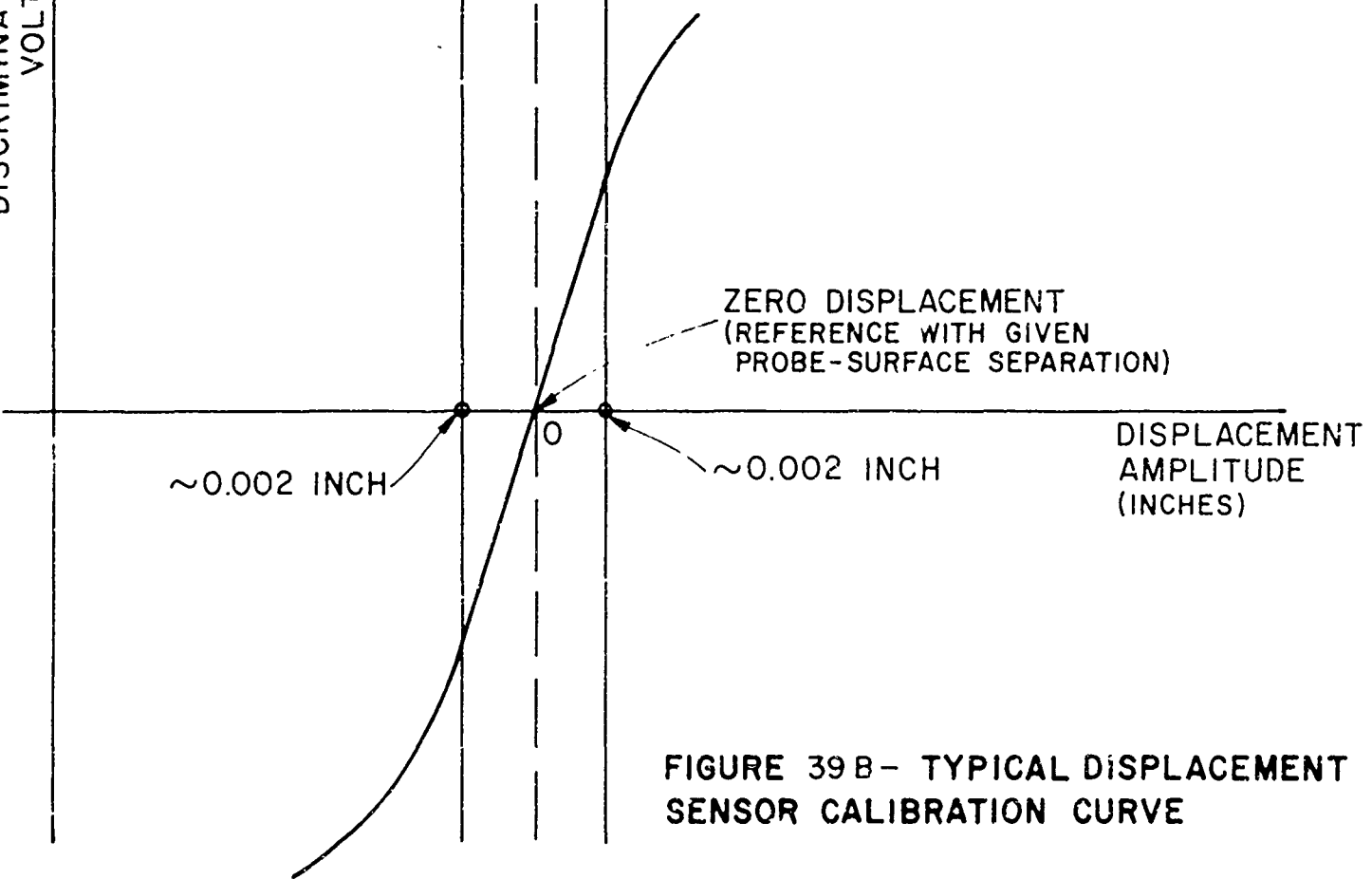


FIGURE 39B - TYPICAL DISPLACEMENT SENSOR CALIBRATION CURVE



A second technique which has also been under investigation, utilizes a CW laser beam as the light source in a Michelson interferometer. The principal advantage of this technique is that it does not alter the acoustic properties of the system under test and lends itself well to remote sensing such as for vibrating surfaces under water. A simplified schematic of a typical laser displacement measuring system is shown in Fig. 40.

The laser light beam (S) is directed through a distance  $L_0$  to the beam splitter (B) where it is separated into two beams. One light beam is reflected from B and traverses path  $L_1$  to a fixed mirror  $M_1$ . The other light beam is transmitted through B and along path  $L_2$  to the sound source and its surface  $M_2$ . Now, since the laser light is highly monochromatic, small alterations in  $L_2$ , produced by vibrating the surface  $M_2$  at a frequency  $\omega_a$ , will cause the reflected light to become phase modulated. However, since  $M_1$  is fixed,  $L_1$  remains fixed and its reflected beam is unmodulated. Thus, the reflection from  $M_1$  fills the role of a local oscillator when it is recombined with the reflection from  $M_2$  at the photo-sensitive surface of the square law detector (D). The displacement amplitude of  $M_2$  is directly related to the total light flux or electric field impinging on the photosensitive surface of the detector since the total electric field is the sum of the electric fields from the two reflected beams. Consequently, the output current of a photo multiplier tube, being a function of the square of the real part of the total electric field, is also related to the displacement amplitude of  $M_2$ . The absolute magnitude of the displacement can be obtained by several different mathematical techniques [15].

The laser interferometer technique has been proven to be capable of measuring displacements in the range of 0.1 to 5000 Å, in air, at acoustic frequencies to 20 kHz [16]. Further, recent underwater tests, carried out at Catholic University,

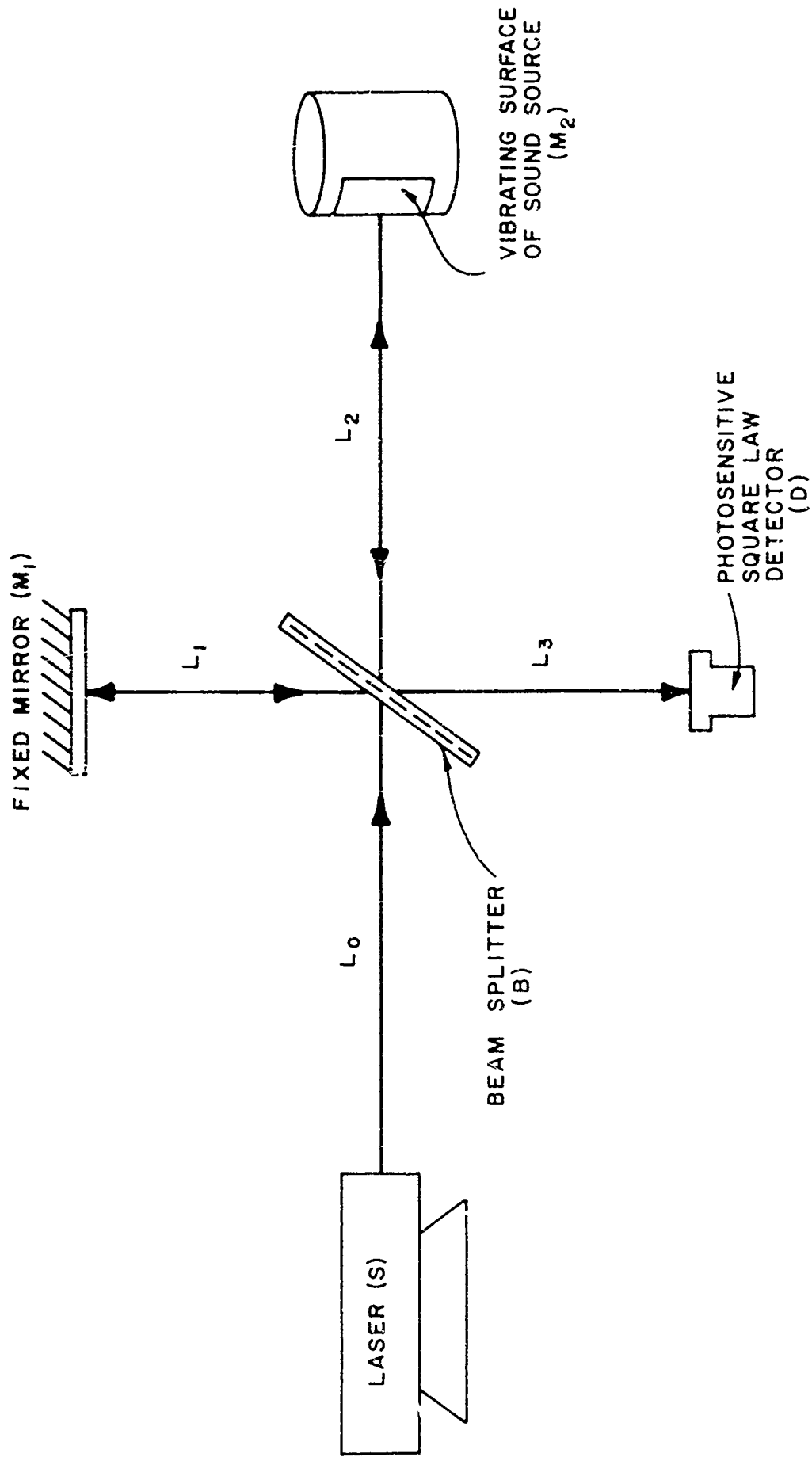


FIGURE 40 - SIMPLIFIED EXPERIMENTAL ARRANGEMENT FOR THE MEASUREMENT OF SMALL DISPLACEMENT AMPLITUDES USING A LASER INTERFEROMETER

have shown the technique (1) to work at frequencies in excess of 200 kHz, (2) to provide measurement of pulsed surfaces, (3) to have an underwater sensitivity of better than 10 Å, and (4) to verify the fact that reflecting surfaces need not be mirror-like, but can be diffuse or granular. Present plans include the implementation of a laser installation in the test facility.

### 7.3 BEAM PATTERN MEASUREMENTS

In addition to the detailed displacement profiles of the transducer element, corresponding azimuthal and vertical radiation patterns are also required. A schematic drawing of the underwater test facility is shown in Fig. 41. The test tank is 16 feet long, 8 feet wide, and 7 feet deep. Two independent traverse mechanisms, affixed to the top of the tank, allow precise location and rotation of both hydrophone and projector elements.

Prior to carrying out extensive measurements on the model sound sources and source-dome configurations, a thorough evaluation of the test facility was deemed necessary. Of particular importance was the identification of spurious signals which arise through multiple reflections within the tank as well as from sound generating sources external to the tank. Additional factors such as acceptable pulse lengths, frequencies of operation, pulse rise times, electrical grouping, stray electrical pickup, cross-talk, geometrical placement of source and hydrophone and other normally encountered experimental difficulties had to be anticipated and resolved. Since the sound sources under consideration were designed to have operating frequencies between 100 and 250 kHz, and active areas measuring 5 water wavelengths in the azimuthal plane and from 1 to approximately 20 water wavelengths in the vertical plane, tests were necessary to verify experimentally those regions which represented the near-

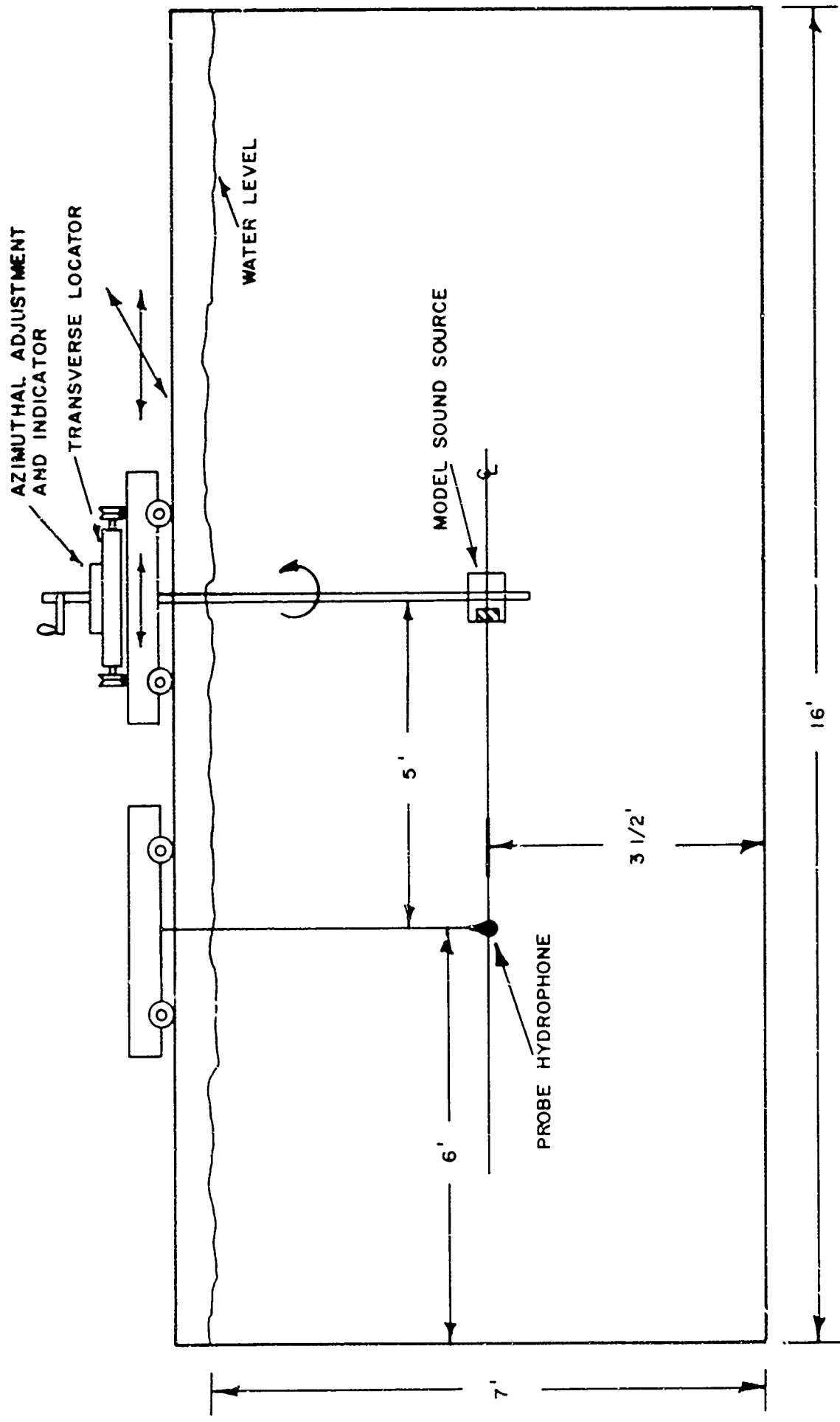


FIGURE 41 GEOMETRICAL ARRANGEMENT OF PROBE HYDROPHONE AND MODEL SOUND SOURCE FOR MEASUREMENT OF AZIMUTHAL BEAM PATTERNS.

and farfields. Finally, probe hydrophones required evaluation to determine whether or not their physical dimensions, sensitivities, and resonant frequencies would allow detailed mapping of both near- and farfield radiation patterns.

It was found that the commercial probe hydrophone (Edo type 197) which is approximately  $\frac{1}{2}$  inch in length, by  $\frac{1}{2}$  inch in diameter, was too large to provide the desired detailed information and resolution of both near- and farfield beam patterns. In addition, its resonant frequency, 150 kHz, put it in the middle of the frequency range of the experimental source. Consequently, a new probe hydrophone was designed and constructed using a 0.125 inch length of PZT 5A ceramic tubing, having an outside diameter of 0.064 inch and a wall thickness of 0.010 inch. This hydrophone was mounted on the end of a length of RG 174/u cable and encapsulated with an electrically conductive epoxy resin. A relative calibration of the hydrophone showed it to have a sensitivity of approximately -155 dB re 1 volt/microbar. Since the data to be taken with this hydrophone did not require the absolute source level, an absolute calibration of the hydrophone was unnecessary. Beam pattern measurements of the probe hydrophone showed it to be omnidirectional in its vertical plane as well. Further tests showed its lowest resonant frequency to be about 500 kHz, far removed from those frequencies of interest in these investigations.

#### 7.4 MEASUREMENT APPARATUS

The experimental apparatus used for obtaining the azimuthal beam patterns is shown in Fig. 42. A CW signal produced by a wide band oscillator is coupled, via the frequency counter, to the General Radio tone-burst generator. The output of the tone-burst generator is a pulse of variable cyclic duration and repetition time. It is applied to the input terminals of the power amplifier used to drive the model sound source. The signal received by the probe hydrophone is passed through the Rohde and Schwarz tunable amplifier which, in this case, fills the dual role of amplifying a very low level signal while at the

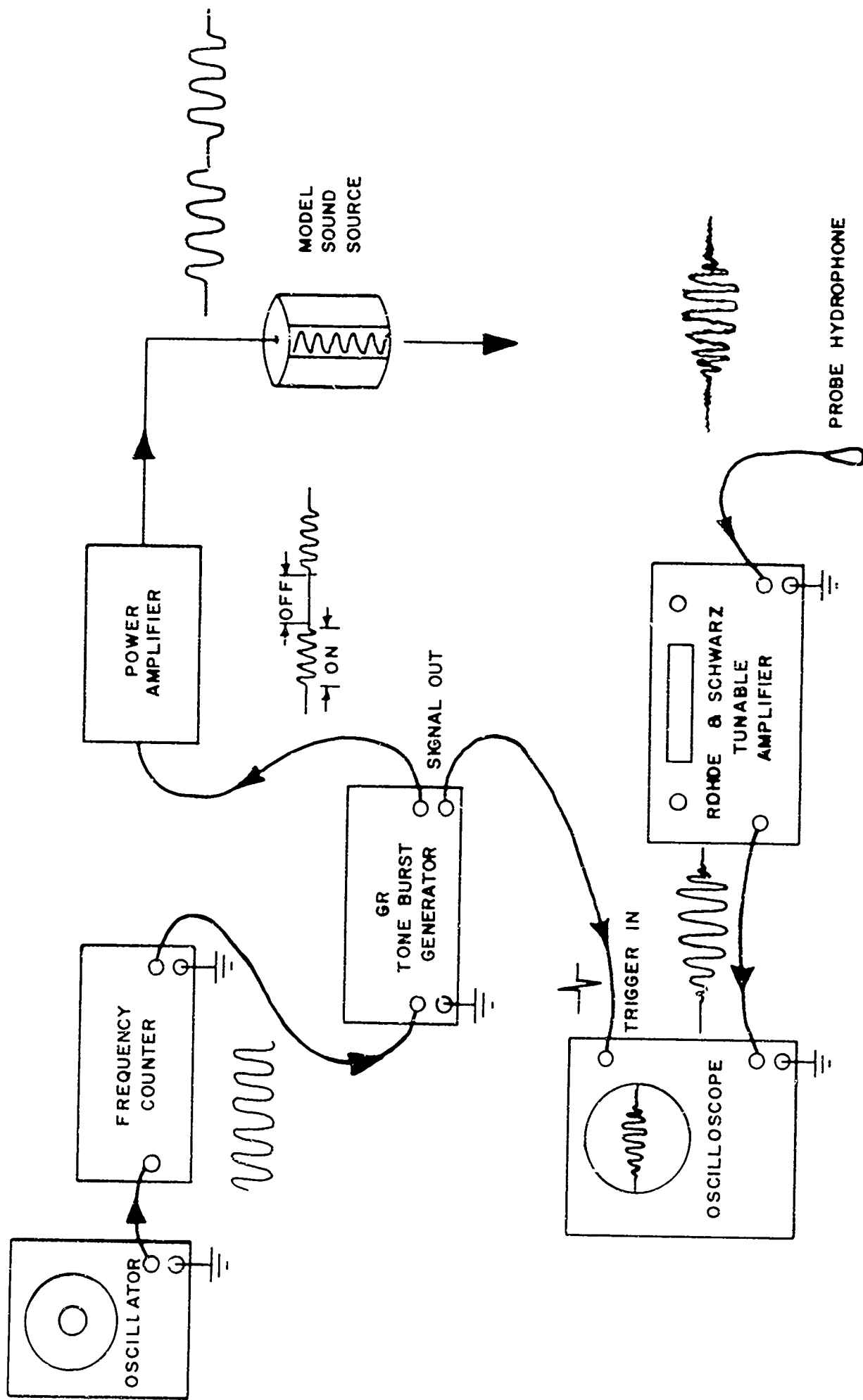


FIGURE 42-ELECTRONIC APPARATUS FOR MEASURING BEAM PATTERNS OF THE MODEL SOUND SOURCE. (BY USING VARIABLE LENGTH PULSE TECHNIQUES SPURIOUS SIGNALS ARE TIME SEPARATED FROM DESIRED SIGNAL INFORMATION.)



same time acting as an active filter. Thus, the signal that is applied to the oscilloscope for measurement is of very clean waveform and of such a level as to facilitate easy measurement. A trigger signal from the tone-burst generator is used to synchronize the sweep of the oscilloscope and allows identification of the received signal based upon travel time.

Poor repeatability of azimuthal beam patterns during the early phases of this investigation were attributed to insufficient buildup time of the transmit pulse. Subsequent tests showed that with typical transducer Q's running about 40, and operating frequencies between 100 and 250 kHz, a pulse length of about 64 cycles duration was required for most of the model sources to reach a repeatable steady state condition. In practice, this pulse duration requirement has been checked on an individual basis. The measured beam patterns, which are presented in a later section of this report, can be repeated to within about  $\pm 1$  and  $\pm 2$  dB.

#### 7.5 MODEL SOURCE DESIGN

Since the experimental models are designed to furnish direct support to the analytical work, the experimental source or transducer must be capable of simulation through mathematical analysis. This has placed the following constraints on the model source design:

1. The model source should be cylindrical.
2. The model source must be capable of producing a fairly directive beam pattern in order to assess dome effects.
3. The azimuthal velocity distribution should be a reasonably smooth function of position because this distribution (boundary condition) must be represented by a Fourier series in the mathematical model.



4. The vertical velocity distribution must be uniform.
5. The axial length of the source must be variable.

During the initial stage of this program, a range of possible sound source designs was reviewed. Consideration was first given to the idea of piezoelectric ceramic segments placed in solid metal rings or, possibly, in lucite baffles, while yet another idea involved the preferential excitation of a mechanically continuous but segmentally polarized, piezoelectric ring element. The most attractive of these initial source designs was the continuous piezoelectric ring.

After some preliminary investigations with a small ceramic cylinder to determine the feasibility of the segmental polarization scheme, a segmentally polarized cylinder of 6.3 in. outside diameter, 2.7 in. height, and 0.48 in. thickness was procured. This cylinder was polarized such that the azimuthal aperture was approximately five water wavelengths at 230 kHz, the wall-thickness resonant frequency. It was estimated that this aperture would produce a beamwidth on the order of 30°-35°, adequate for the purposes of the study.

Upon receipt of the first segmentally polarized ring, a series of displacement measurements was carried out in air. The height of the ring was divided into four equal parts as shown in Fig. 43 and azimuthal scans were completed through each of these sections. The preliminary displacement profiles, Fig. 44, showed the segmentally polarized element to have very uniform displacement over its active portion, and to drop approximately 10 dB in immediately adjacent nonactive areas. These profiles were judged suitable in terms of the mathematical requirements. Upon completion of the displacement profile, the single ring was placed in the water tank and its azimuthal beam pattern (Fig. 45) was obtained. Subsequently, several rings were stacked and azimuthal beam patterns were obtained in order

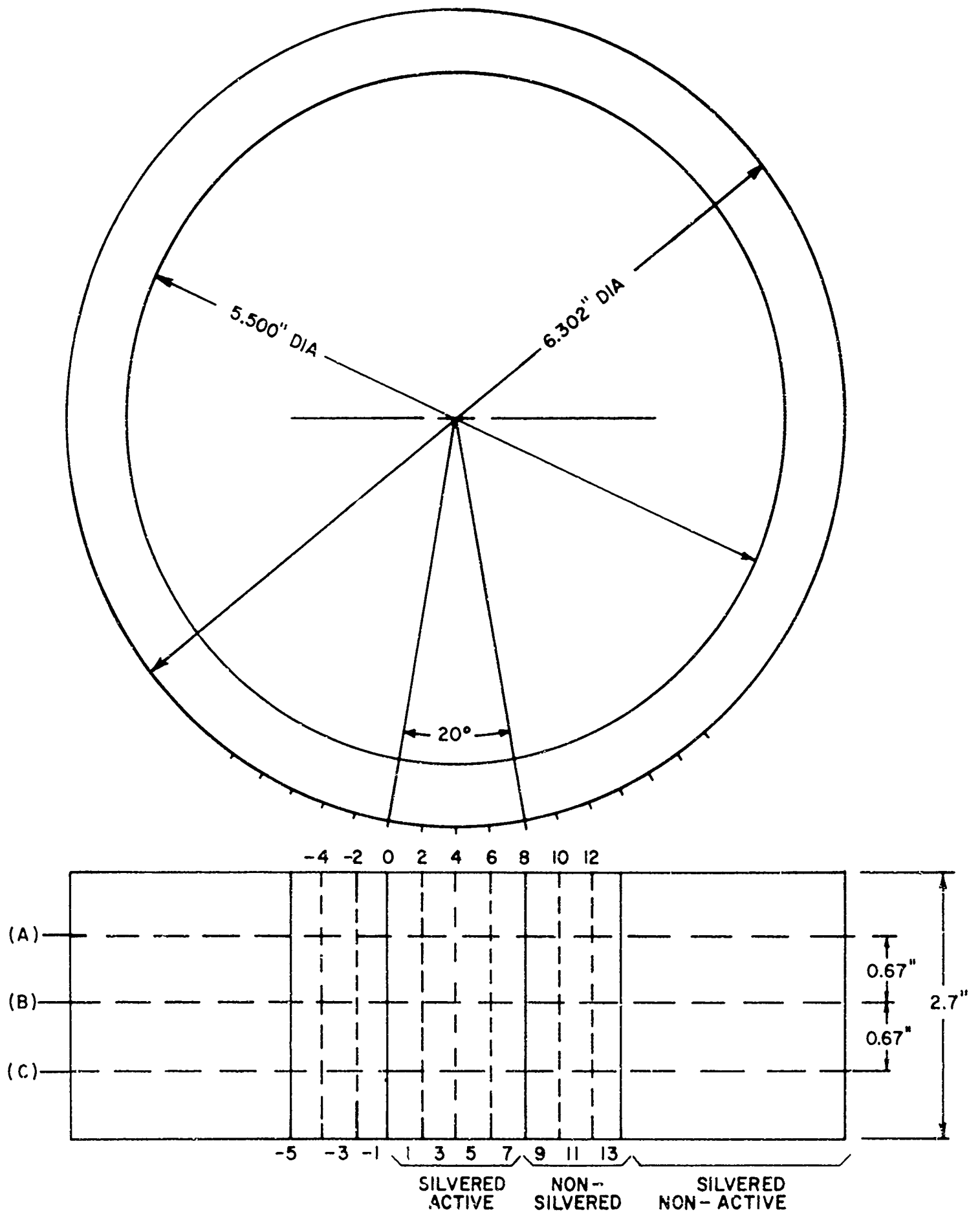


FIG. 43 DISPLACEMENT MAPPING SCHEME FOR A DOUBLE SEGMENTALLY ACTIVE PIEZOELECTRIC RING SOURCE

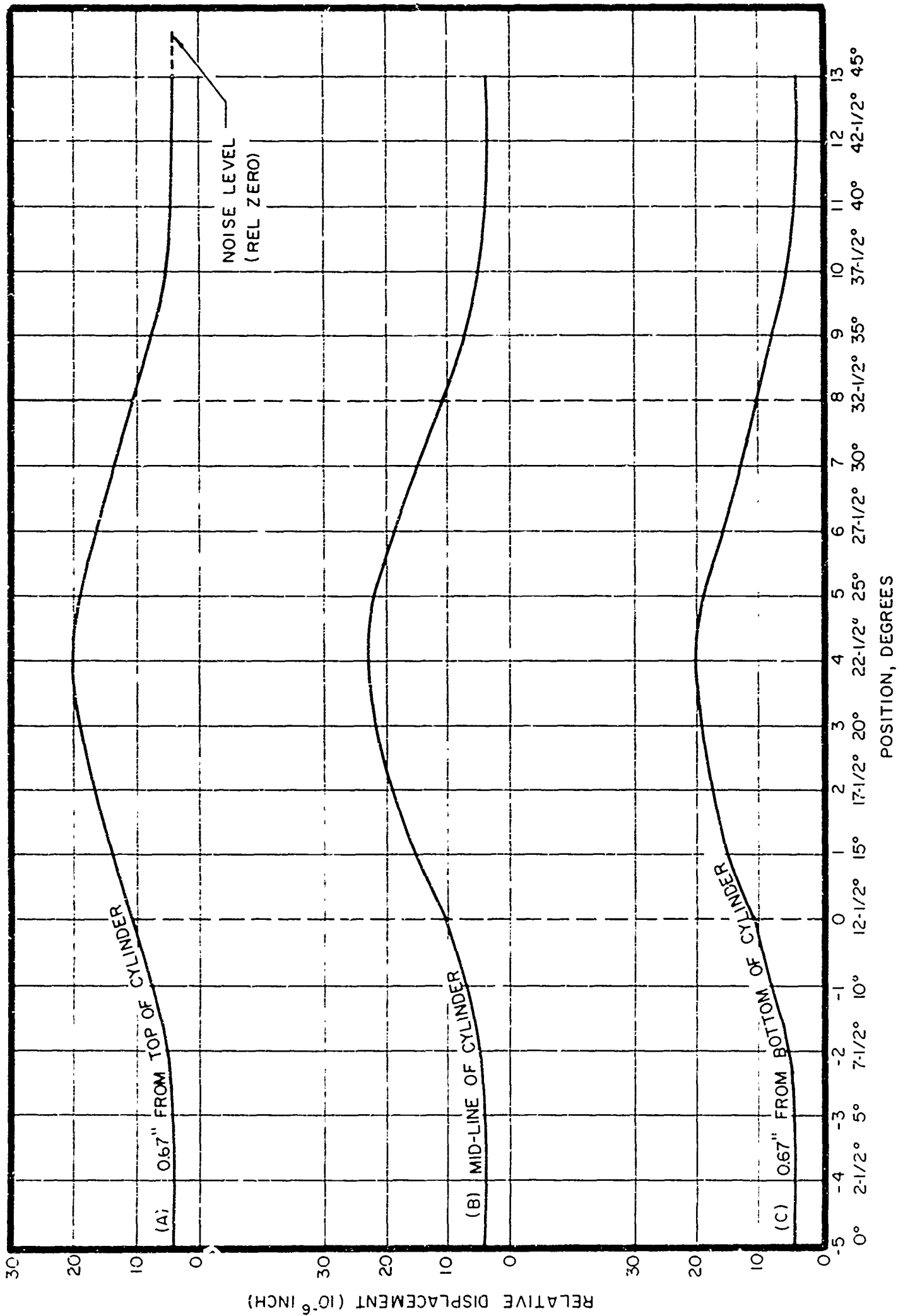
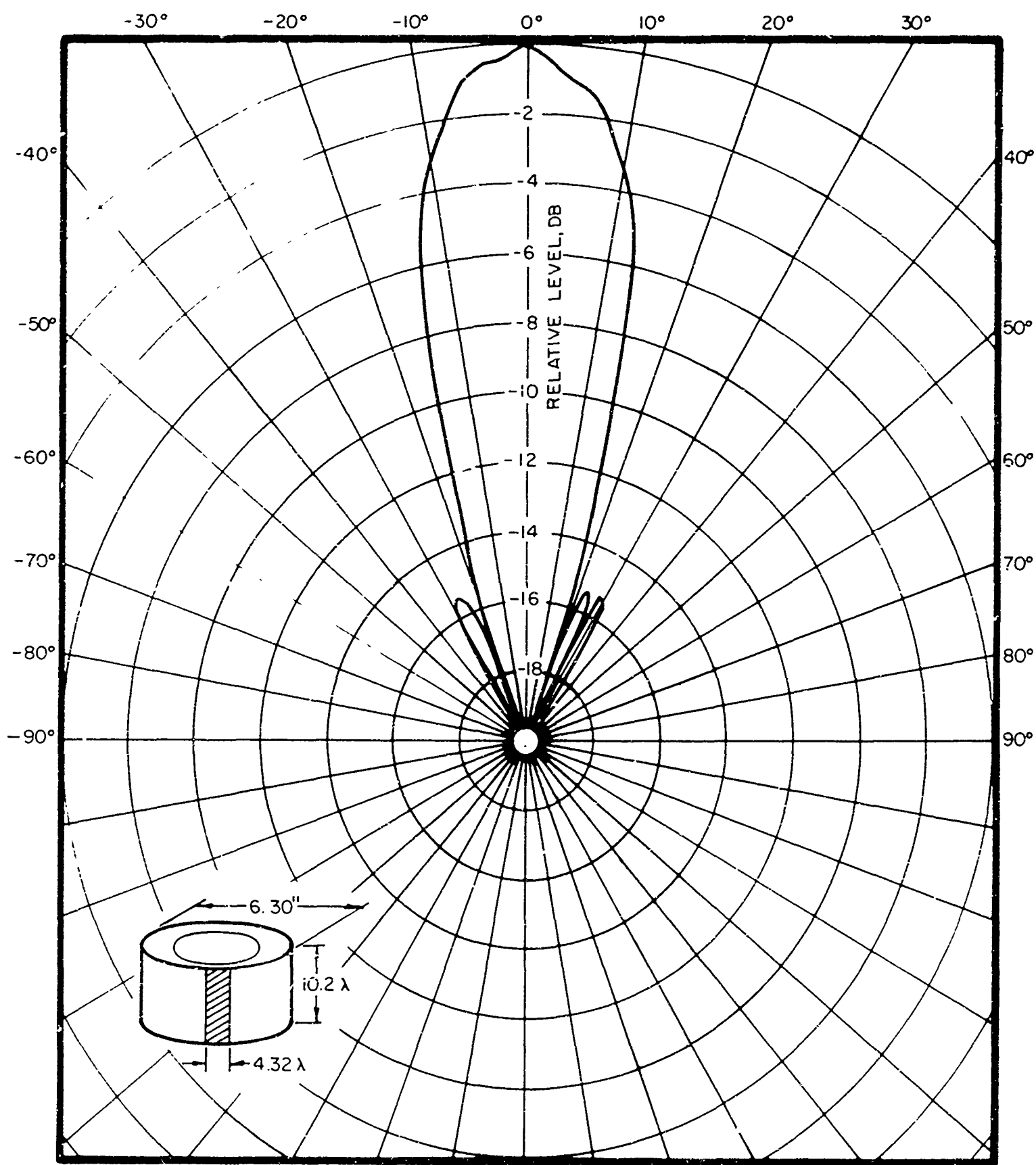


FIG.44 - RELATIVE DISPLACEMENTS OF 6.3" DIA SEGMENTALLY POLARIZED CYLINDER



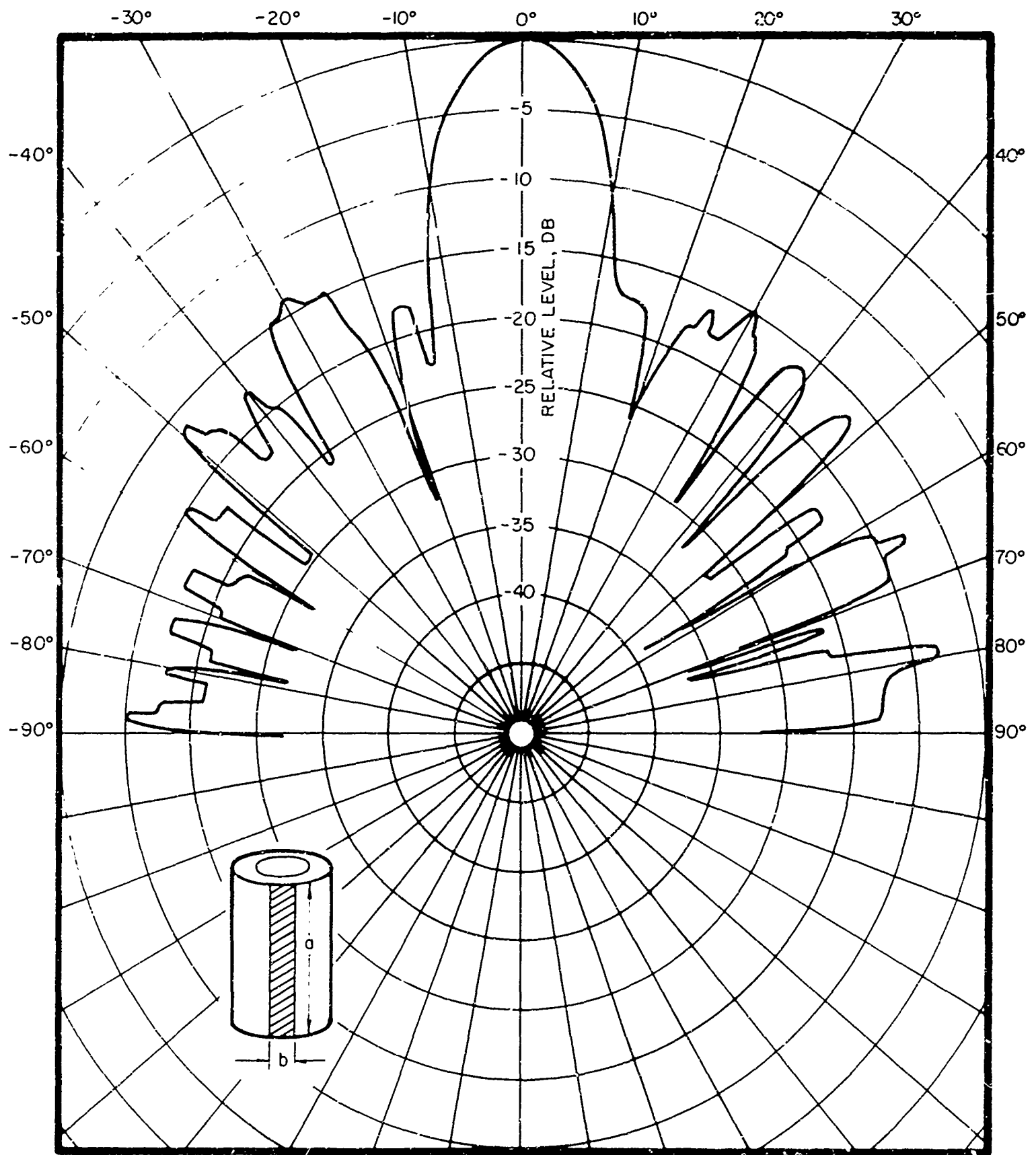
FREQUENCY = 230 KHz .  
 HORIZONTAL FARFIELD ( $d/2 \cong 180$ )

FIG. 45 -HORIZONTAL BEAM PATTERN FOR SEGMENTALLY EXCITED  
 PZT CYLINDER

to determine the dependence of the patterns on the axial length of the source. A pattern obtained with four stacked rings is shown in Fig. 46. The disparity between Figs. 45 and 46 led to the suspicion that the velocity profiles did not have the desired distribution.

More detailed velocity profiles were obtained on single rings and on stacked rings. Results obtained for a single ring are shown in Fig. 47. The apparent coupling of axial modes to the radial mode and subsequent non-uniformity of the vertical profiles render this particular source design useless in view of the requirements outlined above.

In an effort to eliminate the mode coupling in the segmentally polarized ring, a new source was constructed by mounting a polarized ceramic slab in a lucite baffle. The overall dimensions of the source and operating frequency remained the same as the segmentally polarized source. The active slab was mechanically isolated from the lucite baffle to minimize any coupling. An extensive series of velocity profile measurements was made with the ultramicrometer for cases of air and water backing of the active slab. The measurements revealed the existence of several spurious modes, probably attributable to non-uniform polarization and lack of symmetry in the ceramic slab. Despite the undesirable velocity profiles, beam pattern measurements were made as a function of axial length of the source, the length varying from five to fifteen wavelengths. The results shown in Figs. 48-50 demonstrate reasonable agreement; however, it is felt that improvements must be made in the source design before meaningful experiments can be conducted.



$a = 22.5 \lambda$  (4 RING HEIGHTS)  
 $b = 4.4 \lambda$   
 $f_R = 230 \text{ KHz}$

FIG. 46 -- HORIZONTAL BEAM PATTERN AT 5 FT.

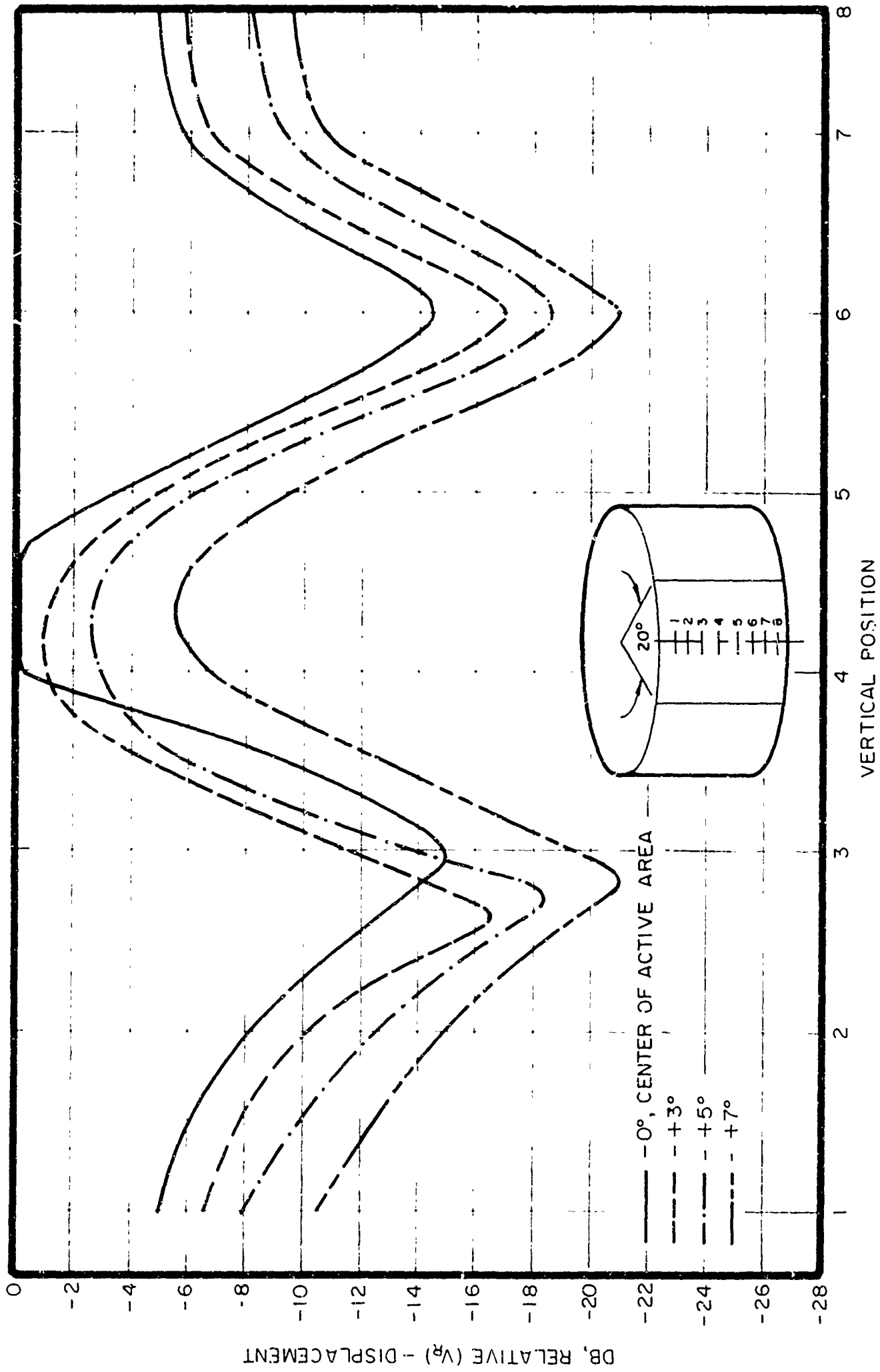


FIG. 47 - RELATIVE DISPLACEMENT, DB, VS VERTICAL POSITION FOR SINGLE CYLINDER

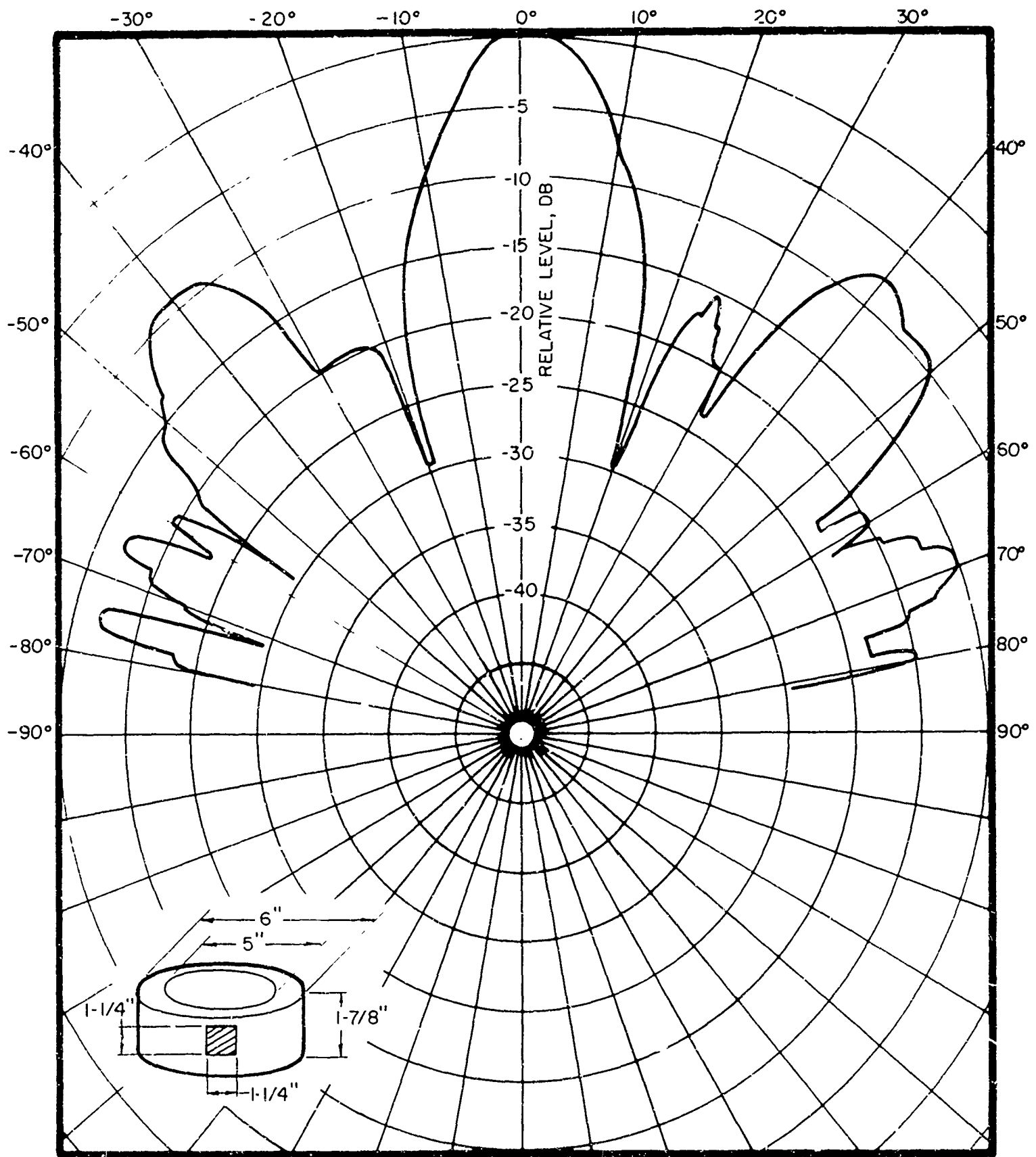
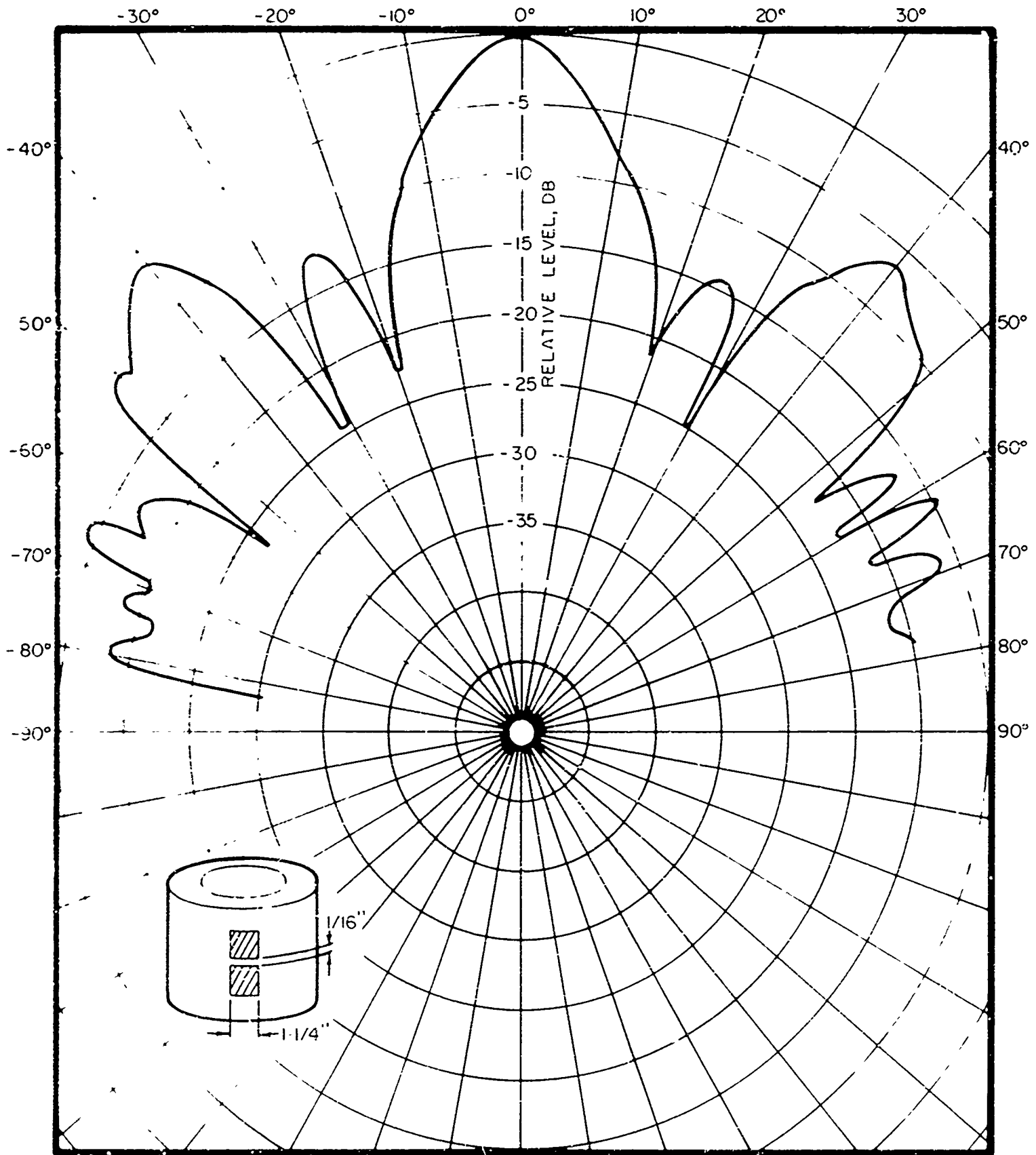
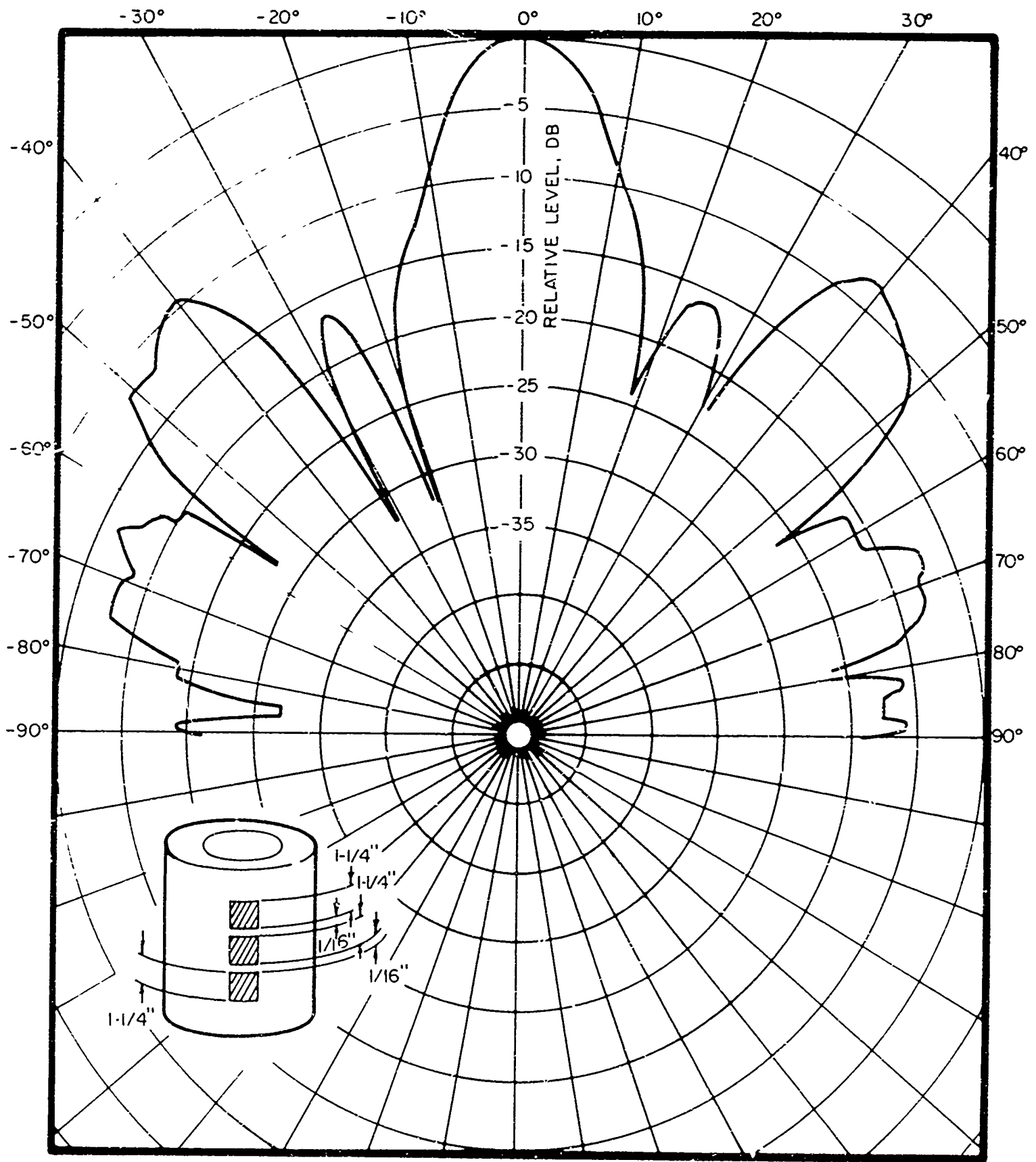


FIG. 48 - FARFIELD HORIZONTAL BEAM PATTERN - SINGLE ELEMENT SECTION (FREE FLOODED INSIDE)



FREQUENCY = 230.8 KHz

FIG. 49 - FARFIELD HORIZONTAL BEAM PATTERN - DOUBLE ELEMENT SECTION (FREE FLOODED INSIDE)



FREQUENCY = 230.8 kHz

FIG. 50 - FARFIELD HORIZONTAL BEAM PATTERN - TRIPLE ELEMENT SECTION (FREE FLOODED INSIDE)



6500 TRACOR LANE AUSTIN TEXAS 78721

## 7.6 SUMMARY

An analysis of the designs to date suggests that an acceptable velocity distribution is difficult to obtain using a single active element on the order of five wavelengths in aperture. Present effort is being directed toward a mosaic of individually tuned radiators whose dimensions are less than one wavelength square. The array of small radiators will be mounted in a cylindrical baffle as in the previous design. This source design should prove satisfactory for the purposes of the dome program.



## 8. CONCLUSIONS

The program of work during the past year has been concentrated on improving the geometry of dome-transducer models in order to obtain more realistic assessments of the effects of dome-transducer interactions on transmitted beams. The analytical phase of studies has been supported by an experimental phase whose primary purpose, during this period, has been the development of a small, general purpose transducer which can be modeled with existing analytical techniques. This transducer will be used in experimental studies of dome structure and geometry effects on the near- and farfields. In addition to these investigations, several problems related to dome construction and three-dimensional dome-transducer geometries were analyzed. Specific conclusions resulting from the past year's studies include the following:

1. Studies of integral techniques for solving the scalar wave equation have led to methods which permit the treatment of larger radiating bodies than heretofore possible. As a result, the integral formulation now offers considerable promise for analyzing dome-transducer systems of fairly general geometries.

2. An analysis of (a) the nonconcentric cylindrical dome model and (b) the elliptical dome model indicates no beam steering errors occur for any beam steering angle. In general, the side lobe structure is not symmetric about the beam axis for these steering directions, however, and side lobe levels can be considerably higher than those found with the concentric dome model. The higher side lobes are always located on the side of the beam pattern which corresponds to maximum dome-transducer spacing.

3. The source level computed with the elliptic dome model varies with beam steering angle. (This is attributed to a varying radiation loading on the active staves.) The dependence

is not the simple periodic one found in several models for which the dome-transducer spacing is constant.

4. Studies of thick homogeneous cylindrical domes and cylindrical domes with simple supporting structure show that, for the former, the results (beam patterns) agree with thin shell theory up to dome thicknesses of approximately 0.06 wavelengths. Thicknesses of metal domes are somewhat less than this number, while the thickness of the rubber dome for the AN/SQS-26 is greater. Because of the method of constructing the rubber dome, the ratio of dome thickness to wavelength increases as the beam steering angle increases towards broadside. For the dome with supporting structure, the limited results indicate the ribs modify the side lobe structure and decrease the source level, compared to a homogeneous dome for which the mass of the ribs has been "smeared out" over the whole dome surface.

5. Computation of beam patterns for a spherical transducer and concentric shell-type dome produced results qualitatively similar to those for the concentric cylinder model; namely, an increase in side lobe level compared to the bare transducer, and no change in main lobe width. A comparison of radiation interaction coefficients for circular pistons in a spherical baffle and equal-area rectangular pistons in an infinite-length cylindrical baffle of similar  $ka$  (product of wave number and radius) showed strong similarities as a function of piston separation. These results suggest the possibility of synthesizing the analysis of real dome transducers with several simpler analytical models. The extent to which such synthesis is valid is yet to be determined.

6. Instrumentation for successful beam pattern and displacement (in air) measurements for a small, high-frequency sound source has been developed. Attempts at using a single element of several wavelengths' dimension in the sound source were not successful due to the non-uniformity of the measured displacement profile. These results point out the necessity of using

**TRACOR** 6500 TRACOR LANE AUSTIN TEXAS 78721

several elements of small dimensions (less than one water wavelength at the transmit frequency) in fabricating an active array. Preliminary results indicate the required elements can be constructed.

## **DISCLAIMER NOTICE**

**THIS DOCUMENT IS BEST QUALITY PRACTICABLE. THE COPY FURNISHED TO DTIC CONTAINED A SIGNIFICANT NUMBER OF PAGES WHICH DO NOT REPRODUCE LEGIBLY.**

*OR ARE  
Blank pgs.  
that have  
Been Removed*

**BEST  
AVAILABLE COPY**



## 9. PROPOSED PROGRAM FOR SECOND YEAR OF STUDIES

The program proposed for the second year of studies is divided into five tasks:

### 1. General Analytical Methods

The integral formulation will be applied to larger bodies representative of, for example, the AN/SQS-26 dome. The procedure then can be employed in obtaining realistic farfield patterns from measurements of dome displacement. This application complements several nearfield-farfield techniques currently under investigation elsewhere. The integral formulation also will be extended to two-body (dome and transducer) problems.

### 2. Elliptical Dome Model

Computations will be extended to determine nearfield and farfield dome effects as a function of dome eccentricity. Configurations approximating the AN/SQS-23 and AN/SQS-26 sonar equipments will be included. Computations of source level as a function of steering angle and dome eccentricity will be performed. A limited study of the influence of dome thickness on transducer performance also will be conducted.

### 3. Spherical Dome-Transducer

A complete set of element interaction coefficients will be computed for a typical array. These, together with an appropriate transducer element model, will be used to study dome-array interactions for cases with and without transducer element velocity control. Where possible, system parameters corresponding to the AN/BQS-6 sonar equipment will be used in the computations.

### 4. Dome Structure

The present structure model will be studied to determine the dependence of farfield patterns on size and spacing



6500 TRACOR LANE AUSTIN TEXAS 78721

of structural members. Possible methods of treating more realistic structural members will be investigated.

#### 5. Experimental Program

Upon completion of the experimental transducer, experiments will be conducted to determine (a) the dependence of azimuthal beam patterns on axial length of the transducer, and (b) farfield patterns with elliptic dome and other dome shapes of interest. Further experiments will be conducted to determine dome structure effects on farfield patterns.



## REFERENCES

1. Moyer, W. C. and J. D. Morell "A Parametric Analysis of Dome-Transducer Interactions," TRACOR Report 66-136-U, February 10, 1966.
2. Douglass, R. E. and B. E. Jay "Radiation Characteristics of a Spherical Transducer Surrounded by a Concentric Shell," TRACOR Report 67-178-U, February 10, 1967.
3. Moyer, W. C. "Radiation Characteristics of a Circular Transducer Surrounded by a Nonconcentric Circular Shell," TRACOR Report 66-579-U, October 11, 1966.
4. Morse, P. M. and H. Feshbach Methods of Theoretical Physics, Vol. 1, Chap. 7, McGraw Hill, New York (1953).
5. A summary of the relevant integral equations arising from acoustic scattering problems is given in the work by G. W. Soules and K. M. Mitzner, "Pulses in Linear Acoustics," Underwater Acoustics Program Report ARD66-60R, Office of Naval Research Code 468, Nonr 4802(00), November 1966.
6. Chen, L. H. and D. G. Schweikert "Sound Radiation from an Arbitrary Body," JASA, 35, No. 10, 1626 (1963).
7. Schenck, H. A. U. S. Navy Electronics Laboratory, Private Communication.
8. Chertock, G. "Sound Radiation from Vibrating Sources," JASA, 36, No. 7, 1305 (1964).
9. Banaugh, R. P. and W. Goldsmith "Diffraction of Steady Acoustic Waves by Surfaces of Arbitrary Shape," JASA, 35, No. 10, 1590 (1963).
10. Copley, L. G. "Two Approaches to the Helmholtz Integral for Slender Axisymmetric Sound Radiators," Final Report U-186-131 Contract Nonr 3845(00)(X), June 1964.

11. Copley, L. G. "Integral Equation Method for Radiation from Vibrating Bodies," JASA, 41, No. 4, 807 (1967).
12. Douglass, Richard Doctoral Dissertation, University of Texas, June 1967.
13. "Acoustic Interaction Effects and the Theoretical Calculations of the Farfield Transmit Beam Patterns for the AN/SQS-26(CX) Sonar," TRACOR Report 67-437-C, September 1967.
14. "Sonar Dome Design Guide," Final Report on Contract NObsr-91145, Raytheon Company, Submarine Signal Division, July 1965 (Confidential).
15. Darby, R. A. "Experimental Techniques for Measuring Vibrations Using a Laser Interferometer," MEL Tech. Memo, 9/67, (AD 650-720), March 1967.
16. Defarrari, H. A. and F. A. Andrews JASA, 39, 1405, 979, (1966).

UNCLASSIFIED

| DOCUMENT CONTROL DATA - R&D  |   |   |
|--|---|---|
| <i>(Security classification of title body of abstract and indexing annotation must be entered when the overall report is classified)</i>   |   |   |
| 1 ORIGINATING ACTIVITY (Corporate author)<br>TRACOR, Inc.<br>6500 Tracor Lane<br>Austin, Texas 78721   |   | 2a REPORT SECURITY CLASSIFICATION<br>UNCLASSIFIED |
|  |   | 2b GROUP  |
| 3 REPORT TITLE<br>"EXPLORATORY DEVELOPMENT DOMES STUDY" Volume I   |   |   |
| 4 DESCRIPTIVE NOTES (Type of report and inclusive dates)<br>Summary Report   |   |   |
| 5 AUTHOR(S) (Last name, first name, initial)<br>Moyer, William C.  |   |   |
| 6 REPORT DATE<br>9 October 1967  | 7a TOTAL NO. OF PAGES<br>110  | 7b NO OF REFS<br>16                               |
| 8a CONTRACT OR GRANT NO<br>NObsr-95349   | 9a. ORIGINATOR'S REPORT NUMBER(S)<br>67-917-U   |   |
| b PROJECT NO<br>SFF101-03-17   |   |   |
| c<br>Task 8139   | 9b OTHER REPORT NO(S) (Any other numbers that may be assigned this report)  |   |
| 10 AVAILABILITY/LIMITATION NOTES   |   |   |
| 11 SUPPLEMENTARY NOTES   | 12. SPONSORING MILITARY ACTIVITY<br>Naval Ship Systems Command<br>Department of the Navy<br>Washington, D. C. 20360 |   |
| 13 ABSTRACT<br>This report presents the results obtained during the first year of a program for the analysis of the effects of sonar dome-transducer interactions on transmit performance. The analytical work has been directed toward (a) modeling a cylindrical transducer surrounded by an elliptical dome, (b) the application of an integral formulation of the radiation problem to sonar domes and transducers, and (c) limited analysis of a spherical transducer and concentric dome and a cylindrical dome with supporting structure. The analytical phases of the program have been supported by an experimental study whose main purpose has been the development of a small, high frequency transducer and appropriate instrumentation for measuring beam patterns and transducer displacements. |   |   |

DD FORM 1473  
1 JAN 64

UNCLASSIFIED

Security Classification

| 14<br>KEY WORDS                       | LINK A |    | LINK B |    | LINK C |    |
|---------------------------------------|--------|----|--------|----|--------|----|
|                                       | ROLE   | WT | ROLE   | WT | ROLE   | WT |
| Dome Geometry (Sonar)                 |        |    |        |    |        |    |
| Dome-Transducer Interactions (Sonar)  |        |    |        |    |        |    |
| Radiation Models (Mathematical)       |        |    |        |    |        |    |
| Dome-Transducer Configuration (Sonar) |        |    |        |    |        |    |
| Transducer Scale Models (Sonar)       |        |    |        |    |        |    |

## INSTRUCTIONS

1. **ORIGINATING ACTIVITY:** Enter the name and address of the contractor, subcontractor, grantee, Department of Defense activity or other organization (*corporate author*) issuing the report.
- 2a. **REPORT SECURITY CLASSIFICATION:** Enter the overall security classification of the report. Indicate whether "Restricted Data" is included. Marking is to be in accordance with appropriate security regulations.
- 2b. **GROUP:** Automatic downgrading is specified in DoD Directive 5200.10 and Armed Forces Industrial Manual. Enter the group number. Also, when applicable, show that optional markings have been used for Group 3 and Group 4 as authorized.
3. **REPORT TITLE:** Enter the complete report title in all capital letters. Titles in all cases should be unclassified. If a meaningful title cannot be selected without classification, show title classification in all capitals in parenthesis immediately following the title.
4. **DESCRIPTIVE NOTES:** If appropriate, enter the type of report, e.g., interim, progress, summary, annual, or final. Give the inclusive dates when a specific reporting period is covered.
5. **AUTHOR(S):** Enter the name(s) of author(s) as shown on or in the report. Enter last name, first name, middle initial. If military, show rank and branch of service. The name of the principal author is an absolute minimum requirement.
6. **REPORT DATE:** Enter the date of the report as day, month, year, or month, year. If more than one date appears on the report, use date of publication.
- 7a. **TOTAL NUMBER OF PAGES:** The total page count should follow normal pagination procedures, i.e., enter the number of pages containing information.
- 7b. **NUMBER OF REFERENCES:** Enter the total number of references cited in the report.
- 8a. **CONTRACT OR GRANT NUMBER:** If appropriate, enter the applicable number of the contract or grant under which the report was written.
- 8b, 8c, & 8d. **PROJECT NUMBER:** Enter the appropriate military department identification, such as project number, subproject number, system numbers, task number, etc.
- 9a. **ORIGINATOR'S REPORT NUMBER(S):** Enter the official report number by which the document will be identified and controlled by the originating activity. This number must be unique to this report.
- 9b. **OTHER REPORT NUMBER(S):** If the report has been assigned any other report numbers (either by the originator or by the sponsor), also enter this number(s).
10. **AVAILABILITY/LIMITATION NOTICES:** Enter any limitation on further dissemination of the report, other than those

imposed by security classification, using standard statements such as:

- (1) "Qualified requesters may obtain copies of this report from DDC."
- (2) "Foreign announcement and dissemination of this report by DDC is not authorized."
- (3) "U. S. Government agencies may obtain copies of this report directly from DDC. Other qualified DDC users shall request through \_\_\_\_\_."
- (4) "U. S. military agencies may obtain copies of this report directly from DDC. Other qualified users shall request through \_\_\_\_\_."
- (5) "All distribution of this report is controlled. Qualified DDC users shall request through \_\_\_\_\_."

If the report has been furnished to the Office of Technical Services, Department of Commerce, for sale to the public, indicate this fact and enter the price, if known.

11. **SUPPLEMENTARY NOTES:** Use for additional explanatory notes.
12. **SPONSORING MILITARY ACTIVITY:** Enter the name of the departmental project office or laboratory sponsoring (*paying for*) the research and development. Include address.
13. **ABSTRACT:** Enter an abstract giving a brief and factual summary of the document indicative of the report, even though it may also appear elsewhere in the body of the technical report. If additional space is required, a continuation sheet shall be attached.
- It is highly desirable that the abstract of classified reports be unclassified. Each paragraph of the abstract shall end with an indication of the military security classification of the information in the paragraph, represented as (TS), (S), (C), or (U).
- There is no limitation on the length of the abstract. However, the suggested length is from 150 to 225 words.
14. **KEY WORDS:** Key words are technically meaningful terms or short phrases that characterize a report and may be used as index entries for cataloging the report. Key words must be selected so that no security classification is required. Identifiers, such as equipment model designation, trade name, military project code name, geographic location, may be used as key words but will be followed by an indication of technical content. The assignment of links, rules, and weights is optional.